Philipps Universität Marburg

Structural and functional studies on the homeostasis and type-III-secretion of flagellin

Dissertation
zur Erlangung des Doktorgrades
der Naturwissenschaften
(Dr. rer. nat.)

dem Fachbereich der Biologie
der Philipps-Universität Marburg
vorgelegt

von

Florian Altegoer
Master of Science
aus Witten (Nordrhein-Westfalen)

Marburg Februar 2017

Die Untersuchungen zur vorliegenden Arbeit wurden von März 2013 bis Januar 2017 am LOEWE Zentrum für synthetische Mikrobiologie (SYNMIKRO) der Philipps-Universität Marburg unter der Leitung von Dr. Gert Bange durchgeführt.

Vom Fachbereich Biologie der Philipps-Universität Marburg
als Dissertation angenommen am: 14.02.2017

Erstgutachter: Dr. Gert Bange
Zweitgutachter: Prof. Dr. Martin Thanbichler

Tag der mündlichen Prüfung: 24.03.2017

ACKNOWLEDGEMENTS

I am very grateful to all the people who made this work possible.

First of all, I would like to thank Dr. Gert Bange for providing me with these exciting scientific projects. He always inspired me with interesting topics and fruitful discussions and I am grateful for the excellent support and the enthusiastic atmosphere. Thank you very much, Gert.

I am also deeply grateful to Prof. Dr. Martin Thanbichler for being my second referee and the productive collaboration, although it could not be included in this thesis.

I especially want to thank Prof. Dr. Peter Graumann for many stimulating discussions on various research topics and the opportunity to use his laboratory equipment whenever needed.

Moreover, I am grateful to the whole Bange group. I would like to thank Wieland Steinchen, Devid Mrusek, Jan Schuhmacher, Carina Knauer, Patrick Pausch and Magdalena Rakwalska-Bange for the nice and collaborative atmosphere over the last four years. It was always a pleasure on the balcony and in the lab.

I am thankful to Wieland Steinchen for his contribution to my manuscript and his excellent support during the collection and evaluation of HDX data.

Furthermore, I would like to thank Prof. Dr. Stefan Rensing for his support on the phylogenetic analysis of CsrA and FliW.

I would like to thank all the members of the Graumann group, especially Patricia Bedrunka and Dr. Felix Dempwolff for many nice discussions and their continuous support during fluorescence microscopy and *in vivo* studies, although most of the work could not be included in this thesis.

I appreciate the support of Dr. Thomas Heimerl for introducing me to electron microscopy and always offering me the opportunity to use the facility.

I am also grateful to Prof. Daniel B. Kearns from the Indiana University, Bloomington for the fruitful collaboration and for providing me with strains and antibodies throughout my thesis.

I would like to acknowledge Dr. Matthew McIntosh for his correction and feedback.

Most of all, I am deeply indebted to my family: to my father Dietmar, my mother Barbara and my sisters Annika and Kathrin who always helped me during this time. I am especially grateful to Lynn Binnebesel for her patience and constant support. I enjoy being with you every day.

SUMMARY

The ability to move towards favorable and avoid unfavorable conditions is key to the survival of many bacterial species. Bacterial movement relies on a sophisticated nanomachine, the flagellum. Despite being one of the tiniest motors in the biosphere, the flagellum exhibits a complex architecture and is composed of more than 30 different proteins in diverse stoichiometries. Flagellar architecture can be subdivided into a membrane-embedded basal body, a hook and a long helical filament.

The process of flagellar assembly involves a plethora of accessory factors and is organized at different stages on the transcriptional, post-transcriptional and translational level. Furthermore, biogenesis of a flagellum is strictly sequential and requires the completion of a building phase prior to initiating the next one. The most abundant constituent within a flagellum is the protein flagellin that assembles into a helical filament with more than 20.000 monomers. The two proteins CsrA and FliW regulate flagellin homeostasis via a post-transcriptional mechanism only allowing flagellin translation when cytoplasmic levels are low, thereby ensuring that flagellin is directly secreted after production. A third protein, the intrinsic chaperone FliS is essential for the recognition and efficient secretion of flagellin. Together these proteins couple translation to secretion of flagellin and keep cytoplasmic flagellin concentrations around a low and narrow threshold. This work aims at unraveling the molecular mechanisms by which the above-named proteins regulate flagellin homeostasis.

In enterobacteria CsrA activity is antagonized by small non-coding RNAs (sRNAs) that act as competitive inhibitors. Conversely, the FliW protein allosterically controls CsrA in a variety of flagellated bacteria, which seems to represent the ancestral state of CsrA regulation. This work furthermore demonstrates that interaction of FliW and flagellin seems to be co-translational or strongly associated with translating ribosomes, therefore coupling homeostasis and secretion.

Another level of regulation elucidated in this study is the influence of bactofilins on the process of flagellar biogenesis. This ubiquitous class of proteins is reminiscent of cytoskeleton factors but seems to rather provide a dynamic scaffold for diverse processes. In *B. subtilis* the bactofilins BacE and BacF are involved in flagellar assembly at the stage of hook-completion but BacE also directly interacts with FliW.

Finally, this work includes a model explaining the coupling of homeostasis and secretion of flagellin at atomic resolution.

ZUSAMMENFASSUNG

Die Fähigkeit günstige Lebensbedingungen zu finden und ungünstige zu vermeiden, ist ein zentraler Aspekt für die Überlebensfähigkeit vieler Bakterienarten. Das bakterielle Flagellum stellt einen der kleinsten Motoren in der Biosphäre dar, weist aber dennoch eine komplexe Architektur auf und besteht aus mehr als 30 unterschiedlichen Proteinen. Das Flagellum kann wie folgt untergliedert werden: Der zentrale Basalkörper ist in der Membran verankert und bietet das Grundgerüst für ein langes, helikales Filament, das über einen „Haken“ mit dem Basalkörper verbunden ist.

Der flagellare Assemblierungsprozess umfasst eine Vielfalt an regulatorischen Faktoren und ist hierarchisch sowohl transkriptionell, als auch post-transkriptionell und translational organisiert. Darüber hinaus ist die Biogenese eines Flagellums streng sequentiell und erfordert so die Fertigstellung eines „Bauabschnittes“ bevor ein neuer begonnen werden kann. Das Filament ist aus mehr als 20.000 Kopien des Proteins Flagellin aufgebaut, dessen Moleküle in einem helikalen Muster angeordnet werden.

Zwei Proteine, CsrA und FliW, regulieren die Flagellin Produktion über einen post-transkriptionellen Mechanismus. Dieser stellt sicher, dass nur dann Flagellin translatiert wird, wenn die zytoplasmatischen Level des Proteins niedrig sind, es also direkt sekretiert wird. Ein drittes Protein, das intrinsische Chaperon FliS, ist essentiell für die Erkennung und effiziente Sekretion von Flagellin. Zusammen kontrollieren diese Proteine die Produktion von Flagellin, so dass die zytoplasmatische Flagellin Konzentration um einen schmalen Schwellenwert oszilliert. Ziel dieser Arbeit ist es die molekularen Details der Flagellin Homöostase aufzuklären.

In Enterobakterien wird der CsrA Aktivität durch kleine, nicht-kodierende RNAs (sRNAs), die als kompetetive Inhibitoren agieren, entgegengewirkt. Im Gegensatz dazu kontrolliert FliW das CsrA Protein allosterisch in einer Vielzahl flagellierter Bakterien. Diese Art der CsrA Regulation stellt vermutlich den evolutionär ursprünglichen Zustand in Eubakterien dar.

Weiterhin wird in dieser Arbeit gezeigt, dass die Wechselwirkung von FliW und Flagellin entweder direkt co-translational zu sein scheint oder aber nah im ribosomalen Kontext stattfindet. Dies erlaubt die Kopplung von Flagellin Homöostase und Sekretion.

Weiterführende Untersuchungen, die in dieser Studie durchgeführt wurden, zeigen den Einfluss von Bactofilinen auf den Prozess der Flagellen-Biosynthese. Diese ubiquitäre Klasse von Proteinen erinnert an Zytoskelettproteine, scheint aber eher ein dynamisches Gerüst für

verschiedene Prozesse zu bilden. In *B. subtilis* sind die Bactofiline BacE und BacF am Aufbau der Flagelle beteiligt, möglicherweise am Aufbau des „Hakens“. Weiterhin wird eine Interaktion von BacE mit FliW gezeigt und damit eine Verbindung zur Flagellin Homöostase. Abschließend liefert diese Arbeit ein Modell, dass die Kopplung von Homöostase und Sekretion von Flagellin auf struktureller Basis erklärt.

PUBLICATIONS

The majority of the results presented in this work has been published in the following articles or is part of the following manuscripts:

Altegoer F, Mukherjee S, Steinchen W, Bedrunka P, Linne U, Kümmerer N, Sinning I, Kearns DB, Bange G (2017) Two chaperones couple translation and secretion for favourable flagellin production *in prep.*

Altegoer F*, Rensing SA, Bange G* (2016) Structural basis for the CsrA-dependent modulation of translation initiation by an ancient regulatory protein. *Proceedings of the National Academy of Sciences of the United States of America*, 113(36), 10168–73.

*corresponding authors

Altegoer F, Bange G (2015). Undiscovered regions on the molecular landscape of flagellar assembly. *Current Opinion in Microbiology*, *28*, 98–105

El Andari J, **Altegoer F**, Bange G, Graumann PL (2015). Bacillus subtilis Bactofilins Are Essential for Flagellar Hook- and Filament Assembly and Dynamically Localize into Structures of Less than 100 nm Diameter underneath the Cell Membrane. *PloS One*, *10*(10), e0141546.

Altegoer F, Schuhmacher J, Pausch P, Bange G. (2014) From molecular evolution to biobricks and synthetic modules: A lesson by the bacterial flagellum. *Biotechnol Genet Eng Rev*. 2014; 30:49-64.

Publications not included in this work are listed below:

Quax T, **Altegoer F**, Rodriguez-Franco M, Bange G, Albers SV (2017) Structure and function of the archaeal response regulator CheY. *Proceedings of the National Academy of Sciences of the United States of America*, *in review*

Blauenburg B, Mielcarek A, **Altegoer F**, Fage CD, Linne U, Bange G, Marahiel MA (2016). Crystal Structure of Bacillus subtilis Cysteine Desulfurase SufS and Its Dynamic Interaction with Frataxin and Scaffold Protein SufU. *PloS One*, 11(7), e0158749.

Steinchen W*, Schuhmacher JS*, **Altegoer F***, Fage CD, Srinivasan V, Linne U, Marahiel MA, Bange G (2015). Catalytic mechanism and allosteric regulation of an oligomeric (p)ppGpp synthetase by an alarmone. *Proceedings of the National Academy of Sciences of the United States of America*, 112(43), 13348–53.

*these authors contributed equally

Pausch P, Singh U, Ahmed YL, Pillet B, Murat G, **Altegoer F**, Stier G, Thoms M, Hurt E, Sinning I, Bange G, Kressler D (2015). Co-translational capturing of nascent ribosomal proteins by their dedicated chaperones. *Nature Communications*, 6, 7494.

Schuhmacher JS, Rossmann F, Dempwolff F, Knauer C, **Altegoer F**, Steinchen W, Dörrich AK, Klingl A, Stephan M, Linne U, Thormann KM, Bange G. (2015) MinD-like ATPase FlhG effects location and number of bacterial flagella during C-ring assembly. *Proceedings of the National Academy of Sciences of the United States of America*. 2015 Mar 10;112(10):3092-7

Giessen TW, **Altegoer F**, Nebel AJ, Steinbach RM, Bange G, Marahiel MA. (2015) A Synthetic Adenylation-Domain-Based tRNA-Aminoacylation Catalyst. *Angew Chem Int Ed Engl*. 2015 Feb 16;54(8)

LIST OF CONTENTS

ABBREVIATIONS

Å	Ångström (10^{-10} m)
ATP	adenosine triphosphate
AU	absorption unit
bp	base pairs
CCW	counter clockwise
CM	cytoplasmic membrane
CV	column volume
CW	clockwise
Da	Dalton (1.660538 x 10^{-27} kg)
DNA	desoxyribonucleic acid
EM	electron microscopy
ESRF	European Synchrotron Radiation Facility
fT3S	flagellar type-III-secretion
fT3SS	flagellar type-III-secretion system
GST	glutathione S-transferase
GTP	guanosine triphosphate
h	hours
hag	gene encoding flagellin
HDX	$^{1}H/^{2}H$ exchange mass spectrometry
HEPES	4-(2-hydroxyethyl)-1-piperazineethanesulfonic acid
IM	inner membrane
IPTG	isopropyl β-D-1-thiogalactopyranoside
iT3SS	injectisome type-III-secretion system
LB	lysogeny broth
M	mol/litre
min	minute
MPD	2-methyl-2,4-pentanediol
MR	molecular replacement
MS	mass spectrometry
MW	molecular weight
sRNA	small non-coding ribonucleic acid

NMR	nuclear magnetic resonance
NTA	nitrilotriacetic acid
OD	optical density
OM	outer membrane
PBS	phosphate buffered saline
PCR	polymerase chain reaction
PDB	protein data bank
PEG	polyethylene glycol
PMF	proton motive force
RBS	ribosome binding site
RNA	ribonucleic acid
rpm	revolutions per minute
rt	room temperature
SD	Shine-Dalgarno sequence
SDS-PAGE	sodium dodecylsulfate polyacrylamide gel electrophoresis
SEC	size exclusion chromatography
SRP	signal recognition particle
T3SS	type-III-secretion system
T4P	type-IV-pili
TBS	tris buffered saline
TCA	trichloroacetic acid
TRIS	Tris(hydroxymethyl)aminomethane
UV	ultraviolet

One and three letter codes as well as x for any amino acid residue is used without further reference. Due to the number of bacterial species named in this work, they are also not listed separately.

LIST OF FIGURES

LIST OF TABLES

1 INTRODUCTION

1.1 Bacterial motility

The ability to move towards favorable and avoid unfavorable conditions is key to the survival of many bacterial species. Requirement for this behavior are a chemosensory system that allows sensing of chemical gradients in the environment and a motility structure.

During the course of evolution, bacteria evolved different motility structures, of which some are still poorly understood [1]. These structures allow bacteria to swim through liquids, swarm across surfaces, attach to surfaces and use a combination of both to form multicellular colonies known as biofilms. Motility mechanisms include but are not limited to surface appendages (e.g. flagella, pili and *Mycoplasma* `legs`) and internal structures (cytoskeleton and gas vesicles)[1–5].

Among the motility mechanisms that rely on outer appendages, type-IV-pili (T4P) have long been suspected to mediate motility. Despite these assumptions, first evidence of T4P movement has not been reported until the beginning of this century [6]. Twitching motility is the most common form of T4P related movement and relies on extension and retraction of an outer pilin structure that results in a stepwise movement. The canonical T4P system is closely related to other systems in bacteria and archaea such as the type-II-secretion system (T2S), the Com system for DNA uptake and archaeal flagella [7,8].

In contrast to using outer appendages for movement, some bacteria are motile without the use of extracellular protein complexes. *Myxococcus* species can move on surfaces by focal adhesion complexes that involve the accumulation of cytosolic proteins and the secretion of extracellular matrix “slime”. The intracellular and periplasmic components move along a helical track within the cells and due to the focal adhesion, the cell body glides in one direction (**Figure1B**). In *Myxococcus*, this gliding process is also assisted by T4P, thereby resembling a chimeric type of movement (**Figure1C**) (D. B. Kearns, 2007; Mignot, 2007).

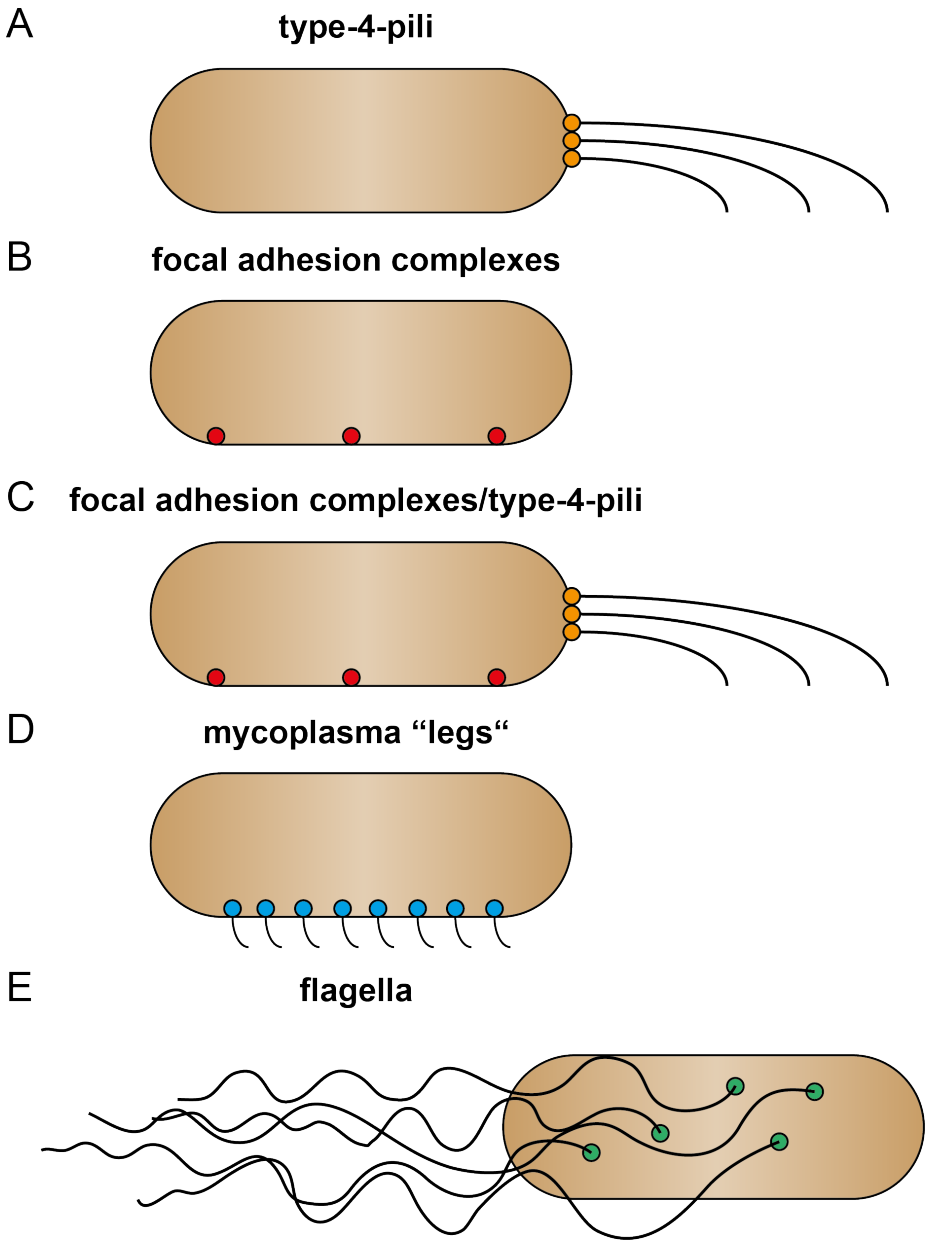

Figure 1: The diverse ways bacteria move. A. Twitching motility is mediated by extension and retraction of T4P**. B.** Focal adhesion complexes allow a surface movement termed gliding. **C.** Gliding can also be assisted by T4P. **D.** Mycoplasma species use a mechanism named “crawling” mediated by “legs” exposed on the cell surface. **E.** Swimming is the movement of individual cells empowered by rotating flagella.

Another mechanism of motility, again relying on outer appendages can be found in *Mycoplasma* species, which belong to the Gram-positive parasitic class of *Mollicutes*. Gliding locomotion is not comparable to any other motility mechanism and allows *Mycoplasma* to attach to sialylated oligosaccharides on the surface of eukaryotic cells. Outer protein complexes are anchored within the cell membrane and can be contracted to generate a propulsion force (**Figure 1D**) (Miyata & Hamaguchi, 2016).

However, bacterial motility has been most extensively studied in enterobacteria of the γ-proteobacterial class, e.g. *Escherichia coli*, *Salmonella typhimurium* and *Pseudomonas aeruginosa*. Due to their size of several micrometer, flagella were the first appendages discovered on the cell body and thus investigated extensively [2,12]. In the late 20th century, advances in electron microscopy facilitated a structural picture of the flagellar composition [13,14]. Nowadays, cryo-electron tomography provides an insight into even the smallest differences within the flagellar architecture of many bacterial species [15–17].

1.2 The bacterial flagellum

Despite the various mechanisms of locomotion which prokaryotes have developed, the overall structure of the bacterial flagellum is conserved and shows only slight differences between Gram-positive and –negative organisms (**Figure 2**). Flagellar architecture can be divided into: the membrane-embedded basal body housing a flagellar type III secretion system (fT3SS), the cytoplasmic C-ring, the motor/stator components, the rod and secondly, the extracellular hook, hook- associated proteins (HAP) and lastly, filament structures. A mature flagellum is made of approximately 30 proteins with different stoichiometries with the long filament extending the cell length by three- or four-fold [4,18,19].

Once assembled, a proton or sodium gradient serves as energy source for the torque generation via Mot/Pom proteins embedded within the cytoplasmic membrane [20,21]. This torque is transmitted to the helical filament, which rotates, thereby generating a propulsion force driving the bacterium forward in a “cork screw” manner. The flagellum can either turn “counterclockwise” (CCW) or “clockwise” (CW) which leads to running or tumbling, respectively, in *E.coli* and close relatives [22,23].

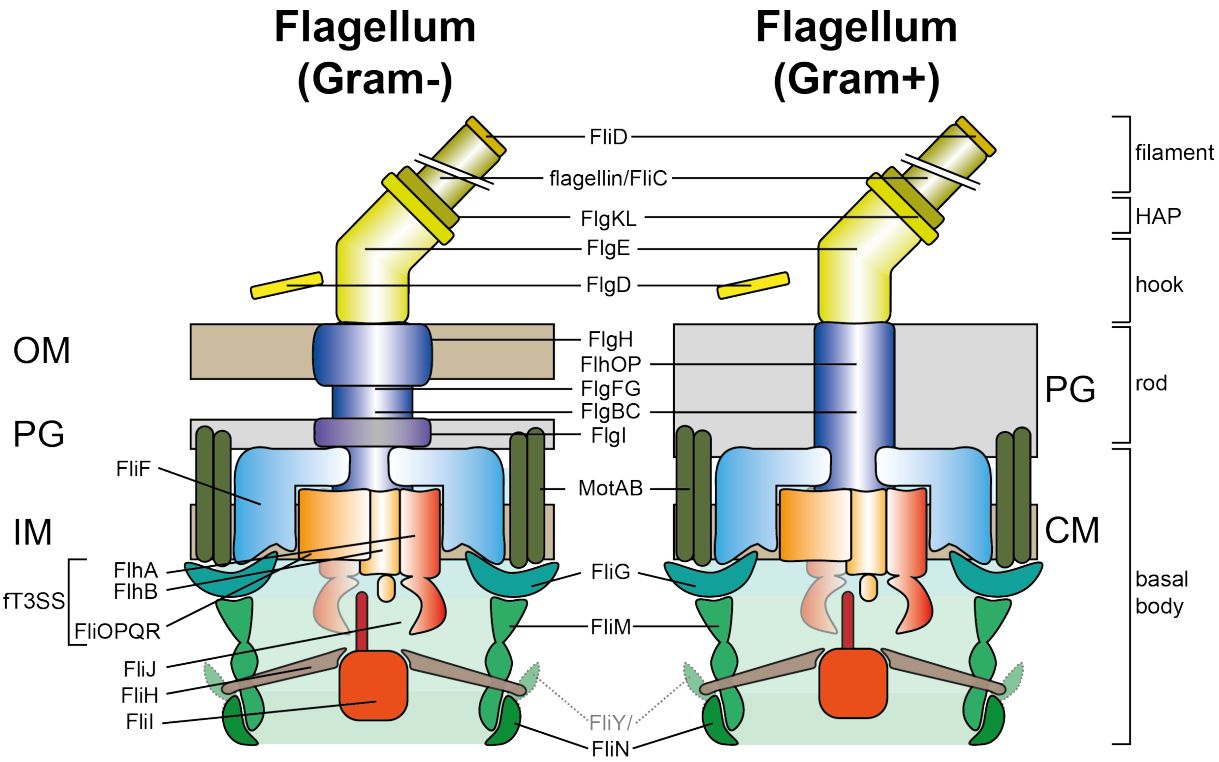

Figure 2: Architecture of the bacterial flagellum in Gram-negative and -positive prokaryotes. Schematic representation of the flagellar architecture that can be subdivided into: basal body, rod, hook, hook-associated proteins (HAP) and filament. Differences between Gram-negative and -positive bacteria are particularly found in the rod structure due to a different membrane composition. (OM: Outer membrane, PG: peptidoglycan, IM: Inner membrane, CM: cytoplasmic membrane)

1.2.1 Architecture of the bacterial flagellum

The basal body

The basal body is the fundament of the bacterial flagellum and houses all components of the motor, the flagellar type III secretion system (fT3SS) and subunits allowing a regulation of the flagellar motor by the chemosensory system.

The fT3SS is composed of the six integral membrane proteins FlhA, FlhB and FliOPQR [24,25](**Figure 2**). FlhA is the largest component of the fT3SS and consists of a transmembrane and a well-characterized cytosolic domain of 42 kDa (FlhA-C). It plays an important role in receiving and secreting building blocks that assemble into extracellular parts of the flagellum, i.e. hook-associated proteins (HAP) and the filament forming protein flagellin [26–29]. How many monomers of FlhA are residing in the basal body is still not entirely clear to date and speculations about the stoichiometry range from 5 to 20 molecules [30–32].

Another component of the fT3SS that has been extensively studied is FlhB possessing a transmembrane domain at its N-terminus and cytoplasmic domain at its C-terminus (FlhB-C).

Although the cytoplasmic domain of FlhB is much smaller than that of FlhA, it is very important for the specificity switching during flagellar assembly by an auto cleavage mechanism [33,34]. In *Salmonella typhimurium* FlhB undergoes autocatalytic cleavage between Asn269 and Pro270 within a highly conserved Asn-Pro-Thr-His sequence, which is essential to switch the substrate specificity from rod/hook to HAP and filament [35,36]. In addition to that, a protein termed FliK, interacts with FlhB-C and is involved in hook-length control as its deletion leads to formation of "polyhook" termed aberrations in the hook structure [37].

Not much is known about the remaining four components of the fT3SS, FliOPQR except that no larger cytosolic domains are predicted [38](**Figure 2**). Initial results showed that FliO is important for stability of FliP although certain suppressor mutants can overcome its loss for functional type 3 secretion [39,40].

In addition to the membrane-embedded components, the process of flagellar type III secretion (fT3S) is assisted by the soluble ATPase complex: FliI, FliH and FliJ. The FliI/FliJ complex is structurally reminiscent of the α3β3γ complex of F1-ATPase, where FliH is similar to the peripheral stalk of A/V-type ATPases [41]. Although structural information on all components is available and many studies have focused on the ATP hydrolysis, it is still not entirely clear whether and if so, how the energy is used in the process of fT3S. Instead, fT3S seems to rely on the proton motive force alone [42].

The whole secretion apparatus is embedded into the MS-ring composed solely of the protein FliF that serves as a core platform for different basal body constituents [30,43] (**Figure 2**). FliF is a membrane protein but possesses a cytoplasmic domain at its C-terminus necessary for the interaction with the flagellar C-ring protein FliG. Approximately 26 molecules of FliF are predicted to form the MS-ring [44]. FliF is closely connected to FliG, which also connects the motor/stator (e.g MotAB, MotXY, PomAB) to the C-ring [45–47]. The stator complex couples ion flux to exertion of force on the C-ring and shows a higher degree of diversity among different bacterial species [48]. Depending on the amount and composition of stator complex units and additional periplasmic proteins, the generated torque varies among the species and this allows productive operation of the flagellar motor within the different environmental niches [48].

The C-ring is further composed of the two proteins FliM and FliY (also named: FliN) forming a cup-like structure at the cytoplasmic face of the basal body (**Figure 2**). The C-ring has been studied extensively in the past and found to be central for transfer of chemotactic stimuli, rotational switching and force intake from the motor-complexes [49,50].

The rod

When turning from the cytoplasmic face to the outside of the cytoplasmic or inner membrane, an axial driveshaft (the rod) spans the peptidoglycan and connects the extracellular components to the basal body [51]. Due to the difference in membrane composition between Gram-positive and –negative bacteria, the rod composition has to match the respective requirements (**Figure 2**). The rod is anchored in the peptidoglycan and outer membrane via the P- and L-ring that act as bushings (**Figure 2**, FlgIH). The L-ring also penetrates the outer membrane and both, P- and L-ring are absent in Gram-positive organisms [52].

The hook

At the outside of the peptidoglycan layer or the outer membrane, the rod is connected to a universal joint that has been termed hook due to its intrinsic curvature (**Figure 2**). From a structural point of view, the hook is a hollow cylinder build up by a single protein termed FlgE in proto-filaments of 11 monomers [53]. The size of mature hooks ranges from 55 nm in *E. coli* to 71 nm in *B. subtilis,* which is also reflected by a high variability in amino acid residue composition and sequence length of FlgE [54].

Hook-associated proteins (HAP) and filament

At the distal face of the hook, hook-associated proteins (HAP) serve as connection between hook and filament. These building blocks that assemble extracellularly are sigma28 (σD or FliA) dependent and all have a respective chaperone that is necessary for secretion and to prevent premature polymerization in the cytoplasm [25,55,56]. The long filament is composed of one single protein (flagellin or FliC) in most organisms, which assembles in a helical pattern of more than 20000 monomers [57]. In *S. typhimurium* flagellin monomers form a protofilament of 11 molecules, which was assumed to represent a conserved fold [58]. However, studies in the ε-proteobacteria revealed the presence of protofilaments composed of only 7 flagellin molecules [59]. These findings show that the diversity in flagellar filaments might be higher than assumed so far. Some bacteria also have two or even more flagellin homologues, which can produce a mature filament but the reason for this redundancy has not been clarified to date [60]. In addition to the occurrence of several flagellin homologues, glycosylation of flagellin also plays an important role in some organisms [61].

1.2.2 Assembly of the bacterial flagellum

To build a flagellum, bacterial cells have to coordinate the assembly of soluble and membrane proteins in a strict spatiotemporal order. Determination of the prospective assembly site is achieved by the SRP-type GTPase FlhF in many bacterial species (reviewed in: [62]). Membrane-embedded components of the basal body are the first building blocks to be inserted into the cytoplasmic membrane. Among these transmembrane (TM) proteins, the MS-ring forming FliF and FlhA, part of the fT3SS, are suspected to be the first components in flagellar assembly [24,27,31,43,63] (**Figure 3A**). Although only little experimental evidence exists demonstrating how these membrane proteins are inserted, it is likely achieved by the signal recognition particle (SRP)-machinery via the SecYEG translocon and TM-protein foldases [64,65]. This is supported by studies in *E. coli* where deletion of *yidC* resulted in motility defects [66].

As mentioned earlier (see chapter 1.2.1.), the MS-ring is connected to the C-ring via FliG. Being proximal to the membrane, positioning of FliG seems to be a prerequisite for the remaining C-ring components to be assembled [67,68]. How FliM and FliY are assembled during flagellar biogenesis is unclear but the MinD-type ATPase FlhG is involved in this process by interaction with these two proteins [69] (**Figure 3B**). As mentioned in chapter 1.2.1. the C-ring is required for torque-generation and switches flagellar rotation in response to chemosensory stimuli [70]. Moreover, studies suggested that the ATPase complex interacts with FliM and FliY via FliH [71,72]. This interaction might be important in two respects: Firstly, to anchor the ATPase complex in close vicinity of the fT3SS, and secondly, to change secretion specificity of the fT3SS [73–75] (**Figure 3C**).

Once the basal body components including C-ring and fT3SS are assembled, secretion of rod components that also anchor the basal body within the peptidoglycan, can take place. Whether the rod proteins are subject to fT3S or secreted into the peptidoglycan via a different pathway (e.g. SecYEG-translocon) has not been clarified yet (**Figure 3D**). However, in the closely related type-III-secretion system of the injectisome (iT3SS) (reviewed in: Diepold & Armitage, 2015; Erhardt, Namba, & Hughes, 2010), the inner rod is secreted by the iT3SS and also serves as a plug and a specificity switch, only allowing secretion of the needle protein when desired [78–80]. Interestingly, the iT3SS is also capable of secreting flagellar components, which confirms the evolutionary conservation of the two systems [81].

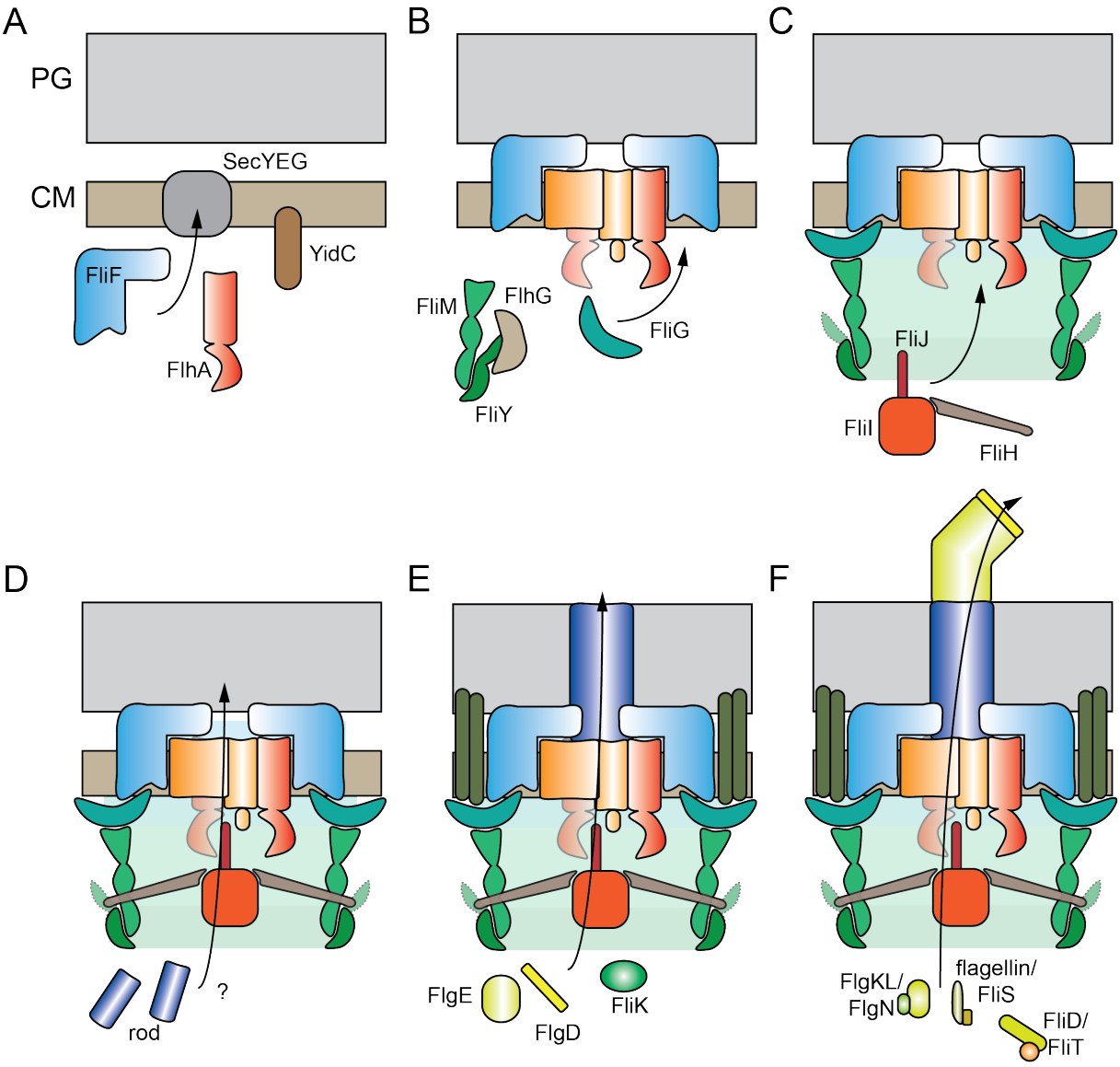

Figure 3: Assembly of the bacterial flagellum. A. Biogenesis starts with insertion of membrane proteins. **B.** FlhG is required for proper C-ring assembly. **C.** The ATPase complex is required for proper fT3S and linked to the C-ring. **D.** Assembly of rod and mot proteins. **E.** FlgE subunits are incorporated via the hook-cap FlgD. **F.** Building blocks of HAP and filament are secreted via the fT3SS. The figure originates from [18] but has been modified. PG: Peptidoglycan, CM: cytoplasmic membrane.

Moreover, the study demonstrates that the hook protein FlgE and its cognate cap FlgD are both secreted by the iT3SS [81]. During flagellar biogenesis, assembly of the hook represents a tightly controlled checkpoint. Briefly, hook-length control is regulated by a "molecular ruler" termed FliK and the fT3S protein FlhB [82–85]. The cytoplasmic domain of FlhB (FlhB-C) exhibits an auto-cleavage activity that is involved in the transition from proximal (rod, hook) to distal components (HAP, filament) [86] (**Figure 3E**).

The last stage in flagellar biogenesis is the assembly of HAP and filament structures, composed of the "late" building blocks FlgL/K, FliD and flagellin. As mentioned earlier, late stage proteins are all secreted by the fT3SS, a process that requires the support of chaperone

proteins to guide their clients to the export gate and prevent premature polymerization in the cytoplasm (i.e. FliS for flagellin, FliT for FliD and FlgN for FlgLK, **Figure 3F**) [27,29,87]. The incorporation of flagellin monomers into the growing filament is further assisted by the cap protein FliD [88,89]. Moreover, due to the high amount of flagellin that needs to be secreted by the fT3SS and its intrinsic property to polymerize, the production of flagellin is tightly controlled not only by its chaperone FliS but also on the post-transcriptional level by the CsrA/FliW regulon [55,90,91].

1.3 Transcriptional regulation of flagellar assembly

In order to control the complex process of flagellar assembly, a sophisticated regulation on the transcriptional, post-transcriptional as well as translational level is absolutely essential (reviewed in: [92,93]. In the Gram-positive bacterium *B. subtilis* most of the genes encoding the integral parts of the basal body are encoded on the *fla/che* operon with a remarkable size of 27 kb [94](**Figure 4**). The first three quarters of the *fla/che* operon encode components of C-ring, MS-ring, rod, fT3SS and hook. Key regulatory factors *flhF* and *flhG* and elements of the chemotaxis apparatus are located within the downstream quarter of the operon. The last genes in the operon encode the alternate sigma factor σD and SwrB (**Figure 4**).

Another level of complexity in *B. subtilis* however, is the σD dependent expression of late flagellar genes that are organized in a second operon (**Figure 4**). The separation of both operons allows a bifurcation of populations during the exponential growth. Individuals are either joined in sessile chains or grow as single but motile cells, a behavior that is advantageous to colonize both the current location and more distant favorable environmental niches [93,95].

This phenotypic heterogeneity is under control of σD in *B. subtilis* [96,97]. Deletion of *σD* results in long non-motile cells that are not able to separate from each other to form single, motile individuals. Interestingly, most laboratory strains are biased towards the OFF-state of σD, which is the result of a frameshift mutation in the *swrA* gene. The product of this gene, SwrA, shifts the population towards either of the two states (σD ON or OFF) by a transcriptional activation of the *fla/che* operon. This regulation can also be observed in the swarming motility of *B. subtilis* when an increased expression of *swrA* results in the enhanced production of flagella [98,99].

The complexity of SwrA and σD interplay is further unveiled by a closer look on the transcriptional regulation of the *fla/che* operon. σD-dependent gene expression is modulated

over a narrow threshold that leads to a high abundance of σD in motile and low levels in sessile cells [94].

Gene positioning within an operon can have drastic effects on the gene expression as transcript abundance has been shown to decrease along the *fla/che* operon [94,100]. The gene encoding σD is located at the downstream end of the *fla/che* operon, which might be crucial for its expression (**Figure 4**). The gradual decrease of *fla/che* operon transcript however, is again controlled by a different factor, the small peptide SlrA. SlrA inhibits *fla/che* operon transcript through the DNA binding proteins SinR and SlrR [101,102].

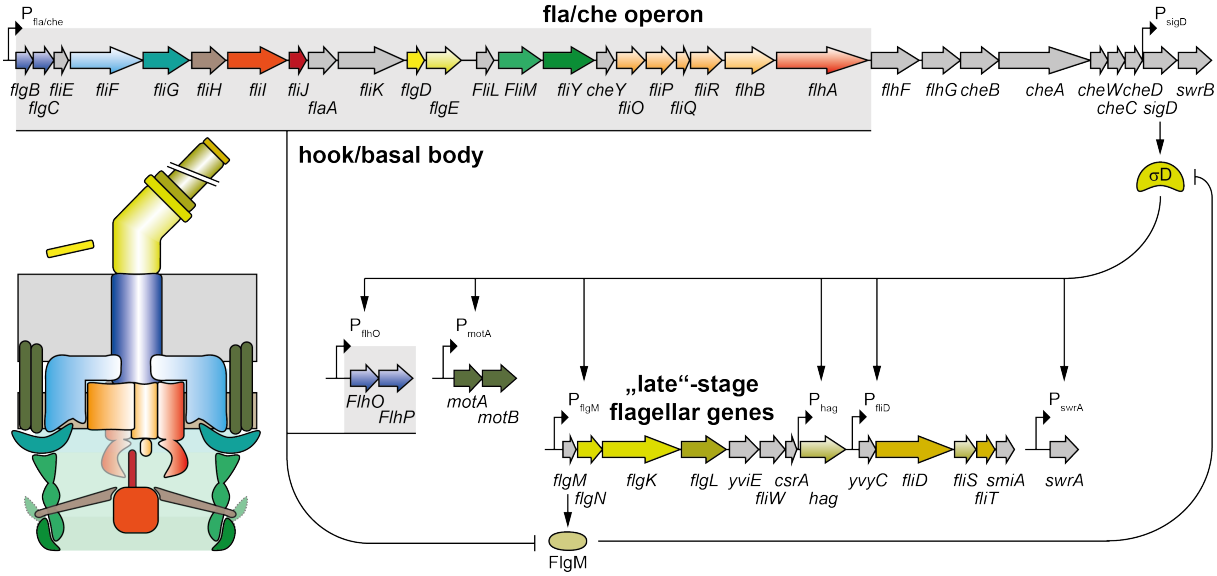

Figure 4: **Transcriptional regulation of flagellar assembly in *B. subtilis*.** The 27 kB *fla/che* operon encodes most of the structural components of the basal body (grey highlight), regulatory proteins and constituents of the chemotaxis apparatus. The alternate sigma factor σD regulates the late flagellar genes and outsourced genes e.g. *flhOP* and *motAB*. It is antagonized by FlgM, which is exported upon the completion of the hook-basal complex (and therefore inhibited). Genes are colored according to their respective position within the flagellum (bottom left).

Another regulatory element, controlling σD activity, is the anti-sigma factor FlgM. Once FlgM is expressed, it binds to σD and prevents association of the latter with the RNA-Polymerase (RNAP). FlgM resembles the α-helical bundle shape that has been reported for other secretion chaperones (e.g. FliS, FliT and FlgN) and wraps around σD [55,103,104]. Although FlgM is encoded on the σD-dependent operon containing late flagellar genes a sophisticated mechanism including DegU and DegS allows prioritization of *flgM* expression over the other genes encoded in this operon [105] (**Figure 4**). Once the hook-basal body complex is completed, FlgM is exported via the fT3SS, thereby liberating σD to start expression of the late flagellar genes [106,107].

1.4 Post-transcriptional regulation

Most of the mechanisms discovered that control the flagellar assembly process act on the transcriptional level, which might be a consequence of techniques used to investigate these findings. However, during flagella biogenesis, transcriptional regulation is only one part and complemented by post-transcriptional and translational control mechanisms.

The ability of ribosomes to access mRNAs at the ribosome-binding site (RBS) is crucial for translation and presents an important element of translational control during bacterial gene expression. The Shine-Dalgarno sequence (SD) is part of the RBS and marks the starting point of translation, as it allows base-pair interaction of the mRNA with the 3'-end of the 16S ribosomal RNA [108,109] (rRNA). Translation is inhibited if an RBS is occluded either by base-paring RNAs or by regulatory proteins. These mechanisms therefore represent a strong regulatory tool to control translation on the post-transcriptional level.

1.4.1 Post-transcriptional regulation by CsrA/RsmA/RsmE proteins

Carbon **s**torage **r**egulator **A** (CsrA) or **r**epressor of **s**econdary **m**etabolite **A** protein (RsmA) has been discovered in the 1990s and represents one of the first examples of post-transcriptional regulation in bacteria [110,111]. A transposon mutagenesis screen originally designed to identify regulators of gene expression during stationary phase revealed that mutating *csrA* had pleiotropic effects on carbon flux pathways but also influenced cell morphology and adhesion [112,113]. The discovery of CsrA was later expanded by studies in the plant-pathogen *Erwinia spp.* showing a broad influence of RsmA on the secretion of secondary metabolites and thus pathogenicity [114]. This research paved the way for extensive research in various pathogenic enterobacteria including *Escherichia coli*, *Pseudomonas spp*., *Legionella pneumophila*, and *Vibrio cholera*.

The structure of CsrA proteins represents a unique fold among all known protein structures determined so far. Structural investigations on several homologues have revealed a homodimer containing five β-strands, followed by a short α-helix and an unstructured C-terminus (**Figure 5B,** [115–118]). The β-strands form an interlaced β-sheet in which β1 of one molecule is part of the opposing β-sheet and vice versa. A compact hydrophobic core stabilizes the two intertwined molecules of CsrA.

The primary interaction interface of CsrA proteins and RNA has been identified by alanine scanning in *E. coli* and includes two motifs at CsrA (**Figure 5,** region 1 and 2, [119]).

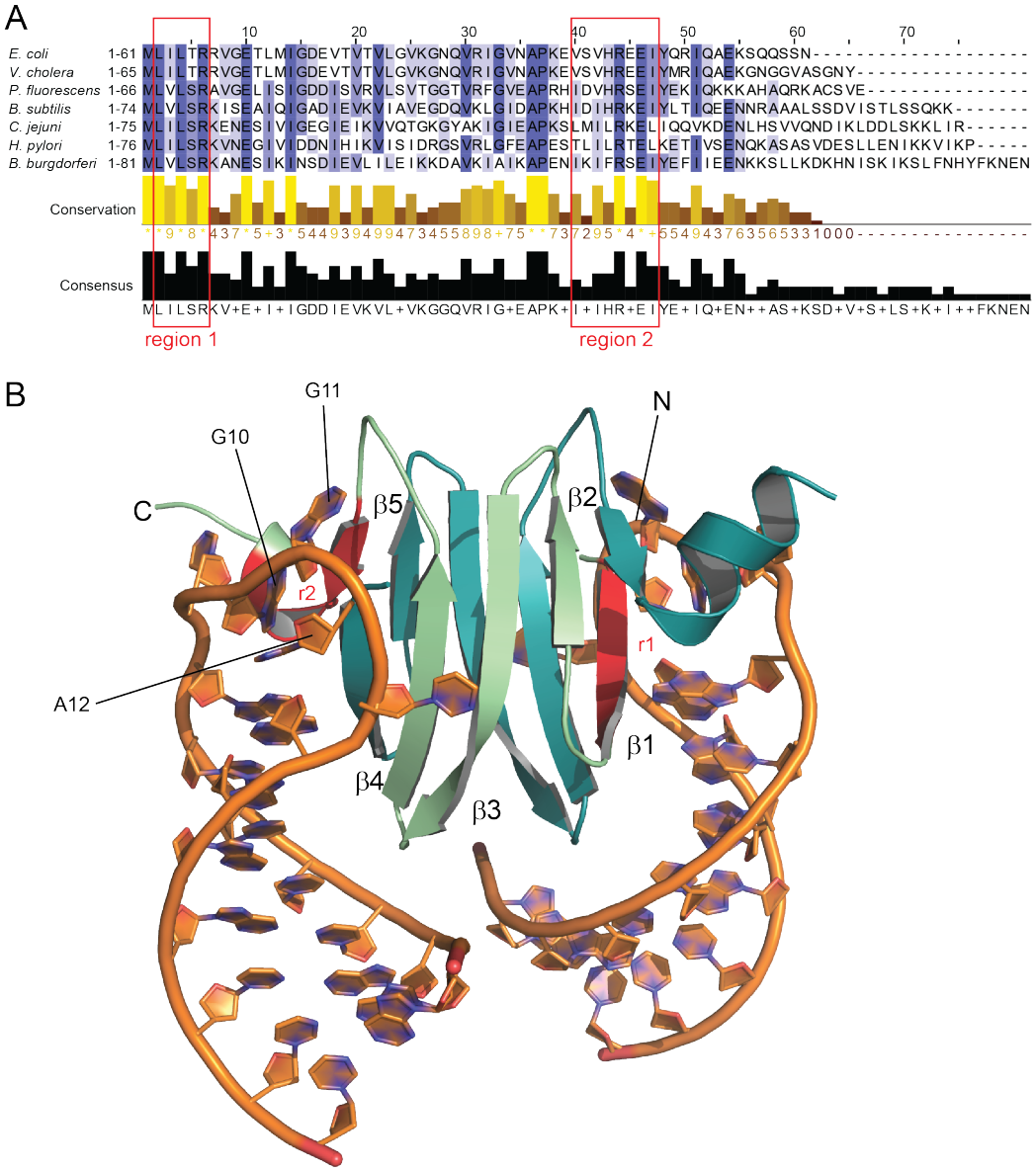

Figure 5: Structure of CsrA/RsmA/RsmE proteins and the RsmE/hcnA RNA complex. A. Sequence alignment from the γ-proteobacteria and species containing a *fliW* homologue in close proximity to the *csrA* gene. The red boxes indicate conserved motifs important for RNA binding. Values next to the species names refer to the amino acids length of the proteins. **B.** Structure of the RsmE/hcnA complex in carton representation (PDB-identifier: 2JPP, [117]. The critical motifs from A are highlighted in red and bases resembling the GGA sequence are indicated by G10, G11 and A12. "N" and "C" represent N- and C-terminus, respectively. Figure based on [111].

CsrA homodimers contain two RNA binding sites that establish contacts with an $A_{/U}$CANGGANGU$_{/A}$ sequence motif present in 5'-leader sequence of many transcripts [117,120]. When bound by CsrA, the ANGGAN core folds into a loop stabilized by a three base-pair stem of the flanking nucleotides (**Figure 5B**, G10, G11, A12). As CsrA always occurs as a stable homodimer with two RNA binding sites, it was assumed that it might also be able to bridge two GGA motifs present on a single RNA. Indeed, CsrA can bind to two

target sites on a transcript, which are separated by 10 to 63 nucleotides [121]. Although the spacing optimal for stability of the CsrA/RNA interaction was shown to be 18 nucleotides, different binding geometries might have consequences for regulatory effects.

The binding to two binding sites has further been demonstrated to occur in a sequential manner and is not restricted to 5'-leader transcripts but also to the regulatory sponge RNAs as CsrB and CsrC that antagonize CsrA activity [122]. The sRNAs act by a mechanism of molecular mimicry as 'protein sponges', which contain multiple binding sites permitting sequestration, storage and release of CsrA [122,125,126]. These small, non-coding RNAs (sRNAs; e.g., CsrB/C or RsmX/Y/Z) antagonize CsrA binding to mRNA in a competitive manner [122–124]. sRNAs such as CsrB/C act as broad-range antagonists of CsrA and in addition to binding CsrA with high specificity, they affect a variety of different processes. The levels of sRNAs CsrB/C are regulated partially by a conserved bacterial two-component system (BarA-UvrY in *E. coli* [127]) but are also subject to stringent response components as (p)pGpp, DksA [128] and DeaD-box helicases (DeaD and SrmB) [129] .

Taken together the interplay between CsrA homologues, 5'-leader transcripts containing conserved binding motifs and sponge RNAs affects a variety of cellular processes that include the central carbon metabolism, secondary metabolite metabolism, motility, biofilm formation and the expression of virulence factors in pathogenic bacteria (summarized in: [111,130,131]).

1.4.2 CsrA and FliW homeostatically control flagellin production

In contrast to the variety of processes controlled by CsrA proteins in enterobacteria, species containing a copy of the *fliW* gene in their genome show a more specific type of regulation that seems to be dedicated to flagellar regulation [132,133].

The release of σD activates the transcription of late flagellar genes encoding the building blocks of hook-associated proteins (HAP), filament and filament-cap [106,107,134,135]. The secretion process of late stage building blocks is not only regulated on the transcriptional level but requires chaperones that are also encoded in the same operon (**Figure 4**).

These specific chaperones prevent futile self-assembly of their cognate building blocks in the cytoplasm (i.e. FliS for Flagellin; FliT for FliD and FlgN for FlgLK) [56,104,136]. However, a folding activity comparable to the classical Heat Shock Protein (Hsp)–type chaperones has never been documented. These chaperones keep their clients in the monomeric state and to prevent futile oligomerization or aggregation. In contrast, the flagellar factors are only limited

to a holding chaperone function. Besides this crucial role, these chaperones guide their respective clients to FlhA-C [27,87]. They might therefore also be viewed as 'targeting factors'. The different substrate/chaperone-complexes have decreasing affinities for FlhA-C according to their order of secretion [29]. Another important value is the amount of secreted building blocks. An estimation of the incorporated amount of HAP proteins showed roughly 11-12 monomers of FlgK and FlgL [44]. The cap protein FliD is assumed to be pentameric [88]. On the other hand, about 20.000 to 25.000 molecules of flagellin are incorporated in a single filament [137]. It is therefore unlikely that these great differences are simply controlled by different affinities towards the export gate.

Research in *C. jejuni*, *B. subtilis* and *B. burgdorferi* has unraveled another level of complexity involved in the regulation of the most abundant flagellar protein flagellin. Many flagellated bacteria possess the conserved CsrA/FliW regulon that homeostatically restricts production of flagellin [110,132,138,139].

CsrA inhibits translation of flagellin by binding to two sites that are present within the 5'-UTR of the *hag* mRNA. One of the binding sites is the Shine-Dalgarno sequence (SD) located within the ribosomal binding site (RBS). Binding of CsrA promotes the formation of a stem-loop, thereby interfering with ribosomal binding and translation initiation [139]. CsrA is sequestered by the flagellar assembly factor FliW, which renders the SD free and allows translation of flagellin.

Upon translation of flagellin, both FliW and its cognate chaperone FliS bind to the emerging amino acid chain. Whether this process is co-translationally or requires mature flagellin, has not been shown yet. Subsequently, CsrA can occlude the SD again and flagellin/FliS is recognized by FlhA-C to be exported [91,132,133]. This cycle is thought to enable homeostasis of cytoplasmic flagellin concentrations over a low and narrow threshold [133]. Additional experiments demonstrated that the flagellin mRNA is not the only target of CsrA, but rather the most abundant in a pool of several motility-related mRNAs that fall under CsrA regulation [132].

Taken together the CsrA/FliW complex represents a conserved regulatory module and might be involved in the control of more processes than anticipated so far.

2 AIM OF THE THESIS

The flagellum represents one of the most sophisticated nanomachines in the biosphere and its biogenesis is a costly process for the cell due to a high structural and regulatory complexity and the fact that many bacteria possess more than one flagellum. More than 30 different proteins assemble within the membrane and peptidoglycan, thereby providing a scaffold and basis for the assembly of outer membrane parts and cytosolic components. A flagellar type-3-secretion (fT3SS) system similar to that of injectisomes (iT3SS) of pathogenic bacteria translocates proteins from the cytosol through the membrane with high efficiency and in large amounts.

Due to functional and structural information obtained in previous work, understanding the process of flagellar type-III-secretion (fT3S) has recently expanded. The crystal structure of the cytoplasmic face of the fT3SS, FlhA allowed a deeper insight into the recognition of substrate/chaperone complexes by the fT3SS. However, how the production of substrates was regulated and whether production and secretion were coupled, could not be fully elucidated.

Therefore, I aimed at determining the crystal structure of the most abundant flagellar protein flagellin in complex with its cognate chaperone FliS. Furthermore, I wanted to gain a mechanistic insight into the post-transcriptional regulation of flagellin by the CsrA/FliW complex. A combined approach of X-ray crystallography, biochemistry and *in vivo* studies should facilitate a thorough explanation of the mechanism of flagellin homeostasis.

In addition to that, I set out to find further interaction partners of the above-named proteins to integrate them into the molecular framework of flagellar assembly.

3 RESULTS

3.1 The CsrA/FliW regulon

3.1.1 CsrA and FliW are conserved among bacterial species

CsrA proteins have been extensively studied in a narrow range of closely related γ-proteobacteria where they are involved in a variety of cellular processes. As all these enteric organisms lack a FliW homologue, the question had to be addressed whether the majority of bacteria possess both, FliW and CsrA or not. In close collaboration with Prof. Dr. Rensing at the Philipps-University Marburg, the NCBI BLAST (http://blast.ncbi.nlm.nih.gov/Blast.cgi) algorithm was employed to collect sequences of CsrA, flagellin and FliW from a variety of different organisms. Per phylum, three representative species were randomly selected and homologous hits acquired by twilight zone filtering according to Rost, 1999.

The species were classified according to the occurrence of flagellin, CsrA and FliW. The existence of flagellin was considered as a criterion for flagellar motility and all species lacking flagellin were therefore considered as "non-motile". In total, five phylae were classified accordingly: the Chlamydiae, Cyanobacteria, Chlorobi, Deinoccocus-Thermus and Fusobacteria (**Figure 6**, red, empty circle). One exception are the Aquificae that possess flagellin but lack both CsrA and FliW. Interestingly, CsrA seems to be present even in the absence of flagellin in some species (**Figure 6**, red).

Phyla marked in yellow contain species that have either CsrA alone or together with FliW. Some representatives from the Planctomycetes and α- and β-proteobacteria were found that possessed CsrA and FliW together but some also lacked FliW (**Figure 6**, yellow). To further understand which species are exceptions, sequences of more species have to be collected. The majority of bacterial phyla are marked in green, which represents the co-occurrence of CsrA and FliW (**Figure 6**, green).

In addition to these findings, a closer look at the amino acid sequence of CsrA revealed that homologues from the γ-proteobacteria, lacking a FliW, also possess a shorter variant of CsrA (**Figure 6**, CsrA-C). This meant in reverse that species containing a FliW also had longer CsrA proteins. The extension indicated a possible interaction interface of FliW at CsrA that was further investigated in the course of this study.

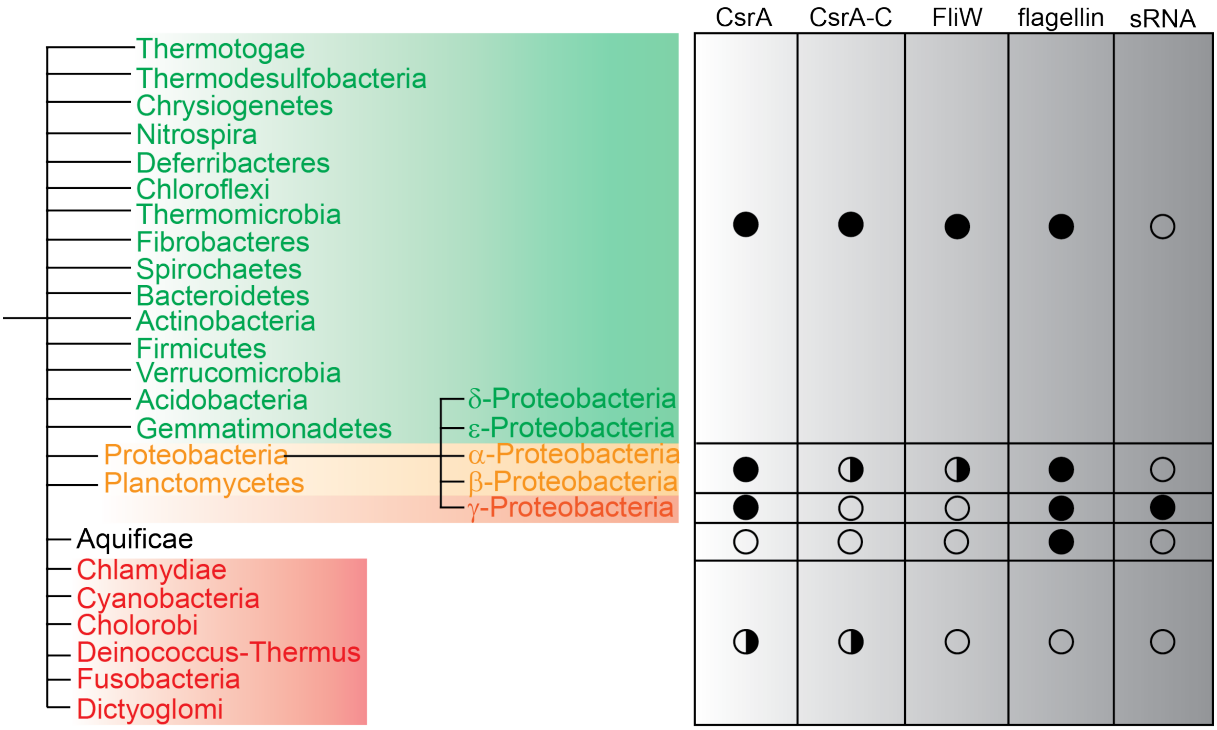

Figure 6: Schematic summary of the phylogenetic analysis of CsrA and FliW. Schematic summary of the phylogenetic analysis of CsrA and FliW. Flagellated species containing FliW and CsrA are shown in green, a full circle marks the general presence of the genes in the respective clades. The flagellin protein serves as a marker for flagella-mediated motility. Some members of the Proteobacteria and Planctomycetes contain FliW, while some lack FliW (yellow), which is also indicated by the split circle (right). sRNAs have only been experimentally confirmed within the class of γ-proteobacteria. The Aquificae only contain flagellin, but lack FliW and CsrA. Species at the bottom (red, half circle) lack all the proteins with the exception of Chlamydiae and Cyanobacteria, in which some species possess a CsrA. The figure originates from [90].

3.1.2 Purification of FliW from *B. subtilis* and *G. thermodenitrificans*

The FliW protein shares no homology on the primary sequence level with any other proteins and its gene is often found in a transcriptional unit together with *csrA*. To better understand the role of FliW, the gene encoding FliW from *B. subtilis* (*Bs*FliW) was cloned to pET24d and expressed in *E. coli* BL21(DE3) (see section 6.6.1). After cell disruption, the protein was enriched via Ni-NTA-chromatography (data not shown) and purified further by size-exclusion chromatography (SEC) using a HiLoad 16/600 Superdex 75 column. The collected fractions (**Figure 7A**, 3) were pooled and the protein was concentrated to a final concentration of 80 mg/ml to further use it to set up crystallization experiments.

No crystals appeared within a time span of several weeks, even when varying concentrations of *Bs*FliW were used (20 and 40 mg/ml). Therefore, the gene encoding the FliW homologue from *Geobacillus thermodenitrificans* (*Gt*) was cloned into pET24d and expressed in *E. coli* BL21(DE3) as described in section 6.6.1. The FliW homologues of *B. subtilis* and *G.*

thermodenitrificans share a high sequence identity on the amino acid level and should be therefore also structurally conserved.

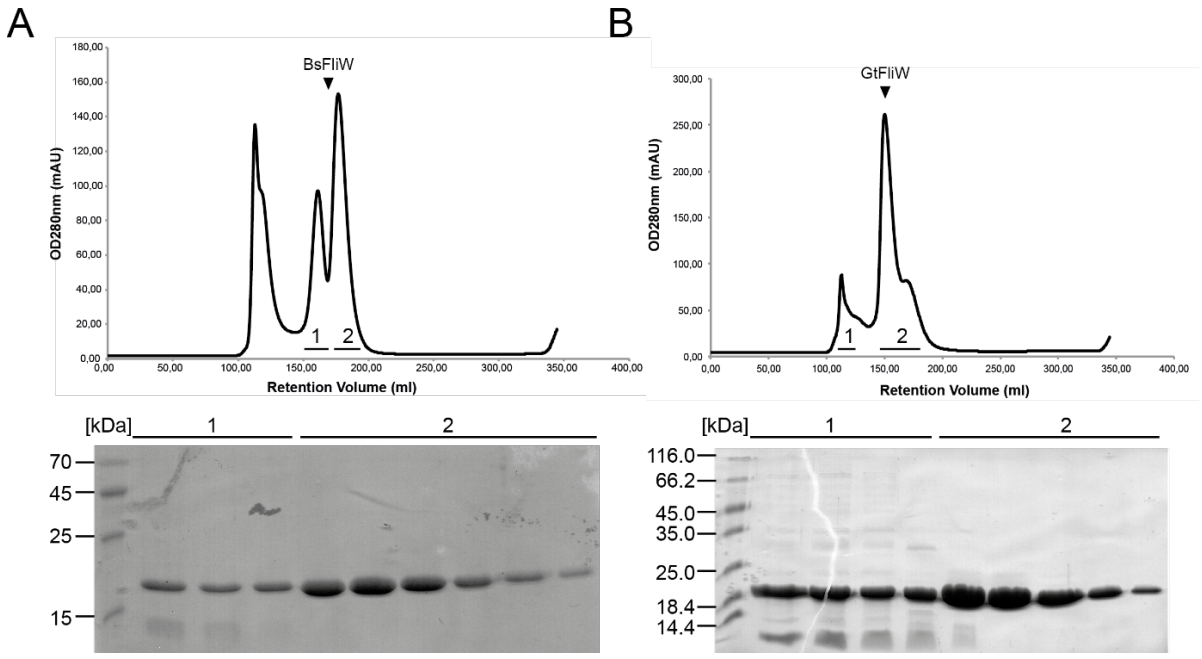

Figure 7: Purification of *Bs*FliW (A) and *Gt*FliW (B). Chromatograms from size exclusion chromatography (SEC) and the respective coomassie-stained SDS-PAGEs are shown. The molecular weight of the marker is given in kDa.

Cells were disrupted and the protein purified by Ni-NTA-chromatography and SEC using a HiLoad 16/600 Superdex 75 column. *Gt*FliW was enriched by concentration of the pooled fractions collected from the main peak (**Figure 7B**, 2) and concentrated to 40 mg/ml.

3.1.3 Crystallization of *Gt*FliW

For the crystallization of *Gt*FliW, 40 mg/ml and 20 mg/ml of protein were used in a sitting-drop experiment. 500 nl of protein was mixed with the same amount of precipitant solution. *Gt*FliW crystallized in several conditions within one week of incubation at room temperature. Two crystallization conditions with crystals suitable for X-ray diffraction experiments were observed: 0.1 M MES pH 6.0, 40 % (v/v) PEG 400, 5 % (w/v) PEG 3000 (**Figure 8A**) and 0.2 M sodium acetate, 0.1 M sodium cacolydate pH 6.5, 30 % (w/v) PEG 8000 (**Figure 8B**).

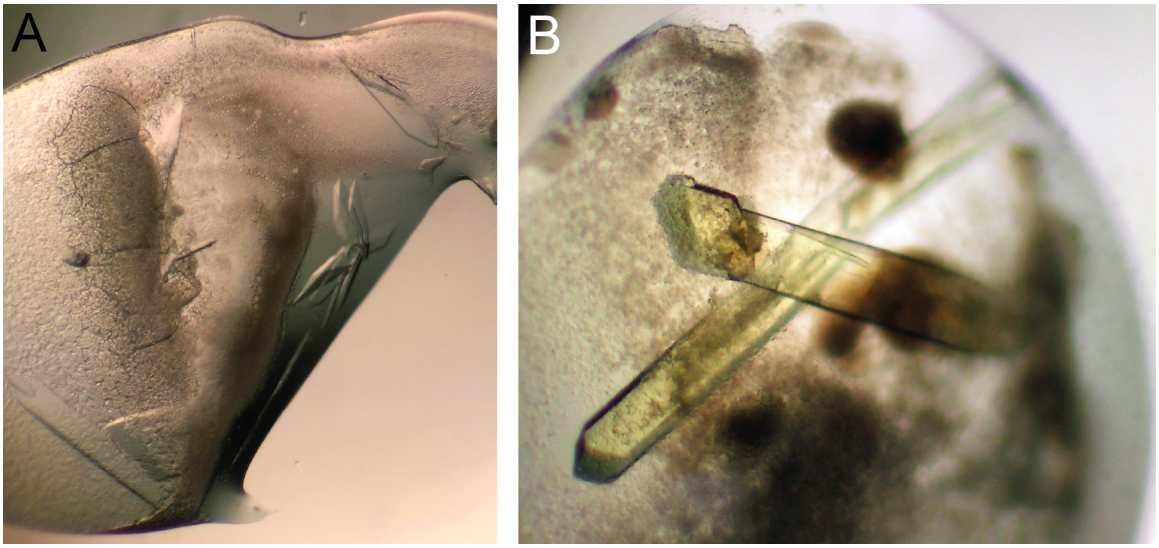

Figure 8: *Gt*FliW crystals observed **in two crystallization conditions.** Two representative crystal forms are shown that were used for X-ray diffraction experiments. **A.** 0.1 M MES pH 6.0, 40 % (v/v) PEG 400, 5 % (w/v) PEG 3000 **B.** 0.2 M sodium acetate, 0.1 M sodium cacolydate pH 6.5, 30 % (w/v) PEG 8000

From both conditions, several crystals were picked with nylon loops and shortly incubated in precipitant buffer with 20 % glycerol prior to flash freezing in liquid nitrogen.

3.1.4 Structure determination of *Gt*FliW

The data were collected at the European Synchrotron Radiation Facility (ESRF; Grenoble, France) at the beamline ID23-1 under cryogenic conditions (**Table 1**).

The data were processed, integrated and scaled with XDS and merged with the program AIMLESS from the ccp4 suite (see chapter 6.8). For phase determination, molecular replacement (MR) was performed using the structure of a putative contractile protein (PDB-identifier: 2AJ7). The two crystal forms resulted in two different crystal lattices, which were determined as spacegroup $P2_1$ and $P22_12_1$, respectively (**Table 1**). The two structures were refined to an R_{work}/R_{free} of 20.4/23.6 and 22.4/24.0, respectively and deposited in the protein data bank (PDB) within the entries 5DMD and 5JAK.

Table 1: Data collection and refinement statistics of the *Gt*FliW structures. Values in parenthesis refer to the highest resolution shell. For Rfree calculation, 5 % of the total reflections from the working set were used.

		***Gt*FliW (A)**	***Gt*FliW (B)**
Data collection			
	Space group	$P2_1$	$P22_12_1$
	Cell dimensions		
	a, *b*, *c* (Å)	47.54	31.24
		42.52	77.99
		71.92	87.05
	α, β, γ (°)	90.00	90.00
		102.66	90.00
		90.00	90.00
	Energy (keV)		
	Resolution (Å)	46.38 - 1.45	43.52 – 1.80
		(1.53 – 1.45)	(1.95 – 1.80)
	R_{merge}	0.056 (0.555)	0.052 (0.51)
	$I / \sigma I$	9.5 (1.9)	18.7 (3.5)
	Completeness (%)	99.4 (96.6)	100.0 (99.8)
	Redundancy	3.3 (3.1)	7.2 (7.5)
Refinement			
	Resolution (Å)	46.38 – 1.45	43.52 – 1.80
	No. reflections	49625	20382
	$R_{work/}$ R_{free}	20.4	22.4
		23.6	24.0
	No. atoms	2658	1226
	Protein	2355	1131
	Ligand	0	0
	Water	303	95
	R.m.s deviations		
	Bond len*Gt*hs (Å)	0.01	0.01
	Bond angles (°)	1.1	1.4
	Ramachandran (%)		
	Preferred	97.49	98.00
	Allowed	1.43	2.00
	Outliers	1.08	0.00

3.1.5 Crystal structure of FliW from *G. thermodenitrificans*

FliW shows no homology to any known proteins on the amino acid sequence level. Determination of the crystal structure should therefore reveal whether the fold reminds of any conserved domain motive. However, search for FliW-related structures employing the DALI server [141] did not result in obvious domain similarities. The only proteins exhibiting a fold reminiscent of a small β-barrel are found in the family of oligonucleotide/oligosaccharide (OB) binding proteins, albeit with large root mean square deviations (r.m.s.d.) over all C-α atoms when superposed to FliW (data not shown).

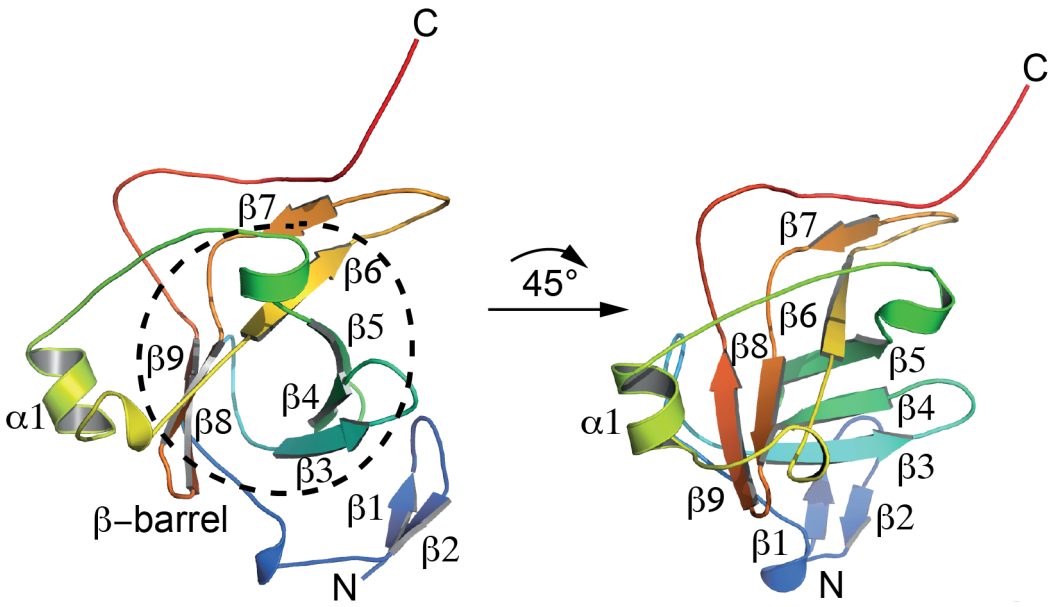

Figure 9: Crystal structure of *Gt*FliW. Cartoon representation of FliW rainbow coloured from N- to C-terminus. The dotted line marks the β-barrel formed by six β-strands. "N" and "C" indicate the N- and C-termini, respectively.

FliW exhibits a minimalistic β-barrel-like fold consisting of six β-strands (**Figure 9**). The strands β3 to 5 form one half, while strands β6, 8 and 9 and close the barrel-structure. A short α-helical segment of 1.5 turns and several loops, as well as three short β-strands (β1, β2, β7) extend from the central barrel to the outside of the molecule. A closer look on the surface of FliW employing the surface electrostatics representation in Pymol revealed several extended grooves that could represent interaction sites (**Figure 10**).

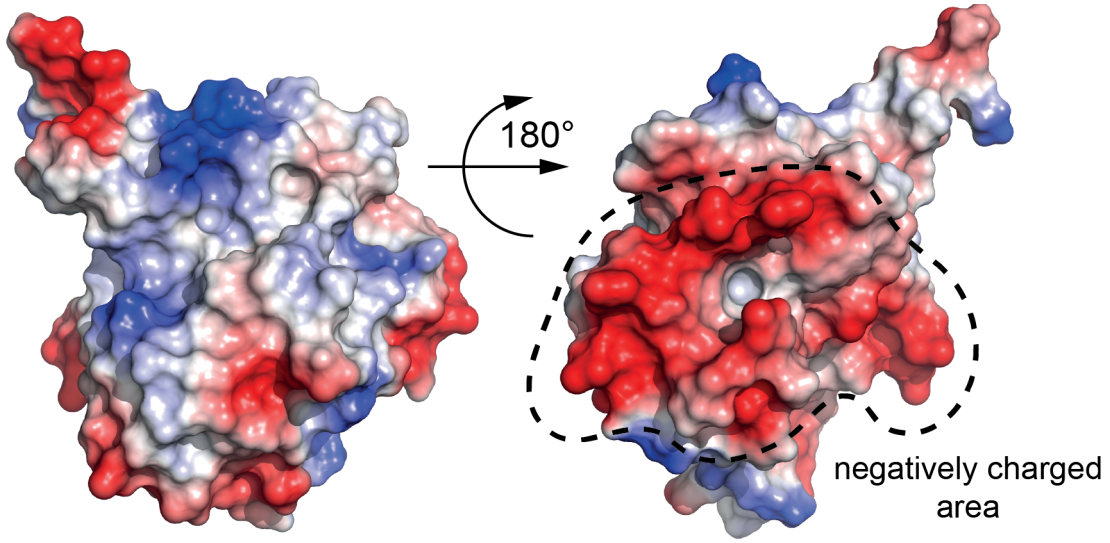

Figure 10: Crystal structure of FliW. Electrostatic surface representation of FliW reveals a negatively charged area on one site of the molecule (dotted line). Surface charges are colour-coded from positive (blue) over neutral (white) to negative (red).

Furthermore, one side of FliW showed a high density of negative charges that might play a role in electrostatic repulsion of negatively charged molecules (e.g., RNA).

3.1.6 Structural conservation of FliW in different crystal forms

*Gt*FliW crystallized in two different crystal forms (see above). The asymmetric unit of the $P22_12_1$ cell contained one FliW molecule, whereas in $P2_1$ two molecules could be placed (**Figure 11**). Despite these differences, no crystal contacts could be identified explaining the differences in crystal packing.

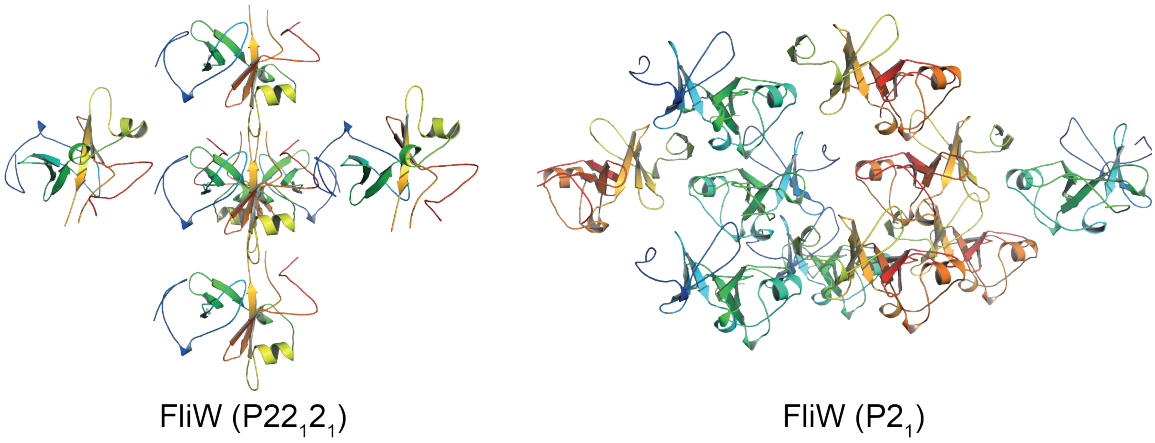

Figure 11: Different crystal packings of *Gt*FliW. The two space groups show that *Gt*FliW can arrange in different lattices. Molecules are displayed as cartoon representation and coloured in rainbow colours from N- to C-terminus. The figure originates from [90].

The two structures were superimposed to identify regions with structural differences or rearrangements (**Figure 12**). A total root mean square deviation (r.m.s.d.) over all C-α atoms of 0.766 revealed no significant differences.

To calculate this value, the Pymol-implemented align algorithm (www.pymol.org) was applied including all residues of the two crystal forms. This algorithm combines a sequence alignment with a structural superimposition thereby calculating a measure of the average distance between the C-α backbone atoms.

Apart from a small loop in close proximity to β6 that became ordered in the $P2_1$ space group, no major differences were observed.

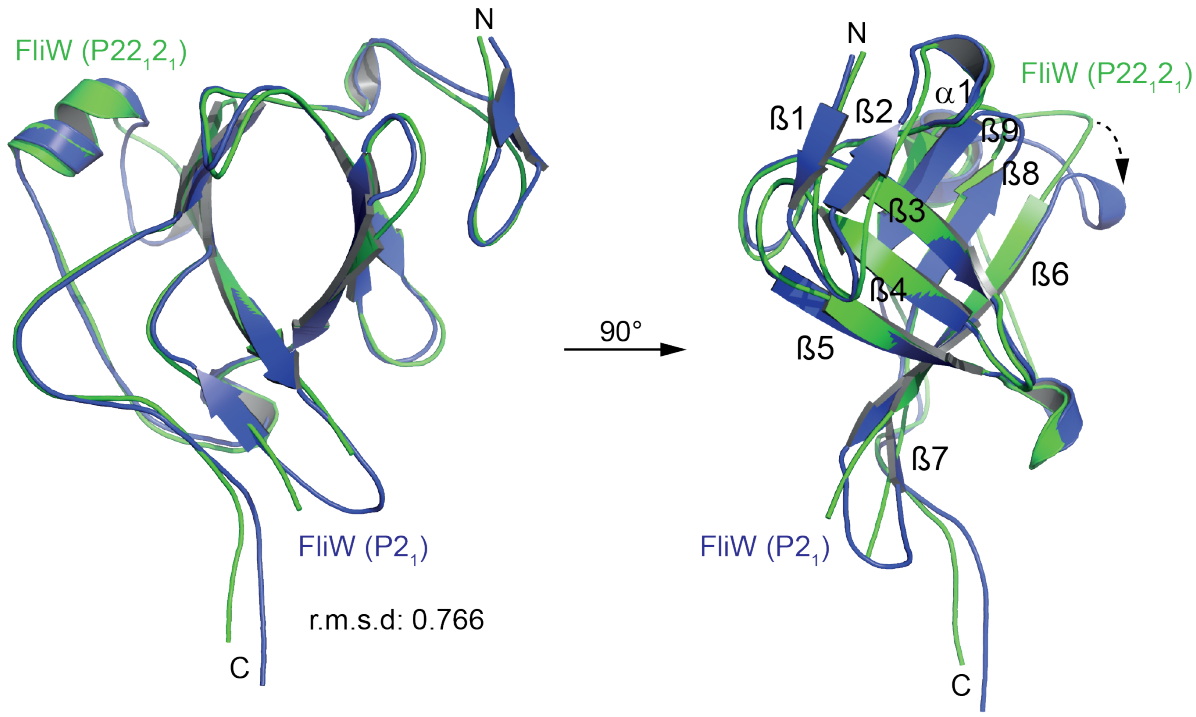

Figure 12: Superposition of *Gt*FliW molecules from different spacegroups. Cartoon representation of *Gt*FliW molecules from $P22_12_1$ (green) and $P2_1$ (blue). The r.m.s.d. calculation revealed a value of 0.766 over all C-α atoms between the two structures. "N" and "C" indicate the N- and C-termini, respectively. The figure originates from [90].

3.1.7 CsrA/FliW from *G. thermodenitrificans* form a heterotetrameric complex

The interaction of FliW and CsrA has been reported earlier [133] but no structural information was available and the exact interaction interface remained unknown. Therefore, the two genes encoding FliW and CsrA from *G. thermodenitrificans* were cloned into pET24d and pET16b, respectively and co-expressed in *E. coli* BL21(DE3) (see section 6.6.1). After cell disruption, the proteins were enriched via Ni-NTA-chromatography (data not shown) and further purified by SEC using a HiLoad 16/600 Superdex 200 column (**Figure 13**).

Only *Gt*FliW was hexahistidine-tagged to enrich the *Gt*CsrA/FliW complex and not any unbound *Gt*CsrA protein. The main peak contained a pure and stoichiometric complex of both proteins as judged from coomassie-stained SDS-PAGE (**Figure 13**, 1). For crystallization experiments all fractions were pooled and concentrated to a final protein concentration of 30 mg/ml.

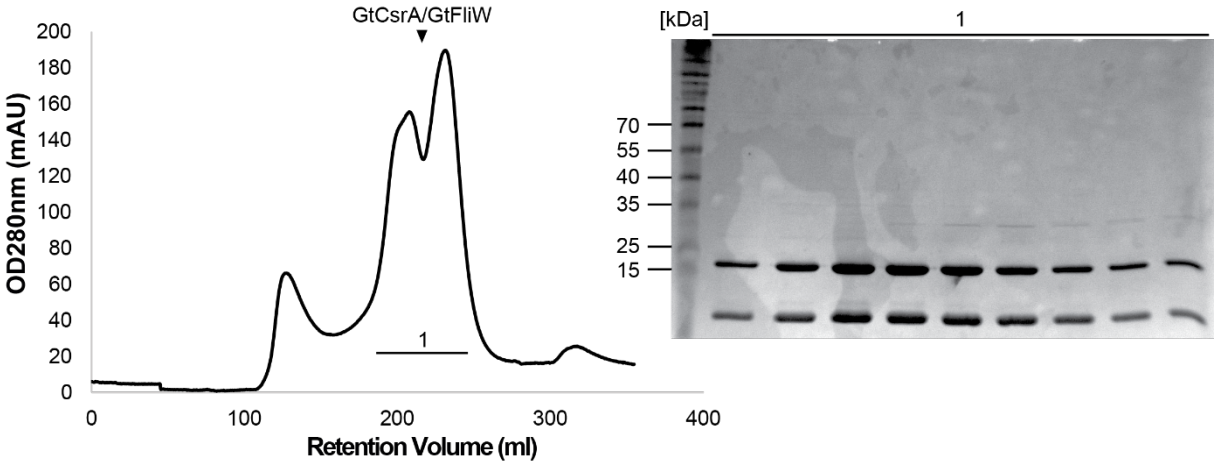

Figure 13: Purification of *Gt*CsrA/FliW. Chromatograms from size exclusion chromatography (SEC) and the respective coomassie-stained SDS-PAGE are shown. The molecular weight of the marker is given in kDa.

To investigate the exact stoichiometry of *Gt*CsrA and *Gt*FliW within the complex, aliquots of all purified proteins were used for analytical SEC. Samples of 200 µM of *Gt*FliW, *Gt*CsrA and the *Gt*CsrA/FliW complex were loaded onto a Superdex 75 10/300 column. *Gt*CsrA always eluted as a stable dimer of 18 kDa, whereas FliW was monomeric with 16 kDa. The complex of *Gt*CsrA/FliW clearly eluted as a heterotetramer indicated by an apparent molecular weight of 40 kDa (**Figure 14**).

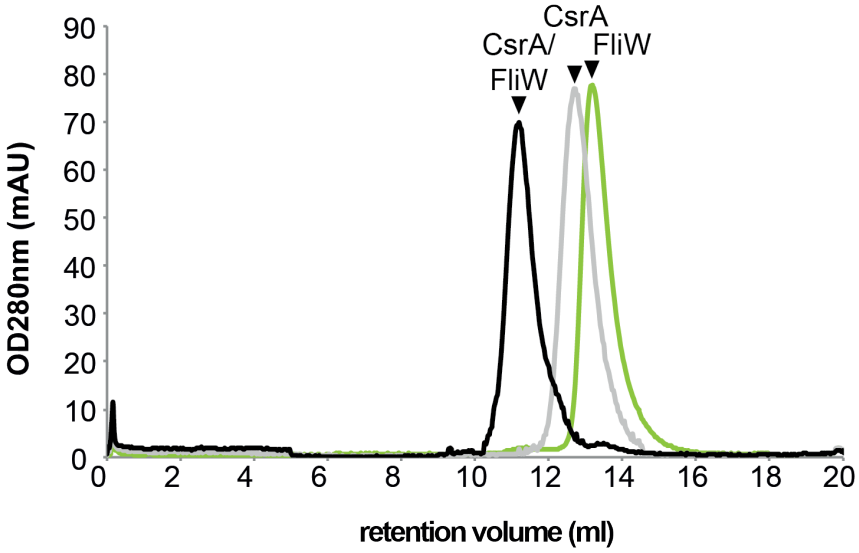

Figure 14: Size-exclusion chromatograms of *Gt*FliW, *Gt*CsrA and *Gt*CsrA/FliW. The chromatogram shows three consecutive SEC runs employing a Superdex 200 10/300 GL (GE Healthcare). The green peak indicates *Gt*FliW, which eluted close to 14 ml. *Gt*CsrA eluted at 13 ml (grey) and the black peak indicates the *Gt*CsrA/FliW complex.

3.1.8 Crystallization of *Gt*CsrA/*Gt*FliW

To crystallize the *Gt*CsrA/FliW complex, a sitting-drop experiment was set up with 30 mg/ml and 15 mg/ml of protein. 500 nl of protein was mixed with the same amount of precipitant solution. *Gt*CsrA/FliW crystallized in 0.2 M potassium fluoride, 20 % (w/v) PEG 3350 within one week of incubation at room temperature (**Figure 15**). Prior data collection, crystals were flash-frozen in liquid nitrogen employing a cryo-protectant solution consisting of mother liquor supplemented with 20 % (v/v) glycerol.

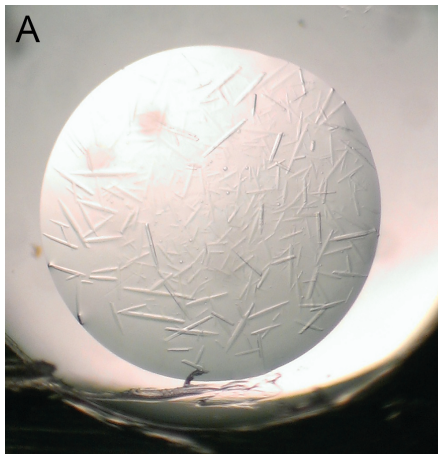

Figure 15: Crystallization of *Gt*CsrA/FliW in one crystallization condition: Crystals were observed in a condition containing: 0.2 M potassium fluoride, 20 % (w/v) PEG 3350

3.1.9 Structure determination of *Gt*CsrA/FliW

The data were collected at the European Synchrotron Radiation Facility (ESRF; Grenoble, France) at the beamline ID30A under cryogenic conditions. Data were processed, integrated and scaled with XDS and merged with the program AIMLESS from the ccp4 suite (see section 6.6.1.). For phase determination, molecular replacement was performed using the structures of a putative contractile protein from *Bacillus halodurans* (PDB-identifier: 2AJ7) and a CsrA homologue from *Pseudomonas fluorescence* (PDB ID code: 2JPP). Data collection and refinement statistics are listed in **Table 2**.

Table 2: Data collection and refinement statistics of the *Gt*CsrA/FliW complex. Values in parenthesis refer to the highest resolution shell. For R_{free} calculation, 5 % of the total reflections from the working set were used.

		***Gt*CsrA/FliW**
Data collection	Space group	C2
	Cell dimensions	
	a, *b*, *c* (Å)	108.88
		61.68
		42.90
	α, β, γ (°)	90.00
		98.08
		90.00
	Energy (keV)	
	Resolution (Å)	42.48 – 2.30
		(2.42 – 2.30)
	R_{merge}	0.055 (0.492)
	I / σI	12.0 (1.8)
	Completeness (%)	99.5 (99.6)
	Redundancy	3.1 (2.9)
Refinement		
	Resolution (Å)	42.48 – 2.30
	No. reflections	11552
	R_{work}/ R_{free}	22.7
		29.0
	No. atoms	1762
	Protein	1689
	Ligand	0
	Water	73
	R.m.s deviations	
	Bond len*Gt*hs (Å)	0.01
	Bond angles (°)	1.45
	Ramachandran (%)	
	Preferred	90.87
	Allowed	7.69
	Outliers	1.44

The structure was refined to an R_{work}/R_{free} of 22.7/29.0 and deposited in the protein data bank (PDB) within the entry 5DMB.

3.1.10 Crystal structure of the heterotetrameric *Gt*CsrA/FliW complex

To gain insight into the interface of the *Gt*CsrA/FliW complex, its crystal structure was determined at 2.30 Å resolution. The structure of *Gt*FliW could almost be built to completeness and only lacked the first 2 N-terminal residues and the last 9 amino acid residues at its C-terminus. The crystal structure of *Gt*CsrA/FliW shows a heterodimer within the asymmetric unit composed of two molecules of *Gt*FliW and *Gt*CsrA. The heterotetramer could be reconstituted along the crystallographic two-fold axis and is composed of a symmetric *Gt*CsrA homodimer and two molecules of FliW that reside on helical C-terminal extensions of *Gt*CsrA (**Figure 16A**, CsrA-C).

In perfect agreement with many other CsrA structures determined by X-ray crystallography and nuclear magnetic resonance (NMR), the interface of the CsrA homodimer is established by five β-strands with β1 being part of the opposing monomer.

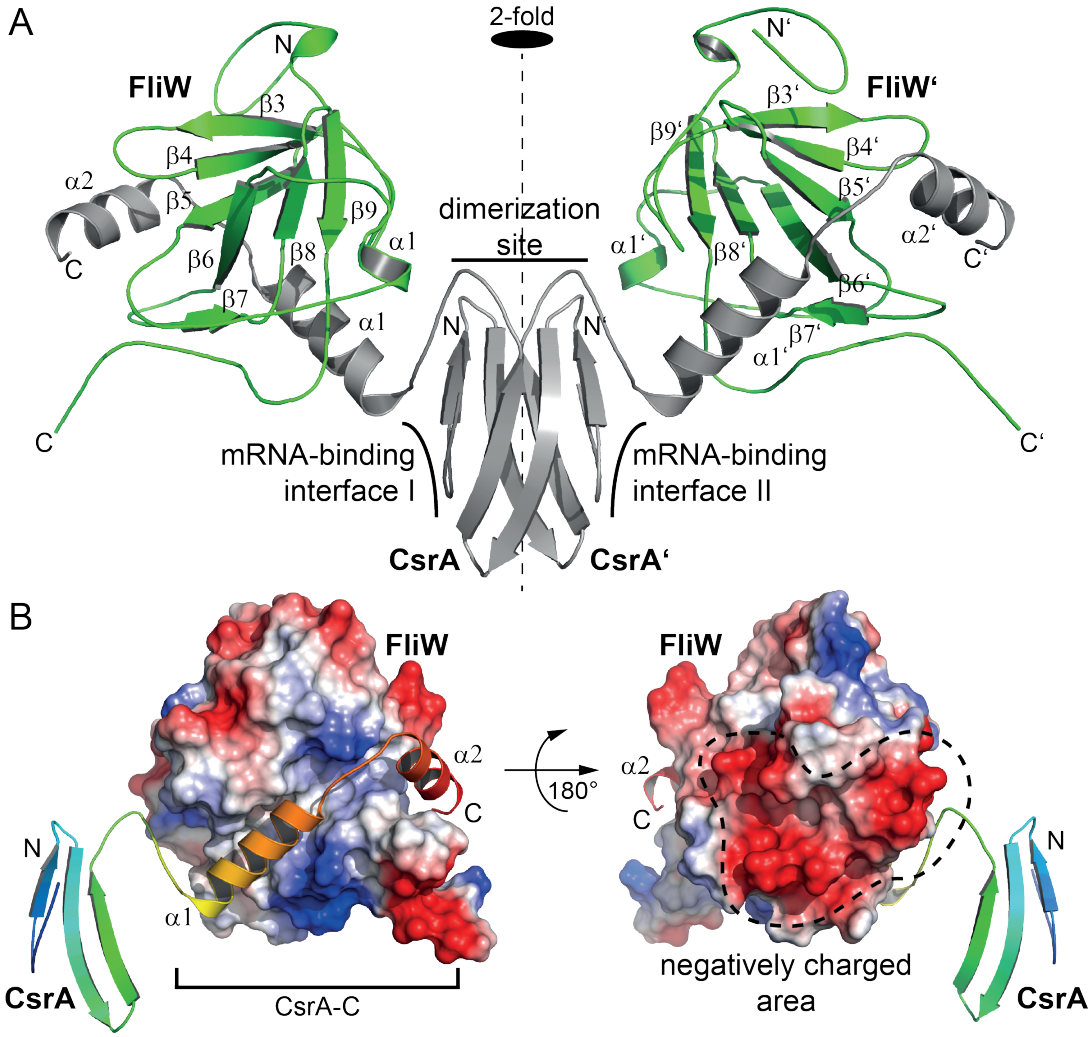

Figure 16: Crystal structure of the CsrA/FliW complex. A. Cartoon representation of CsrA coloured in grey and FliW shown in green. **B.** Electrostatic surface representation of FliW and cartoon representation of CsrA in rainbow colours from N- to C-terminus. Surface charges are colour-coded from positive (blue) over neutral (white) to negative (red). "N" and "C" indicate the N- and C-termini, respectively. Figures were generated with Pymol (**www.pymol.org**). The figure originates from [90].

The binding site of *Gt*FliW at *Gt*CsrA is primarily formed through CsrA-C and covers a buried surface area of approximately ~1405 Å^2. As mentioned earlier (compare **Figure 10**), *Gt*FliW exhibits a highly negatively charged area, which is on the opposite site of the interaction interface. CsrA-C is composed of two α-helices, α1 (residues: 44 to 59) and α2 (residues 60 to 74) that are connected by a short loop. These helices bind into an extended

surface groove of *Gt*FliW and wrap around the molecule via an extensive network of polar and hydrophobic interactions (**Figure 16B**).

3.1.11 Mutational analysis of the CsrA/FliW interface

As outlined in the phylogenetic analysis (see 3.1.1), CsrA-C is only present in species that harbor a copy of both genes encoding FliW and CsrA but not when CsrA is present alone as in case of theγ-proteobacteria. Determination of the crystal structure clearly showed the importance of CsrA-C as the major binding interface. Therefore, constructs of CsrA were generated lacking the first helix (Δα1) and both helices (Δα1α2) and tested for their interaction capability with FliW. The successive deletion of both helices abolished the interaction *in* vitro (**Figure 17A**).

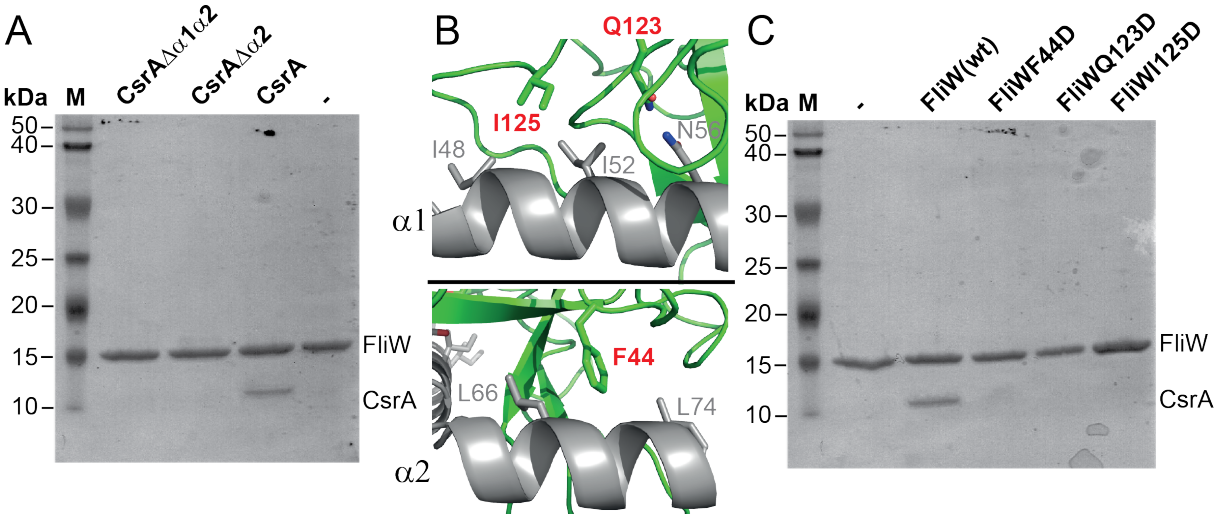

Figure 17: Mutational analysis of the CsrA/FliW interaction. A. Coomassie-stained SDS-PAGE of an interaction assay employing hexahistidine-tagged FliW and different variants of CsrA without an affinity tag. **B.** Close-up of the two α-helices forming the CsrA/FliW interface as cartoon representation. Side chains of varied residues are colored in red. **C.** Coomassie-stained SDS-PAGE of an interaction assay employing hexahistidine-tagged FliW variants and CsrA without affinity tag. The molecular weight of the marker is given in kDa. The figure originates from [90].

A closer inspection of the interaction interface of CsrA and FliW within the *Gt*CsrA/FliW complex revealed several residues at *Gt*FliW that seemed to be important for the interaction. Variation of these residues again abolished the in vitro formation of the *Gt*CsrA/FliW complex (**Figure 17BC**).

Taken together, the structural and biochemical analysis shows that FliW interacts with CsrA-C. The CsrA-dimer is therefore able to recruit two molecules of FliW, yielding in a wing-shaped heterotetramer.

3.1.12 FliW abolishes RNA interaction with CsrA

To understand the molecular mechanism by which FliW antagonizes CsrA binding to the SD-containing 5'-UTR of the *hag* mRNA, the crystal structure of *Gt*CsrA/FliW (compare 3.1.9) was compared with a that of a CsrA homologue from *P. fluorescens* (also named: RsmE) bound to a short SD that is present within the 5'-UTR of the *hcnA* mRNA (PDB-identifier: 2JPP, [117]).

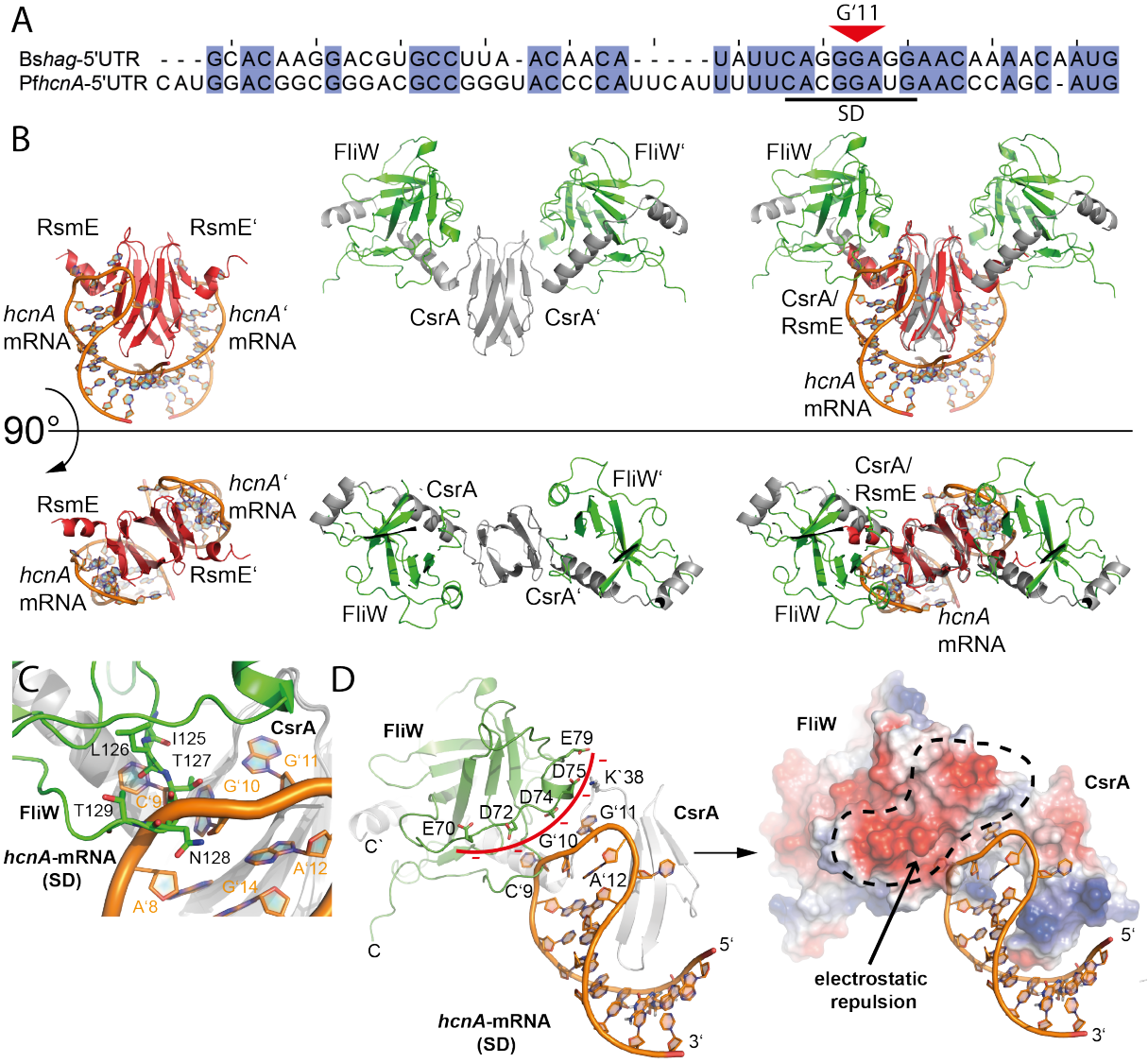

Figure 18: Superposition of the CsrA/FliW complex with a SD-bound CsrA homologue from *P. fluorescens*. A. Sequence alignment of the *hag* and *hcnA* 5'UTR regions. The Shine-Dalgarno (SD) sequence is marked with a black line. **B.** Superposition of the NMR structure of RsmE bound to a SD sequence and the CsrA/FliW complex in cartoon representation. **C.** Close-up of residue 125-129 at FliW (green) and the bases C9 and G10 of the SD sequence (orange). **D.** Overlapping region of the SD and FliW in cartoon representation (left) and electrostatic surface representation (right). Surface charges are colour-coded from positive (blue) over neutral (white) to negative (red). The figure originates from [90].

The sequence recognized by CsrA proteins is the highly conserved 'CANGGANG' motif, which is also present within the ribosomal binding site (RBS) of the flagellin encoding *hag* mRNA (**Figure 18A**). This conservation allowed a direct comparison of both CsrA homologues that share a high structural similarity with a root mean square deviation (r.m.s.d.) of 0.746 over all Cα atoms.

The SD-sequence and FliW occupy similar regions at CsrA, which includes several side chain contacts and therefore charge distributions (**Figure 18CDE**). A detailed investigation of the area that is occupied by FliW in the *Gt*CsrA/FliW complex revealed a clash between the FliW molecule and the SD sequence. This overlap includes the residues 125-129 of FliW and bases G9 and G10 of the SD (**Figure 18CD**).

The negatively charged area of FliW (i.e., amino acids E70, D72, D74, D75, E79) reside in close proximity to the SD-binding interface at CsrA, which would interfere with the phosphate backbone (**Figure 18DE**).

Taken together, the in-depths structural investigation of the CsrA/FliW complex revealed why CsrA-activity can be modulated by FliW. Only unoccupied CsrA can bind to the SD sequence and FliW precludes this interaction by binding allosterically to CsrA-C, therby exposing a negatively charged patch that interferes with the phosphate backbone of the bound 5'-leader transcript.

3.2 Structural investigation on the flagellin/FliS complex

The CsrA protein regulates production of flagellin on the post-transcriptional level and is antagonized by FliW. In the previous chapter, the crystal structure of the *Gt*CsrA/FliW complex was determined to unveil the molecular mechanism by which FliW sequesters CsrA from the SD sequence of the *hag* mRNA. However, FliW can also interact with flagellin, which allows CsrA to again bind to the SD sequence.

To integrate the FliW/flagellin interaction into the model of flagellin regulation, an in-depths structural understanding of flagellin was necessary. Previous work showed that the cognate chaperone FliS facilitated folding of flagellin [57]. Subsequently, the flagellin/FliS complex from *B. subtilis* was used for structure determination.

3.2.1 Purification of flagellin/FliS reveals a heterodimer on SEC

Structural information on the flagellin/FliS interaction is so far only available for FliS from Aquifex aeolicus (*Aa*) bound to the very C-terminus of its cognate flagellin (D0-C, residues 478-518; pdb: 1ORY). The *Aa*FliS/D0-C complex, however, only resembles a partial model and is especially lacking the N-terminal parts of flagellin. In an attempt to obtain the complete structure, the flagellin/FliS proteins from Bacillus subtilis were first co-expressed and co-purifed by Ni-NTA chromatography followed by SEC using a HiLoad 16/600 Superdex 200 column. Only the flagellin protein was hexahistidine tagged to prevent a contamination with unbound FliS.

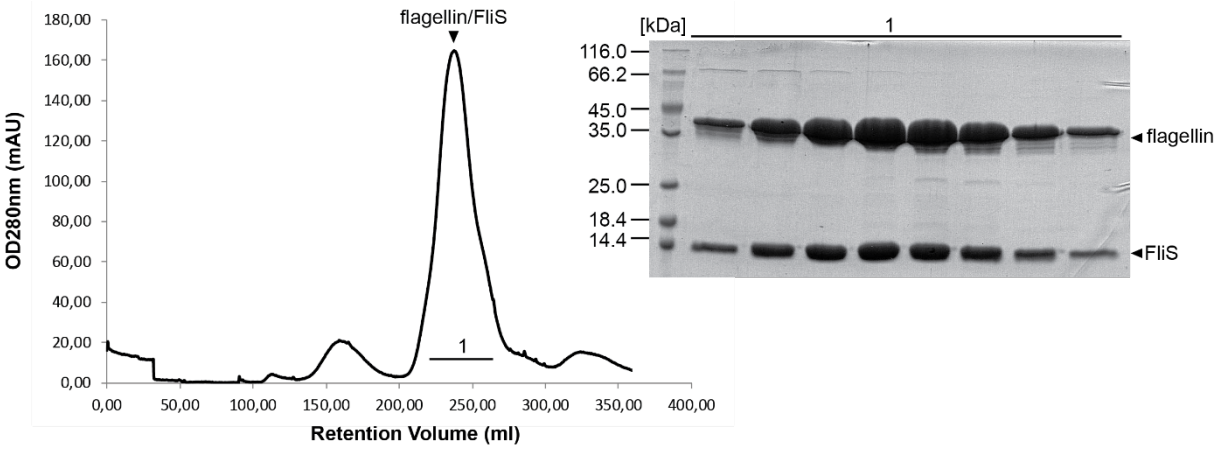

Figure 19: Purification of the flagellin/FliS complex. The chromatogram from size exclusion chromatography (SEC) and the respective coomassie-stained SDS-PAGE is shown. The molecular weight of the marker is given in kDa.

The proteins eluted as a stoichiometric complex from the SEC column (**Figure 19**). Analysis of the SEC fractions by coomassie-stained SDS PAGE always revealed some degradation of the flagellin protein (**Figure 19**). The degradation might be explained by an incomplete saturation of flagellin monomers by FliS. Production of the chaperone was presumably lower than that of flagellin but the slight degradation did not impact further experiments conducted with the complex obtained after SEC.

Therefore, the fractions from peak 1 were collected, pooled and concentrated to 100 mg/ml for crystallization experiments.

3.2.2 Crystallization of the flagellin/FliS complex

To crystallize flagellin/FliS 100 mg/ml and 50 mg/ml of the complex was used in a sitting-drop experiment. 500 nl of protein was mixed with the same amount of precipitant solution. Flagellin/FliS crystallized in various conditions within 24 hours. Crystals from a condition containing 0.2 M Lithium sulfate, 0.1 M Tris pH 7.0 and 2.0 M Ammonium sulfate were harvested and flash-frozen in liquid nitrogen employing a cryo-solution that consisted of mother-liquor supplemented with 20 % glycerol (**Figure 20**). Data were collected under cryogenic conditions at the European Synchrotron Radiation Facility (ESRF, Grenoble) at beamline ID29.

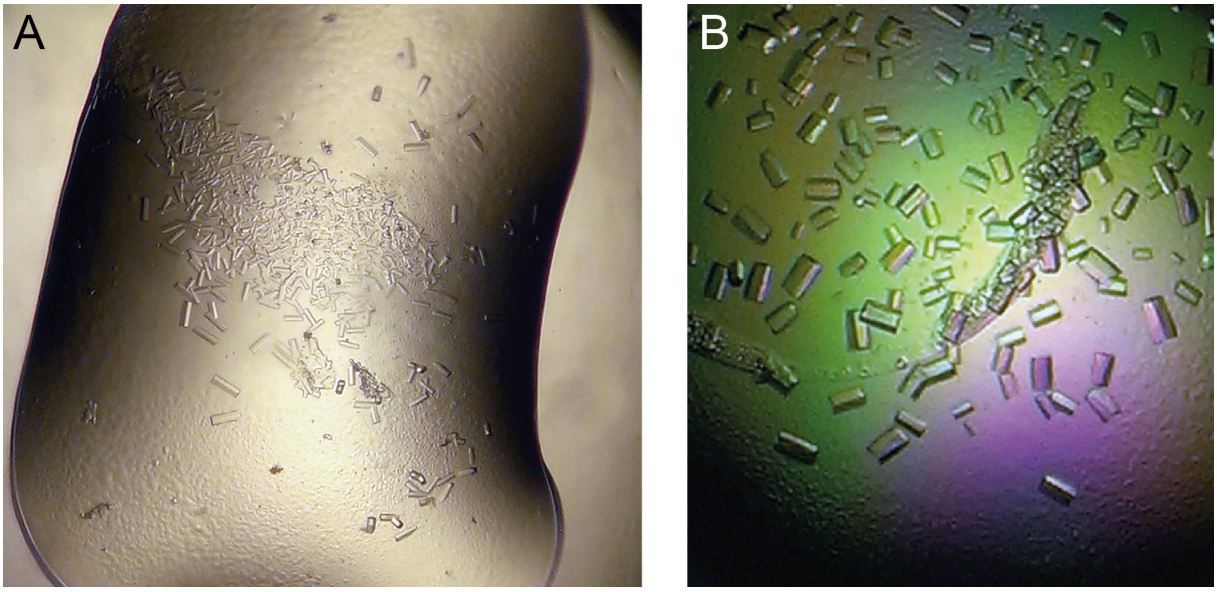

Figure 20: Crystals of the flagellin/FliS complex. Crystals were observed in 0.2 M Lithium sulfate, 0.1 M Tris pH 7.0 and 2.0 M Ammonium sulfate.

3.2.3 Structure determination of flagellin/FliS

Crystals of the flagellin/FliS complex were obtained that belonged to the monoclinic space group $P2_1$. The data were processed, integrated and scaled with XDS and merged with the program AIMLESS from the ccp4 suite (see chapter 6.8.). The structure of the flagellin/FliS complex was determined by molecular replacement using the crystal structures of the *S. typhimurium* flagellin core (pdb: 1IO1) and *B. subtilis* FliS (pdb code: 1VH6) as search models. The crystal form contained one flagellin/FliS heterodimer within the asymmetric unit, which had the overall dimensions of 95 Å, 40 Å and 40 Å.

Table 3: Data collection and refinement statistics of the flagellin/FliS complex. Values in parenthesis refer to the highest resolution shell. For R_{free} calculation, 5 % of the total reflections from the working set were used.

		flagellin/FliS
Data collection	Space group	$P2_1$
	Cell dimensions	
	a, *b*, *c* (Å)	52.13
		62.35
		65.07
	α, β, γ (°)	90.00
		111.33
		90.00
	Energy (keV)	0.9724
	Resolution (Å)	48.57 - 1.5
		(1.55 - 1.5)
	R_{merge}	0.0439 (0.23)
	$I / \sigma I$	18.17 (5.40)
	Completeness (%)	0.99 (0.99)
	Redundancy	4.1 (4.2)
Refinement		
	Resolution (Å)	48.56 - 1.50
	No. reflections	61470
	R_{work}/ R_{free}	17.9 (20.9)
		20.1 (24.7)
	No. atoms	3209
	Protein	2846
	Ligand	0
	Water	363
	R.m.s deviations	
	Bond lengths (Å)	0.009
	Bond angles (°)	0.97
	Ramachandran (%)	
	Preferred	98.33
	Allowed	1.4
	Outliers	0.27

The structure was refined to an R_{work}/R_{free} of 17.9/20.1 and deposited in the protein data bank (PDB) within the entry 5MAW.

3.2.4 Crystal structure of the flagellin/FliS complex

The overall architecture of flagellin is highly conserved among the different bacterial species and can be divided into the D0N, D1 and D0C-domains (**Figure 21A**). The structural model obtained from the crystals is complete, except for the N-terminal 40 residues of flagellin, which were only poorly visible in the electron density maps (**Figure 21AB**, dashed line). Unlike the limited contact observed with partial structures, full length-flagellin and FliS were found to interact with each other by an extensive network of hydrophobic and electrostatic interaction with an interface area of about 2600 Å2 (**Figure 21B**, **Figure 22**), and form a rather compact particle.

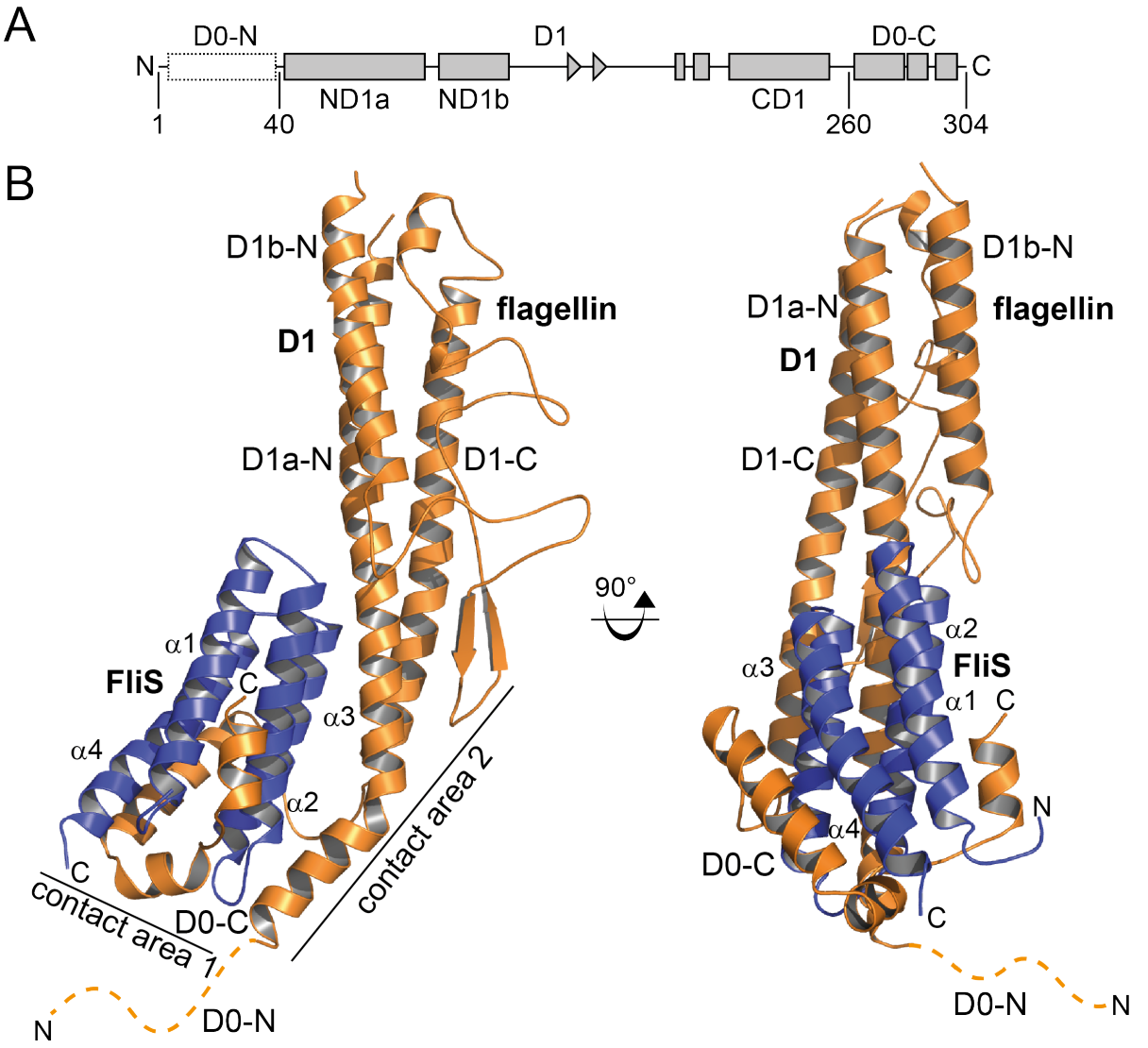

Figure 21: Crystal structure of the flagellin/FliS complex. A. Domain architecture of flagellin. **B.** Crystal structure of flagellin (orange) in complex with its chaperone FliS (blue) in cartoon representation. "N" and "C" indicate the N- and C-termini, respectively.

The interface between flagellin/FliS can be divided into two main areas. Firstly, the C-terminus of flagellin (D0-C) is wrapped around the surface of FliS in an extended horseshoe like conformation with a mainly hydrophobic interaction area of 1600 Å (Contact area 1, **Figure 21B**, **Figure 22**). Contact area 1 is highly similar to that in an earlier structure of FliS bound to the C-terminus of flagellin with a Cα r.m.s.d of 2,2 Å over 140 amino acid residues [55]. Interactions of the second area are of a more electrostatic nature and align FliS to the D1 core domain of flagellin (Contact area 2, **Figure 21B**, **Figure 22**). An N-terminal region of flagellin, which is disordered in previous flagellin structures [142–144] formed a helical segment and participated in the interaction with FliS. Taken together, the crystal structure revealed that both the N- and C-termini of flagellin interact with its secretion chaperone FliS.

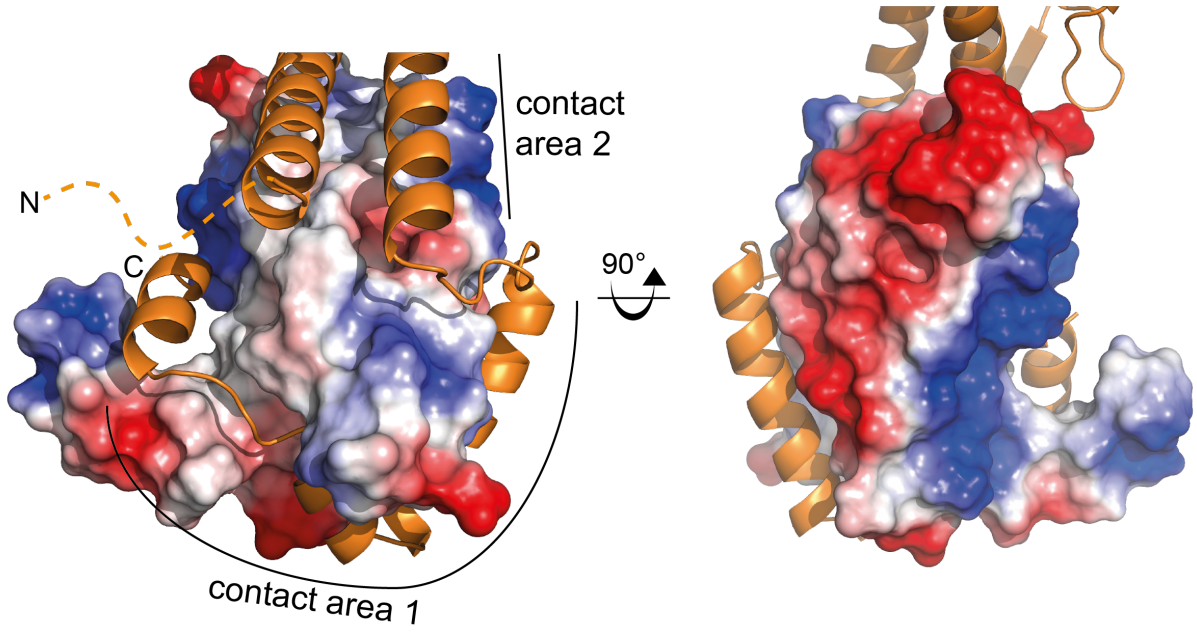

Figure 22: Electrostatic surface representation of the FliS binding site at the flagellin D0C domain. Flagellin is coloured in orange and shown as cartoon representation, whereas the electrostatic surface potential of FliS is shown. Surface charges are colour-coded from positive (blue) over neutral (white) to negative (red).

3.2.5 Comparison of different flagellin homologs

Crystal structures of several flagellin homologues have been determined and all show the overall same architecture [142–144] (**Figure 23**). The D0-domains are not resolved, except for the FliS-bound state in this study, due to flexibility.

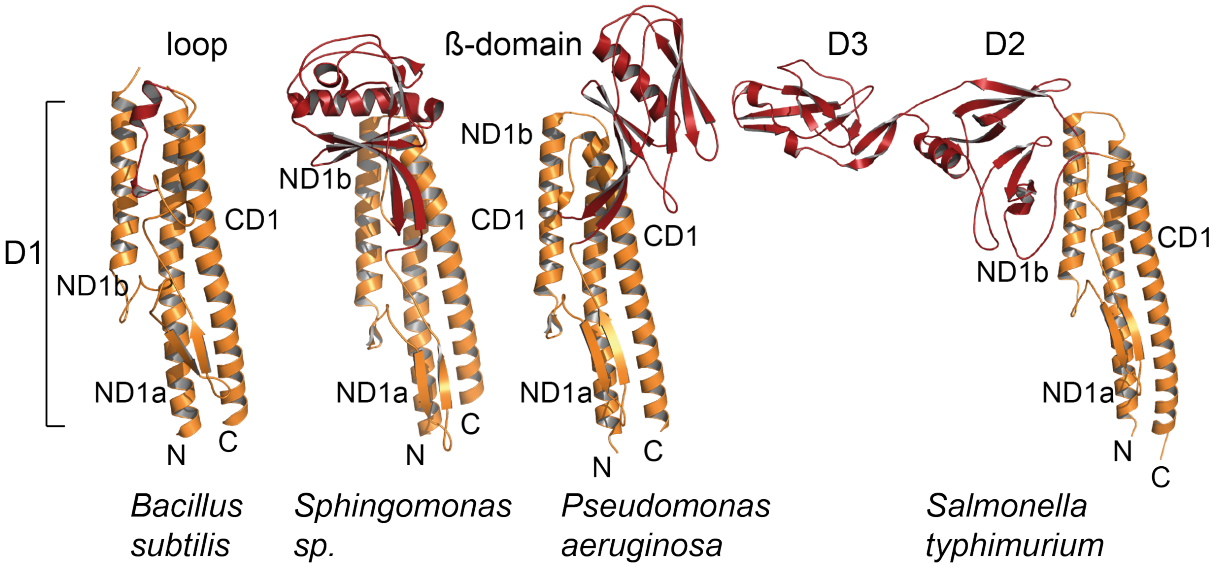

Figure 23: Comparison of different flagellin homologues. The crystal structures of flagellin proteins from different organisms (as indicated) are shown in cartoon representation. The D1 domain is coloured in orange and variable domains (D2, D3, β-domain, loop) in dark red. "N" and "C" indicate the N- and C-termini, respectively.

The conserved fold is clearly visible when the four structures of *B. subtilis, Sphingomonas sp.* (PDB-identifier: 2ZB1)*, P. aeruginosa* (PDB-identifier: 4NX9) and *S. typhimurium* are compared (PDB-identifier: 1IO1, **Figure 23**).
The D1-domains consist of three α-helices and two small β-sheets, which are part of the inner scaffold in a mature filament and connect the variable domain via a short loop region (**Figure 23** orange). The variable domain has a similar fold in the closely related Pseudomonas and Sphingomonas species but shows an additional extension in Salmonella (**Figure 23**, red). The flagellin homologue from *B. subtilis* seems to represent one of the shortest variants, which might also facilitate its ability to crystallize.

3.3 Structural investigation of the flagellin/FliW interaction

Earlier studies suggest the direct interaction of FliW with flagellin and predicted the interface within the D1-C region of flagellin in close proximity to the D0-C domain [91,145]. These findings are in contrast to recent data, which suspect that the FliW binding site to rather be located within the N-terminal region of flagellin [132].

3.3.1 Flagellin and FliW form a complex on SEC

The two genes encoding FliW and flagellin from *B. subtilis* were cloned into pET24d and pET16b, respectively and co-expressed in *E. coli* BL21(DE3) as per described in chapter 6.6.1. After cell disruption, the proteins were enriched via Ni-NTA-chromatography (data not shown) and further purified by SEC using a HiLoad 16/600 Superdex 200 column (**Figure 24**). Both proteins were fused to a hexahistidine-affinity tag to increase the total protein yield.

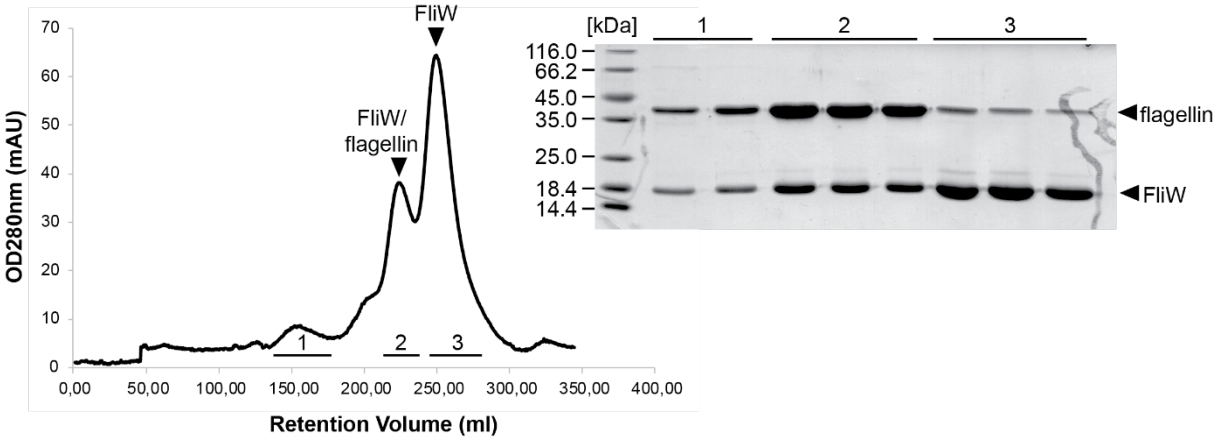

Figure 24: Purification of the flagellin/FliW complex. The chromatogram from size exclusion chromatography (SEC) and the respective coomassie-stained SDS-PAGE is shown. The molecular weight of the marker is given in kDa.

The size exclusion chromatography step revealed three distinct fractions that all contained FliW and flagellin. However, only in the fractions collected from peak 2, a stoichiometric flagellin/FliW complex was detected (**Figure 24**). The fractions from 2 were pooled and concentrated to 60 mg/ml to further use the protein for crystallization experiments. However, all attempts to crystallize the complex were unsuccessful and only resulted in the crystallization of flagellin alone (data not shown).

3.3.2 Flagellin, FliS and FliW form a complex on SEC

The flagellin/FliW complex could be successfully reconstituted on SEC but all crystallization attempts remained unsuccessful. To investigate, whether the binding of FliS to flagellin might facilitate the crystallization process also with FliW present, the heterotrimeric complex was co-expressed in *E. coli* BL21(DE3) as described in chapter 6.6.1. First the flagellin/FliS complex was produced as shown in 3.2.1. In a next step, SEC-pure flagellin/FliS complex was mixed with an equimolar amount of FliW (compare 3.1.2) Complex formation was analyzed by SEC and revealed the presence of one peak that contained flagellin/FliS and FliW in stoichiometric amounts as analyzed by coomassie-stained SDS-PAGE (**Figure 25**). These data show that both FliS and FliW interact with flagellin simultaneously. A size standard was applied to the SEC column and showed that the complex had an apparent molecular weight of ~75 kDa (data not shown). Through this observation, the complex was estimated to be heterotrimeric.

For crystallization experiments all fractions were pooled and the protein concentrated to a final concentration of 60 mg/ml. Again, crystallization of the flagellin/FliS/FliW complex was not successful and only led to crystals containing flagellin/FliS (data not shown).

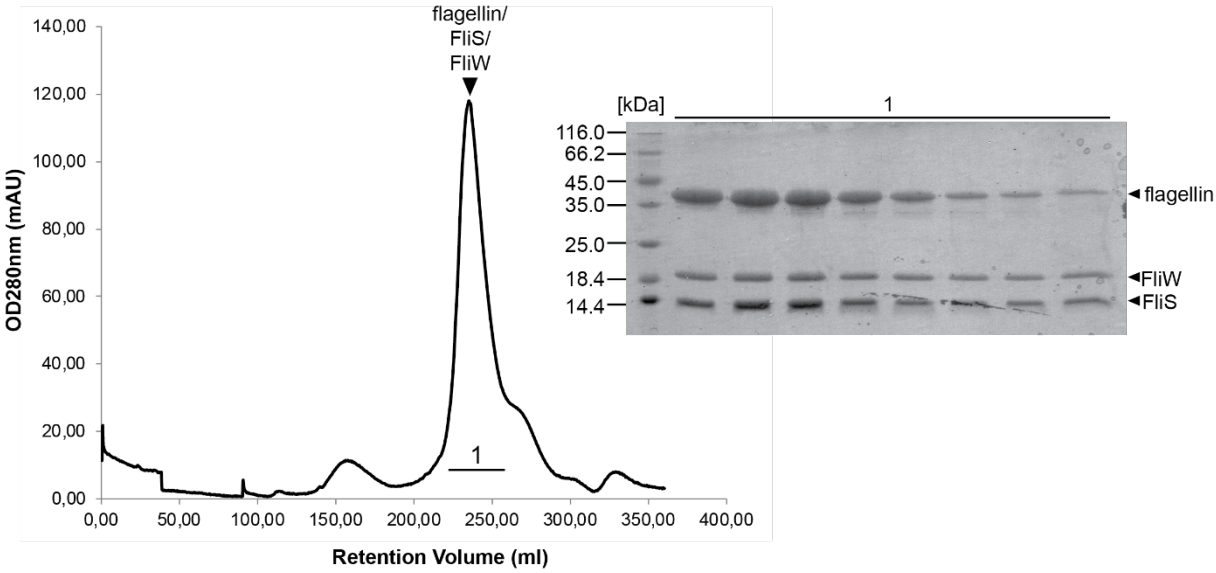

Figure 25: Purification of the flagellin/FliS/FliW complex. The chromatogram from size exclusion chromatography (SEC) and the respective coomassie-stained SDS-PAGE is shown. The molecular weight of the marker is given in kDa.

3.3.3 SAXS analysis confirms the heterotrimeric complex in solution

All attempts to crystallize the heterotrimeric complex did not result in a complete structure of the complex. Both, the heterotrimeric flagellin/FliS/FliW and heterodimeric flagellin/FliW complex were stable on SEC and did neither show degradation or a high degree of flexibility. To assess whether flexibility might be the reason for the failure of the complex to crystallize and gain a deeper insight into the binding site of FliW at flagellin, small angle X-ray scattering (SAXS) was employed. SAXS allows unraveling of both the molecular shape of a particle and the approximate locations of components within this macromolecular complex. *Ab initio* shape restoration bead modelling of FliW revealed an oval shaped volume with a small extension on one side, which resembled the crystal structure of FliW (**Figure 26**, left side). SAXS of the flagellin/FliS complex yielded in a volume into which the crystal structure of flagellin/FliS could be fitted very well (**Figure 26**, middle).

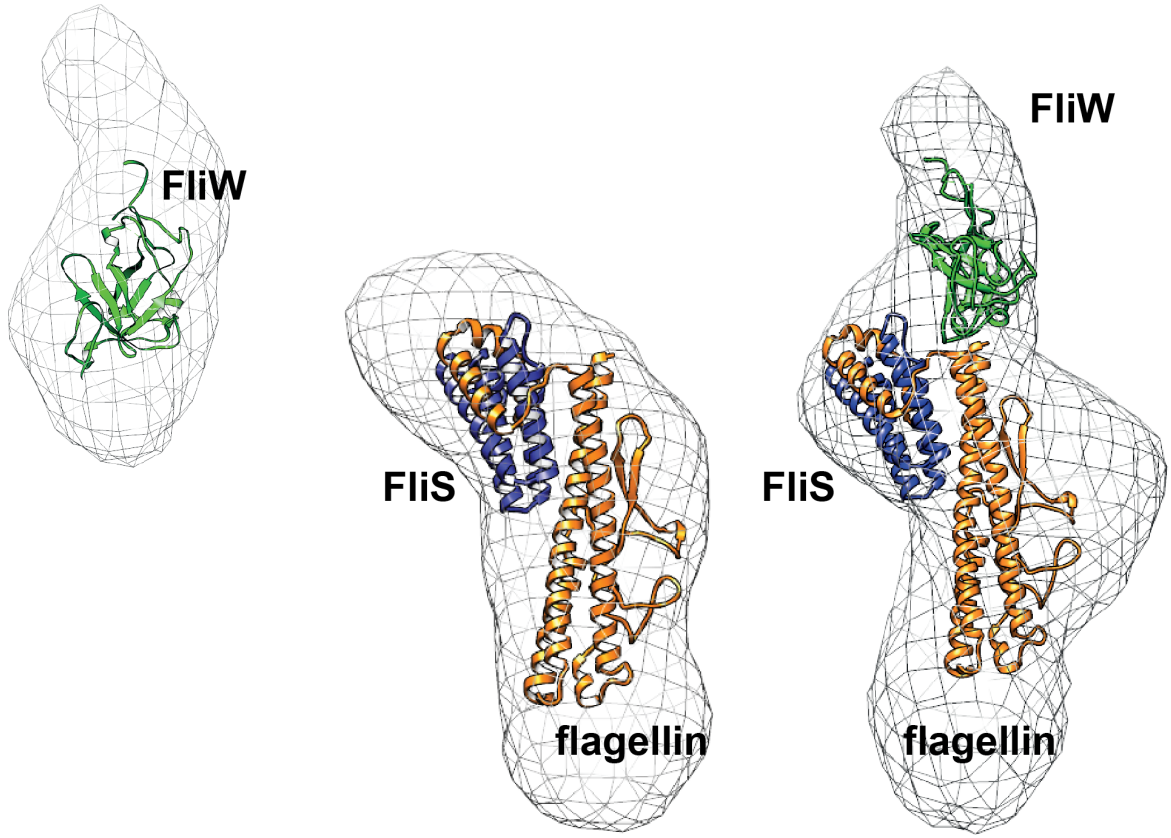

Figure 26: Small-angle X-ray scattering analysis of FliW, flagellin/FliS and flagellin/FliS/FliW. Surface grid representations of averaged and filtered ab initio bead models calculated by Dammif [146]. Structures of FliW, and flagellin/FliS are displayed in cartoon representation and manually fitted to the density. Figures were generated with Chimera (**https://www.cgl.ucsf.edu/chimera/**).

For the heterotrimeric complex, a significant extra density appeared in close proximity to the N-terminus of flagellin and opposite of the FliS binding site at flagellin. The SAXS technique only allows insight into macromolecular complexes at a very low resolution but could already give an idea about the FliW binding site at flagellin and confirm the stability of the heterotrimeric complex in solution.

3.3.4 Hydrogen-deuterium-mass spectrometry of flagellin/FliW reveals the binding site of FliW at flagellin and *vice versa*

To specify the binding site of FliW at flagellin, hydrogen-deuterium exchange mass spectrometry (HDX-MS) was performed. Additionally, this method allows monitoring conformational changes within the proteins involved in complex formation, which might explain the repeated failure to crystallize the proteins.

The proteins FliW, flagellin/FliS and flagellin/FliW were enriched by Ni-NTA-chromatography and purified by SEC. FliW, flagellin/FliS and flagellin/FliW were incubated

in a deuterated buffer for 30 seconds, two minutes and 10 minutes, digested with pepsin and analyzed by electrospray ionization-mass-spectrometry. The heterotrimeric complex flagellin/FliS/FliW was not included in my HDX analysis due to a better exchange in the flagellin/FliW complex without FliS (data not shown).

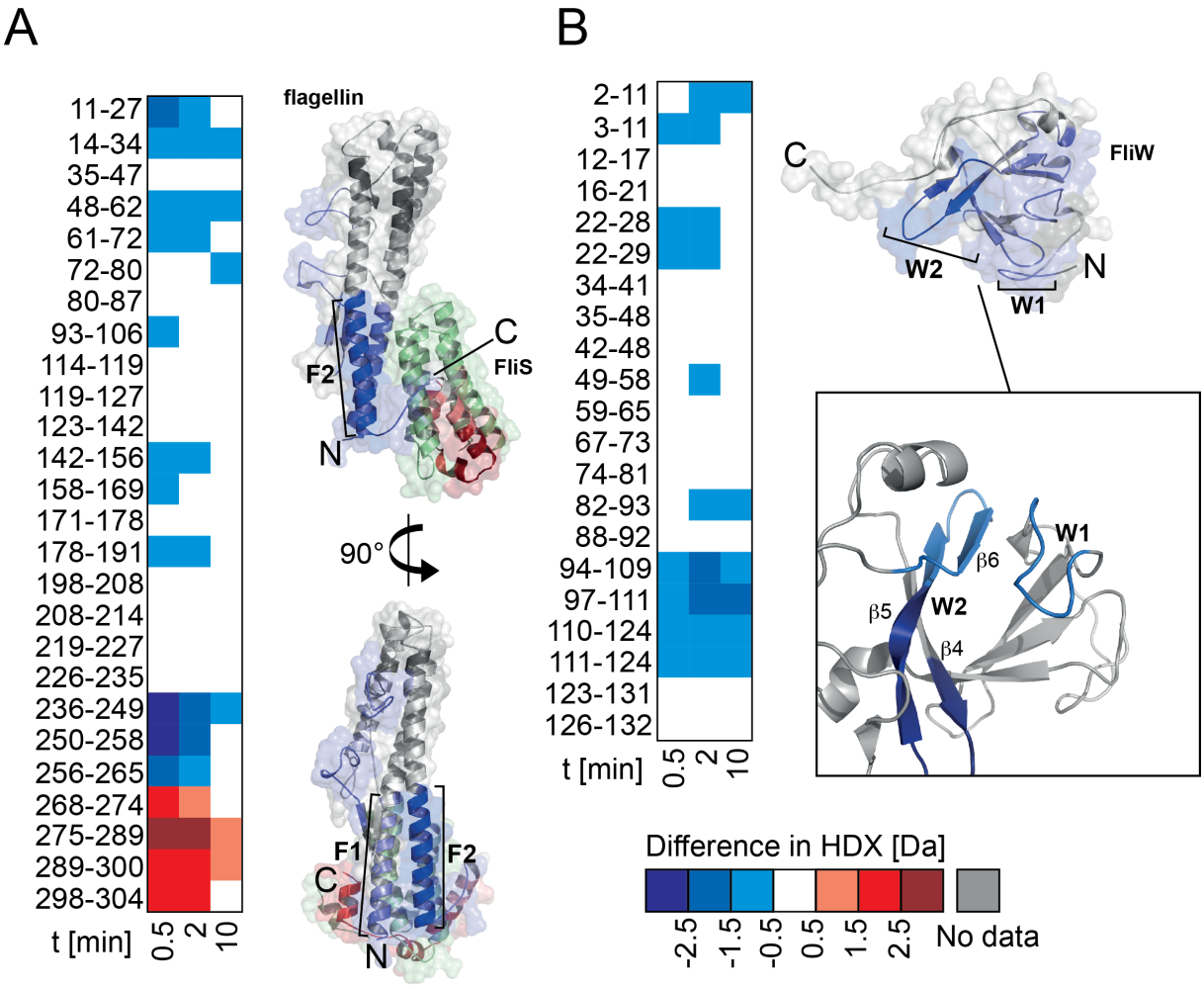

Figure 27: Hydrogen deuterium exchange mass spectrometry (HDX-MS) of flagellin, FliW and the flagellin/FliW complex. A. (Left) Analysis of deuterium exchange in flagellin peptides after 30 seconds, 2 minutes and 10 minutes. Numbers indicate amino acids. (Right) Cartoon representation of flagellin/FliS**.** Regions with less exchange in the flagellin/FliW complex are colored in blue, regions with more exchange are colored in red. **B.** (Left) Analysis of deuterium exchange in FliW peptides after 30 seconds, 2 minutes and 10 minutes. Numbers indicate amino acids. (Right) Cartoon representation of FliW**.** Regions with less exchange in FliW are coloured in blue. "N" and "C" indicate the N- and C-termini, respectively.

FliW protected two adjacent regions at flagellin spanning the N-terminal part (**Figure 27**, residues 11-34, 50-72) of helix D1a-N (region F1) and the C-terminal part (**Figure 27**, residues 240-260) of helix D1-C (region F2). Conversely, flagellin protected a loop region close to the N-terminus of FliW (**Figure 27**, residues 3-11, W1) and the three β-strands β4, β5, and β6 (**Figure 27**, residues 22-28, 95-115; W2). Our HDX data suggest that FliW

interacts with flagellin on the opposite site of the FliS binding site, thus also not interfering with FliS binding as shown earlier [91].

In addition to the binding site definition, our HDX analysis also reveals a strong increase in solvent accessibility of the D0-C domain of flagellin (**Figure 27**, residues 270-304) when bound to FliW. This is in perfect agreement with the flagellin/FliS crystal structure, as the C-terminus is shielded by FliS. Without FliS, the D0-C domain is highly flexible.

3.3.5 FliW interacts with the D0N/D1N-domain of flagellin

To further narrow the interaction site of FliW at flagellin, several truncated flagellin constructs were generated and tested for their interaction proficiency. The crystal structure did not contain the first 40 residues of flagellin (compare 3.2.4), a region putatively targeted by FliW. However, the first 40 residues were not sufficient for FliW binding and neither were the N-terminal 50 residues (data not shown). Due to the small size of both constructs, which increased the possibility of degradation during protein production in *E. coli* BL21(DE3), the cultures were induced at an OD_{600} of 0.5 with 1 mM IPTG for three hours. Although this increased the yield, no binding to FliW was observed.

The next constructs included the first 60 and 72 residues of flagellin, respectively. Both constructs were co-expressed with FliW to decrease the sensitivity to degradation.

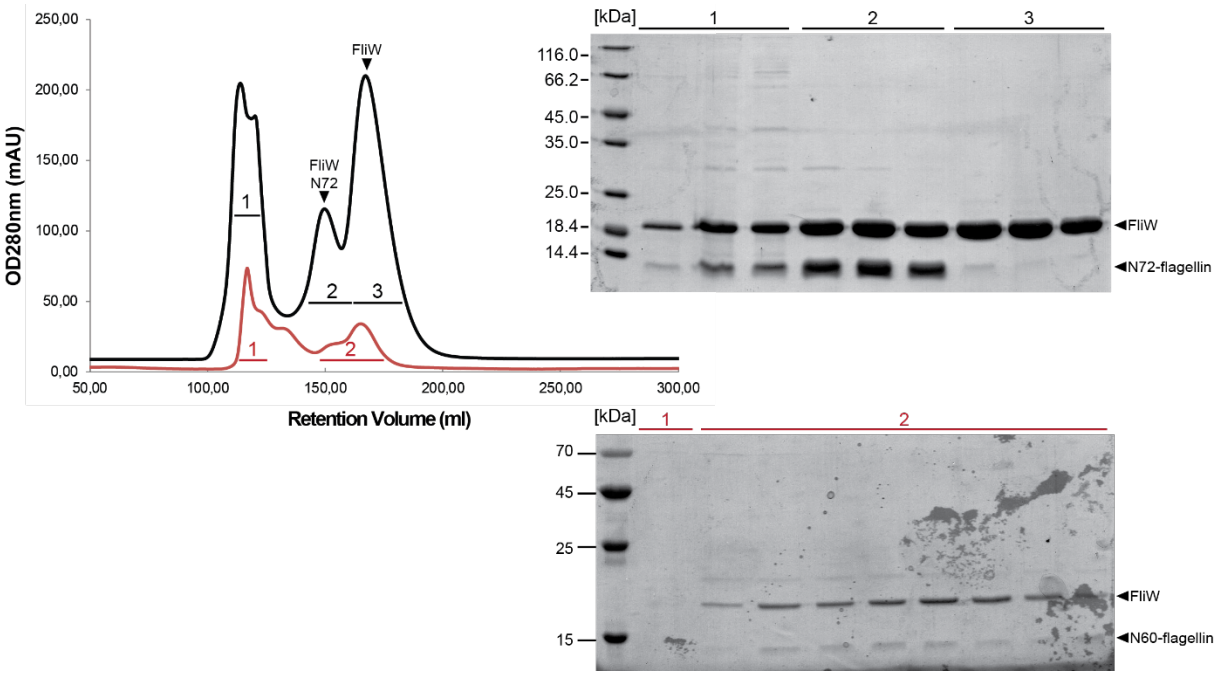

Figure 28: Purification of flagellinN72/FliW and flagellinN60/FliW. The chromatograms from size exclusion chromatography (SEC) and the respective coomassie-stained SDS-PAGEs are shown. The molecular weight of the marker is given in kDa.

The flagellin variants N60 and N72 were both capable of FliW binding and formed a SEC stable complex but the N60-flagellin yield was less than a tenth of N72-flagellin yield (**Figure 28**). Therefore, the longer flagellin constructs was further used to set up crystallization experiments.

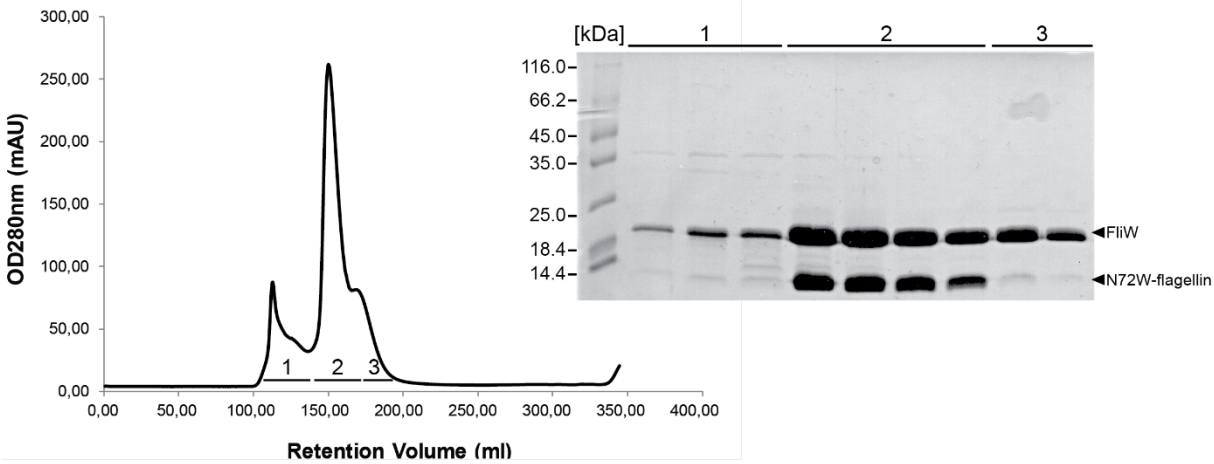

Figure 29: Purification of flagellinN72W/FliW. The chromatogram from size exclusion chromatography (SEC) and the respective coomassie-stained SDS-PAGE is shown. The molecular weight of the marker is given in kDa.

To increase the amount of N72-flagellin/FliW complex and allow a better UV detection at 280 nm, N72-flagellin was C-terminally fused to a hexahistidine tag and an additional tryptophane residue included in the construct (**Figure 29**).

These changes led to a much higher yield of the complex, which now allowed the setup of crystallization experiments (**Figure 29**). The peak fraction 2 was concentrated to 80 mg/ml. The N72-flagellin/FliW complex was used to setup a sitting-drop crystallization experiment and 500 nl of the protein solution mixed with mother liquor in a 1:1 ratio. Although promising precipitation could be observed in several conditions, no crystals appeared after several weeks.

3.4 Coupling of homeostasis and type-3-secretion of flagellin

3.4.1 FliS is necessary for recognition of flagellin by FlhA-C

Earlier work showed that FliS is required for the recruitment of flagellin to FlhA-C in *B. subtilis* [27]. However, the impact of FliW on this important step has not been studied yet.

Therefore, I tested whether and if yes how, the presence of FliW would influence the recruitment of flagellin to FlhA-C.

Flagellin, FliS and FliW were enriched via Ni-NTA-chromatography and further purified by SEC using a HiLoad 16/600 Superdex 200 column according to 6.6.1. Furthermore, a glutathione-S-transferase-tagged (GST) variant of FlhA lacking the first 301 residues (FlhAΔN301) was purified via Ni-NTA chromatography and SEC.

GST-FlhAΔN301 (referred to as FlhA-C) was immobilized on glutathione-sepharose beads at a concentration of 2 µM and incubated with 10 µM of purified flagellin, FliS and FliW. Lane 1 in figure 29 contains FlhA-C alone as a negative control. Flagellin alone cannot bind to FlhA as shown in lane 2 (**Figure 30**, lane 2). Whereas FliS successfully recruited flagellin to FlhA-C (**Figure 30**, lane 3), no interaction of flagellin with FlhA-C was observed in the presence of FliW (**Figure 30**, lane 4). It can therefore be concluded that FliS is essential for flagellin interaction with FlhA but not FliW.

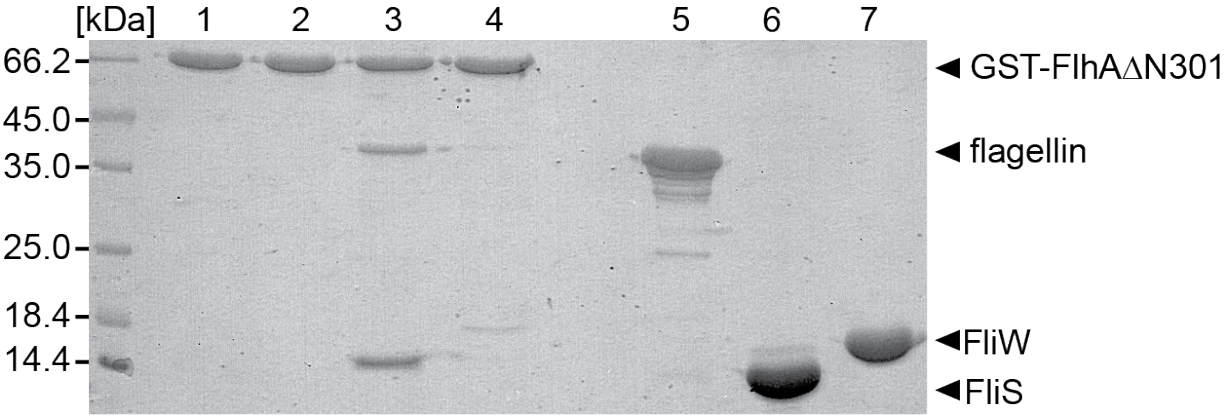

Figure 30: Interaction of flagellin with FlhA requires FliS but not FliW. Coomassie-stained SDS-PAGE of an interaction assay employing GST-FlhAΔN301, flagellin, FliS and FliW. The molecular weight of the marker is given in kDa.

3.4.2 The heterotrimeric flagellin/FliS/FliW complex can bind to FlhA-C

The previous experiment showed that FliS is necessary for flagellin recruitment, whereas FliW is not. However, this does not exclude the ability of the heterotrimeric complex of flagellin/FliS/FliW to bind to FlhA-C. Nothing is known about the recycling process of chaperones that guide their cognate clients to the export gate. To find out whether FliW is released from the flagellin/FliS/FliW complex prior to recognition by FlhA or not, the heterotetrameric complex was reconstituted on SEC. FlhA-C, flagellin/FliS and FliW were enriched by Ni-NTA chromatography and purified by SEC. The fractions containing the

protein were pooled, concentrated and mixed in equimolar amounts (data not shown). All proteins eluted in a stable complex from the SEC column (**Figure 31**).

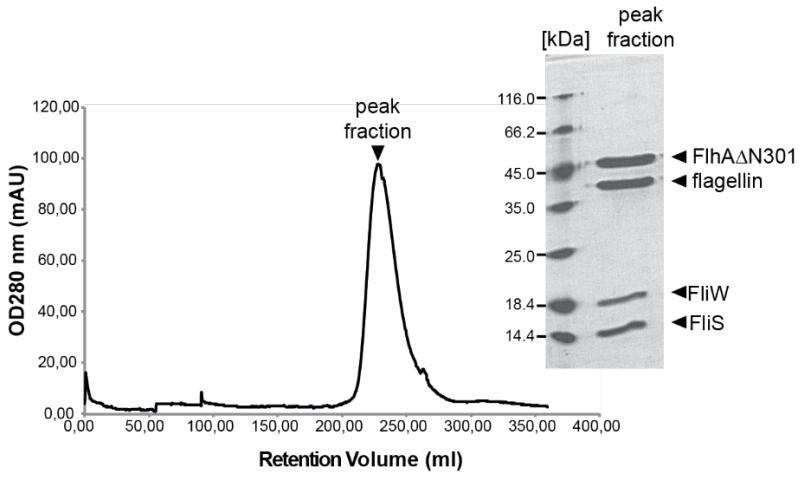

Figure 31: Purification of FlhA/flagellin/FliS/FliW. The chromatogram from size exclusion chromatography (SEC) and the respective coomassie-stained SDS-PAGE is shown. The molecular weight of the marker is given in kDa.

These data confirm that the heterotrimeric complex of flagellin/FliS/FliW is still capable of being recognized by FlhA-C (**Figure 31**).

3.4.3 Hydrogen-deuterium-mass spectrometry of flagellin/FliS/FlhA-C reveals the binding site of flagellin/FliS at FlhA-C and *vice versa*

To understand how the flagellin/FliS complex is recruited to FlhA-C, HDX mass spectrometry was conducted and the changes in deuterium incorporation upon binding of flagellin/FliS to FlhA investigated. The proteins FlhA-C, flagellin/FliS and flagellin/FliS/FlhA-C were enriched by Ni-NTA-chromatography and purified by SEC as described in section 6.6.1. All proteins were then incubated in a deuterated buffer for 30 seconds, two minutes and 10 minutes, digested with pepsin and analyzed by electrospray ionization-mass-spectrometry.

First, the residues within flagellin/FliS that exchange less in the presence of FlhA-C were analyzed. Three regions within the D1-N and D1-C domain and the D0-C are stabilized upon binding (**Figure 32**, F1-F3).

The region F1 belongs to the D1-N domain and comprises a small helical stretch within the residues 60-72 at flagellin (**Figure 32**, F1).

Regions F2 and F3 are located in the C-terminal region of D1 and the D0-C domain, respectively (**Figure 32**, F2, F3). Peptides summarized in F2 include residues 240-260, which are directly adjacent of the F1 patch on the D1-N domain. Additionally, this region is also part of the interaction interface between flagellin and FliS (compare 3.2.4, contact area 2).

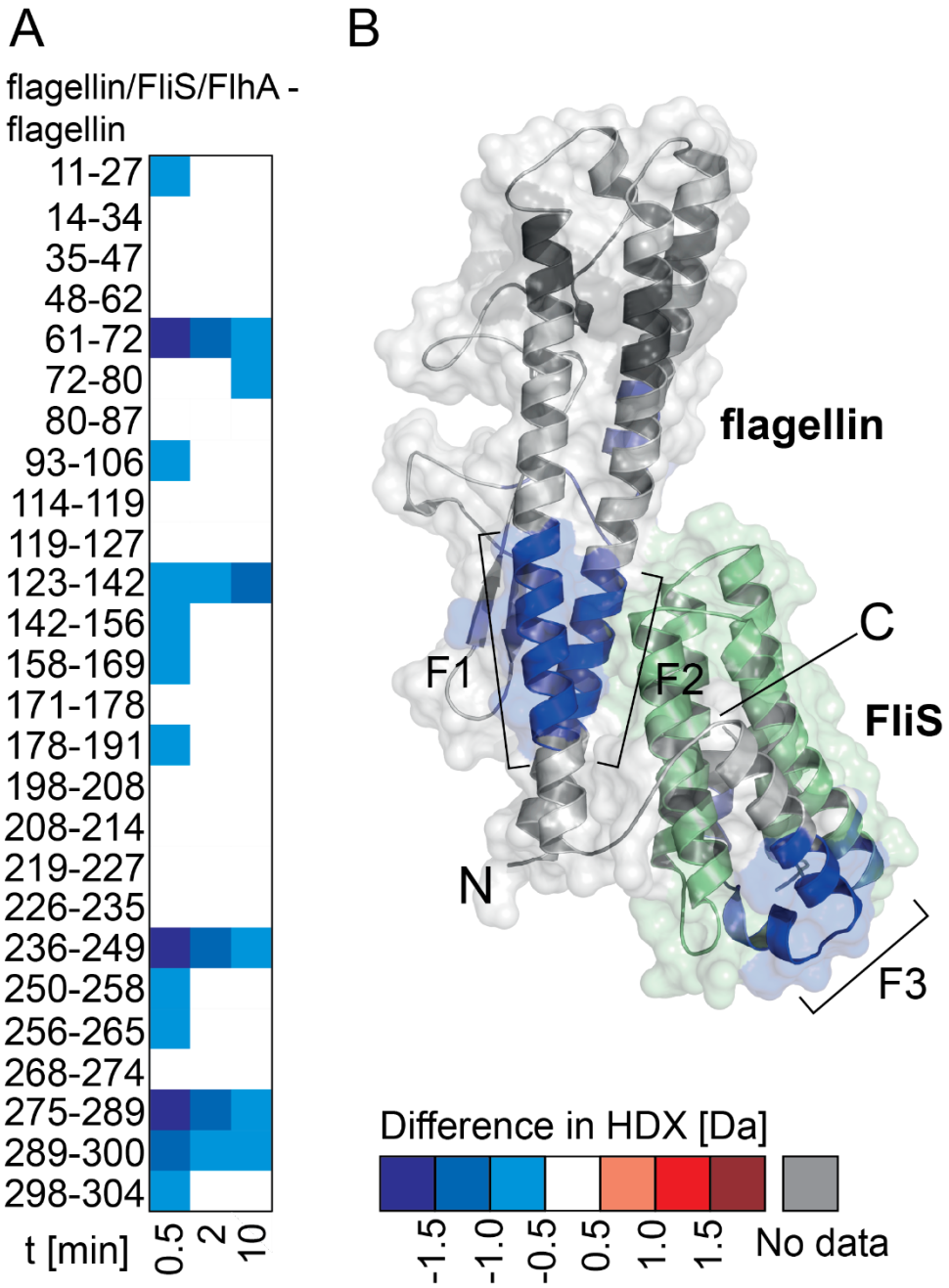

Figure 32: Hydrogen deuterium exchange mass spectrometry (HDX-MS) of flagellin/FliS compared to FlhA/flagellin/FliS A. Analysis of deuterium exchange in flagellin peptides after 30 seconds, 2 minutes and 10 minutes. Numbers indicate amino acids. **B.** Cartoon representation of flagellin/FliS**.** Regions with less exchange in the FlhA/flagellin/FliS complex are colored in blue, regions with more exchange are colored in red.

The most prominent protection of hydrogen to deuterium exchange can be observed in the very C-terminal region of flagellin ranging from residue 280 to 300. These residues are arranged in two short α-helices connected by a loop and wrap around FliS (**Figure 32**, F3).

Taken together, the HDX-MS results show that FlhA-C recognizes a complex interface at flagellin that includes residues located in contact areas to FliW (F1, F2) and the cognate chaperone FliS (F2, F3). The data explain the importance of FliS in recognition of flagellin at FlhA-C as its presence leads to a dramatic rearrangement of the D0-C domain and therefore renders the "client" ready to be exported.

The D1b of FlhA-C together with two adjacent helical segments of D1a and D3 show a dramatic decrease in deuteron incorporation, indicating stabilization or shielding (**Figure 33**). This is in line with findings from *S. typhimurium*, where the interface of flagellin/FliS on FlhA-C was mapped within a hydrophobic "dimple" [29]. This dimple is formed by the interaction sites A1 and A2 (**Figure 33**, A2, A3). Thus, the D1b domain and adjacent regions provide the major interaction site for the flagellin/FliS complex on FlhA-C.

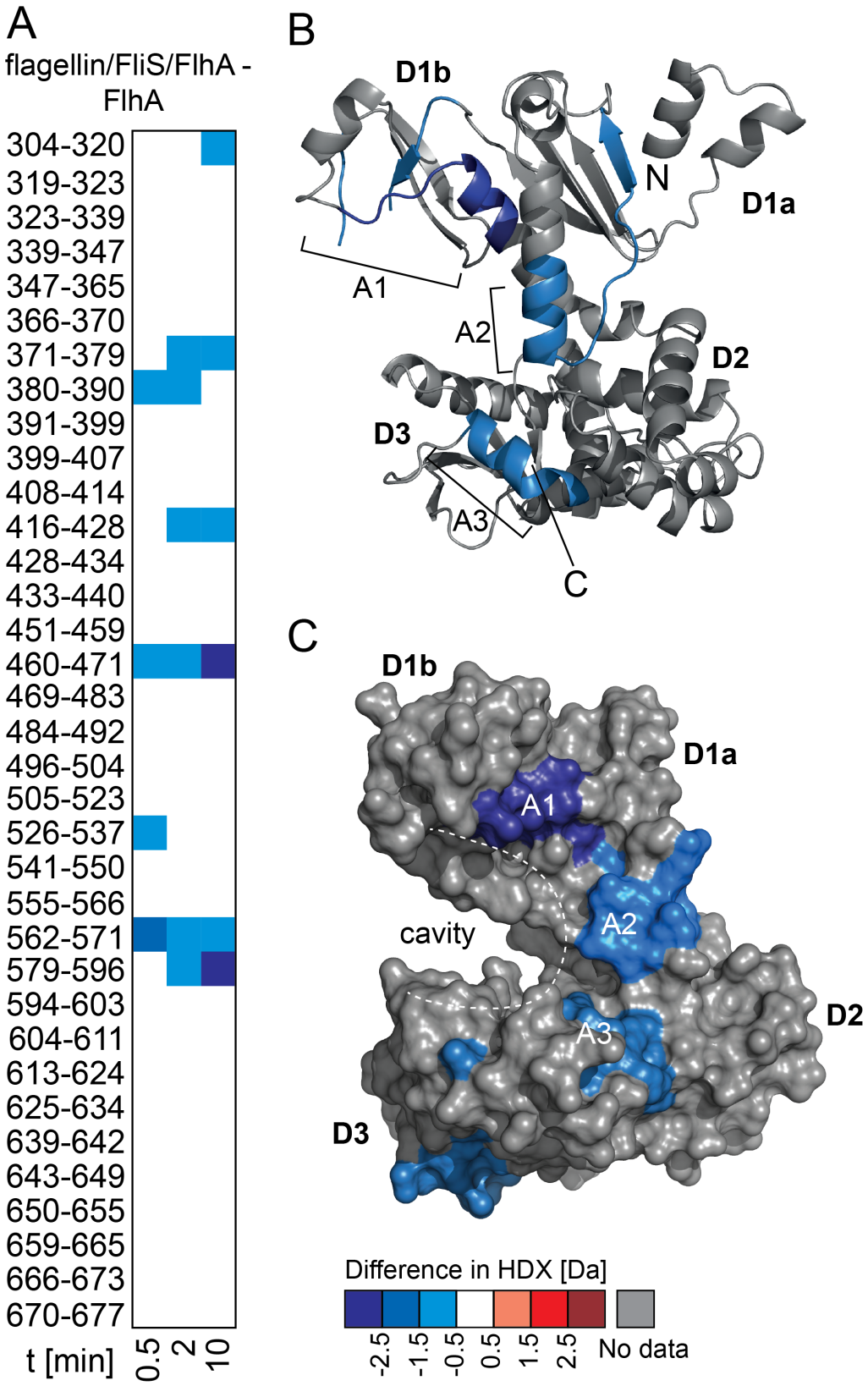

Figure 33: Hydrogen deuterium exchange mass spectrometry (HDX-MS) of FlhA-C compared to FlhA/flagellin/FliS A. Analysis of deuterium exchange in FlhA-C peptides after 30 seconds, 2 minutes and 10 minutes. Numbers indicate amino acids. **B.** Cartoon representation of FlhA-C**.** Regions with less exchange in the FlhA/flagellin/FliS complex are colored in blue, regions with more exchange are colored in red. **C.** Surface representation of FlhA-C. Regions with less exchange in the FlhA/flagellin/FliS complex are colored in blue.

3.4.4 Nascent flagellin is bound to bacterial ribosomes from *B. subtilis*

Determination of the *Gt*CsrA/FliW crystal structure allowed explaining how the binding of FliW sequesters CsrA from the SD sequence at atomic resolution (chapters: 3.1.7 to 3.1.12). Furthermore, FliW recognizes a region at flagellin that is in close proximity to the N-terminus (chapter: 3.3.5). Therefore, one could speculate that FliW might bind shortly after the nascent flagellin chain emerges from the exit tunnel at the ribosome.

To test the scenario in which FliW binds to a nascent flagellin chain directly at the translating ribosome, the flagellin/FliW interaction should be investigated in the context of translating ribosomes. By having a closer look at the recognition of flagellin at the export gate of the fT3SS, FlhA-C, the whole homeostasis mechanism of flagellin could be investigated.

Several biochemical techniques showed that the first 72 residues of flagellin are sufficient for FliW binding, although the interface of the mature flagellin/FliW complex involves also a C-terminal part of the D1-C domain (compare 3.4.3). These findings indicate that the process of FliW binding to flagellin might occur co-translationally as soon as the nascent chain of flagellin emerges from the ribosome.

The process of co-translational capturing is a well-known phenomenon during the production of ribosomal proteins contacting structural RNAs in mature ribosomes [147]. These proteins have highly charged regions (interacting with the negatively charged phosphate backbone of RNAs) and therefore are prone to aggregation within the cytosol. Specialized chaperones recognize the nascent chains and bind to their clients to guide them to the incorporation site and prevent futile polymerization.

To address the idea of a co-translational recognition process by FliW, ribosomes from early- to mid-log phase of *B. subtilis* were purified. Cultures of *B. subtilis* NCIB 3610 were grown to an OD_{600} of 0.6-0.7 and harvested after the addition of 50 µg/ml Chloramphenicol to prevent peptide bond formation and dissociation of 70S ribosomes. Cells were disrupted and the debris removed by centrifugation. Again, chloramphenicol and DDM was added to the cleared lysate and the ribosomes enriched by ultracentrifugation employing a cushion of 17.5 % (w/v) sucrose (**Figure 34**).

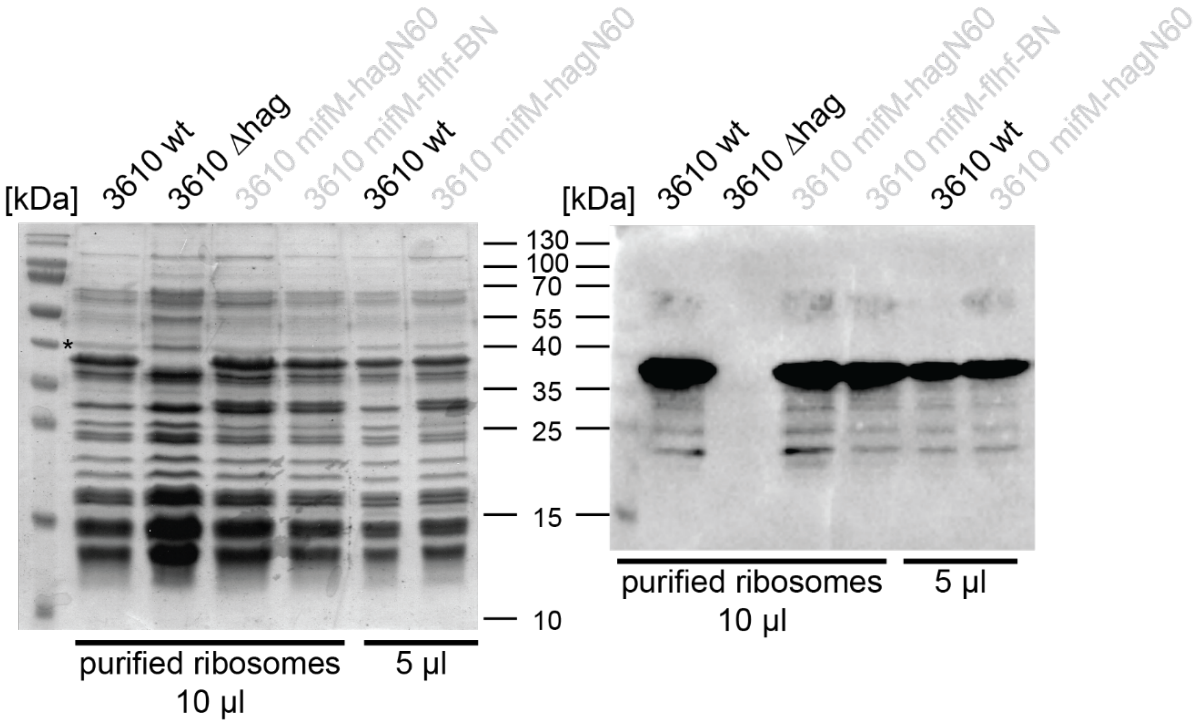

Figure 34: Ribosome purification of *B. subtilis* ribosomes. Coomassie-stained SDS-PAGE and western blot employing an α-flagellin antibody. The molecular weight of the marker is given in kDa.

Interestingly, an SDS-PAGE of the ribosomes after cushion centrifugation showed a prominent signal at 37 kDa reminiscent of flagellin (**Figure 34**, asterisk). It is well known, that *B. subtilis* NCIB 3610 produces high amounts of flagellin during exponential growth but the translation of flagellin *in vivo* has never been monitored before [148]. Therefore, ribosomes of a flagellin deletion strain (Δhag) were purified and the presence of flagellin verified by western blotting employing a flagellin-antibody. Indeed, ribosomes of the wildtype strain exhibited strong flagellin signal which was absent in the flagellin deletion strain, thereby confirming that ribosomes from exponential phase indeed mainly produce flagellin (**Figure 34**). In addition to the signal resembling full-length flagellin, several less prominent signals were visible which could either indicate degradation or translation intermediates of flagellin.

To confirm the purity of ribosomes and to control the presence of 70S ribosomes and polysomes, samples were further separated by a sucrose gradient (**Figure 35**). Sucrose gradients of 10 to 60 % (w/v) were prepared and samples of purified ribosomes added on top of the gradient. By employing an ultracentrifugation step, ribosomes were separated according to their sedimentation constant and then collected by a gradient fractionator.

To investigate whether flagellin is produced by 70S or polysomes, the fractions from gradient centrifugation were analyzed by coomassie-stained SDS-PAGE and western blotting. Indeed,

flagellin can be found in both, the 70S and polysome fractions. However, it is more abundant in the latter (**Figure 35**, B).

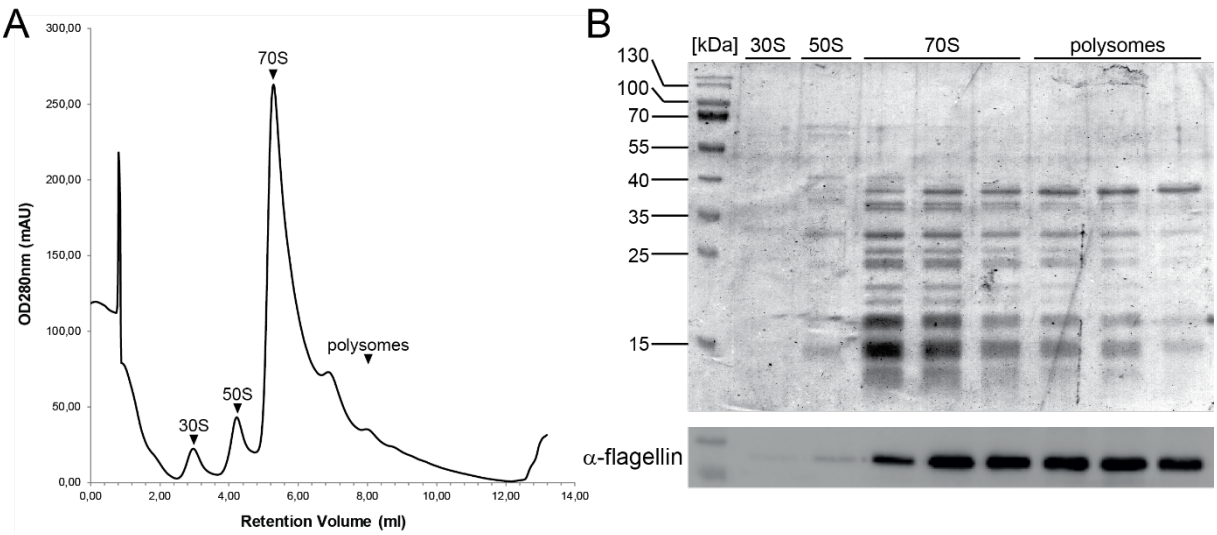

Figure 35: Purification of ribosomes from *B. subtilis*. A. Chromatogram of a ribosome gradient employing *B subtilis* ribosomes. Different ribosomal fractions are highlighted. **B.** SDS-PAGE and western blot of precipitated ribosomal fractions. The molecular weight of the marker is given in kDa.

To verify that the flagellin detected in ribosomal samples did not result from contaminations during the purification process and was indeed a translation intermediate, ribosomes were purified under increasing salt conditions. Only proteins strongly associated with the ribosome and/or nascent chains are not released by increasing KOAc concentrations.

Therefore, ribosomes were purified as described in chapter 6.6.4, incubated in ribosome buffer with different KOAc concentrations and again harvested by ultracentrifugation through a 17,5 % (w/v) sucrose cushion with the respective KOAc concentration. Although some of the signals on an SDS-PAGE corresponding to ribosomal proteins were fainter in the presence of 600 mM KOAc, flagellin amounts did not change significantly (**Figure 36**). This shows that flagellin detected in the purified ribosomes is indeed strongly associated.

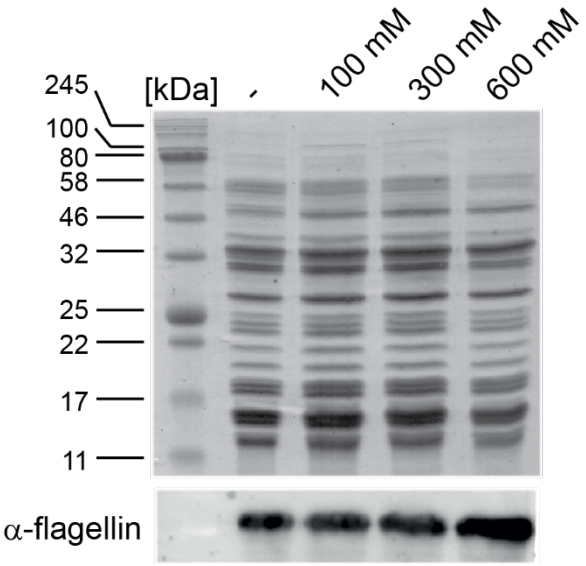

Figure 36: Purification of *B. subtilis* ribosomes with different KOAc concentrations. SDS-PAGE and western blot are shown. The molecular weight of the marker is given in kDa.

Purification of bacterial ribosomes from *B. subtilis* was successfully established, demonstrating that a large sub-population produced flagellin. Gradient fractionation allowed the enrichment of certain ribosomal species, which confirmed that flagellin is not only produced by 70S ribosomes but also and foremost by di- and polysomes.

To get a picture of the purity, samples of 70S ribosomes were spotted on formvar coated copper-grids, stabilized with evaporated carbon film and negatively stained by applying a 2 % (w/v) uranyl acetate solution. Transmission electron microscopy revealed that the samples were almost free of contaminations and contained particles of size and shape similar to bacterial ribosomes (**Figure 37**).

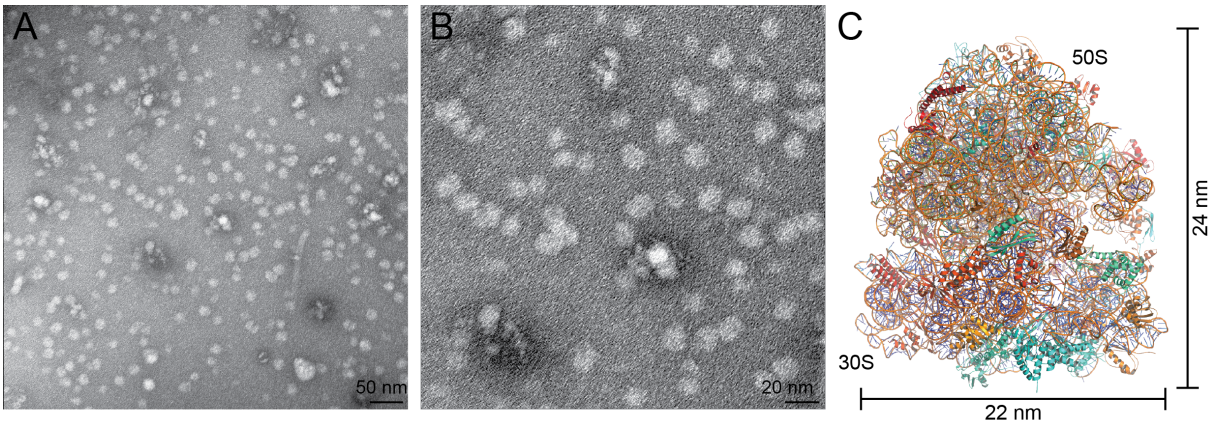

Figure 37: Negative stain electron microscopy images of 70S *B. subtilis* ribosomes. A. *B. subtilis* ribosomes at 15.000-fold magnification. **B**. *B. subtilis* ribosomes at 20.000-fold magnification. **C.** Bacterial ribosome in cartoon representation to display size and shape (PDB-identifier: 3J9W, [149]).

3.4.5 Does FliW interact with flagellin-translating ribosomes?

In the previous chapter, purification of ribosomes from *B. subtilis* was successfully established and purity of the ribosomes verified. However, the main question whether FliW binds to nascent flagellin chains remained to be addressed. The observation that purified ribosomes produce large amounts of flagellin might allow the detection of native FliW, if present.

Therefore, ribosomes from wildtype *B. subtilis* cells and a flagellin deletion strain were enriched by ultracentrifugation, purified FliW added at a final concentration of 10 µM and the binding monitored by western blotting. SDS-PAGE and western blotting confirmed the presence of flagellin only in samples obtained from the wildtype but not the flagellin deletion strain (**Figure 38**).

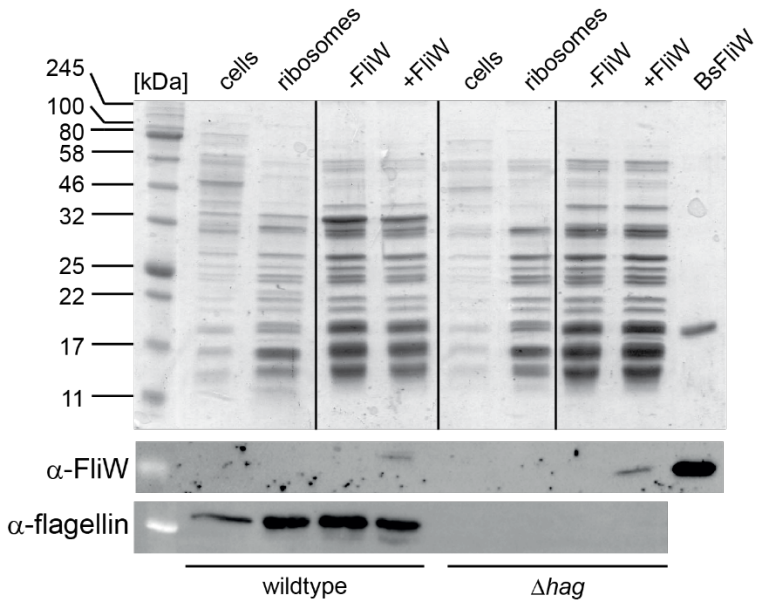

Figure 38: Purification of ribosomes from *B. subtilis* wildtype and flagellin deletion strain. SDS-PAGE and western blot are shown. The molecular weight of the marker is given in kDa.

A FliW signal could not be detected in the ribosomal samples after ultracentrifugation and even after supplementing of purified FliW, the signal remained very faint. In addition to that, a FliW signal was present in both wildtype and flagellin KO strain, indicating that it either bound to ribosomes independently of flagellin presence or just did not properly dissociate during the cushion centrifugation step (**Figure 38**).

Further experiments to investigate the FliW binding are in preparation. However, due to time restraints they could not be included in this thesis.

3.5 Role of the bactofilins BacE and BacF in filament maturation

Bactofilin proteins belong to a widely-conserved protein family that plays a role in cell shape maintenance and bacterial motility [150]. In the Gram-positive model organism *B. subtilis*, two bactofilin homologues (*yhbE* and *yhbF*) can be found in the genome that are part of a transcriptional unit [151]. Based on the presence of a DUF583 (sometimes DUF342), two genes, *yhbE* and *yhbF,* were identified in the *B. subtilis* genome and encode the bactofilins BacE and BacF, respectively. BacE and BacF show 32% sequence identity to each other and 45% and 39% sequence identity to their *Bacillus cereus* orthologs.

It has been shown that a deletion strain of these two genes shows a deficiency in flagellar movement [152]. In addition homologues of BacE and BacF in *Treponema pallidum* were shown to interact with FliS and the flagellar C-ring protein FliY [152]. Both bactofilins form assemblies underneath the cell membrane in close proximity to flagellar basal bodies and can also interact with each other. Recent results could also demonstrate that flagellar assembly is blocked at the stage of hook assembly [151]. However, why flagellar assembly is halted and how BacE and BacF communicate with accessory proteins and/or integral components of the flagellum remains to be shown.

3.5.1 Purification of BacE from *B. subtilis*

Research indicating a link between flagellar proteins and the bactofilins was mostly based on genetic screening and Yeast-2-Hybrid. Therefore, biochemical experiments were required to better understand the role of BacE.

The gene encoding BacE from *B. subtilis* was cloned to pET24d and expressed in *E. coli* BL21(DE3) as described in 6.6.1. After cell disruption, the protein was enriched via Ni-NTA-chromatography (data not shown) and further purified by SEC using a HiLoad 16/600 Superdex 200 column.

Proteins that exceed the columns pore size elute in the “void, which either indicates the presence of a large assembly or aggregation. Only a small sub fraction of BacE eluted in a peak (**Figure 39**, 2). Moreover, most of the protein could be detected in the void fraction (**Figure 39**, 1). In addition to that, impurities resulting from the affinity-purification step could not be separated from the BacE fraction.

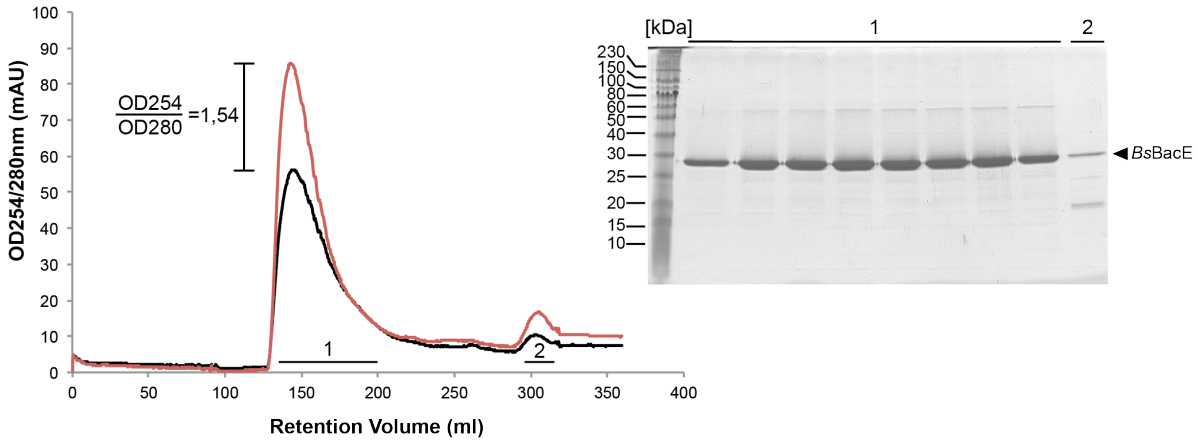

Figure 39: Purification of *B. subtilis* BacE. The chromatogram from size exclusion chromatography (SEC) and the respective coomassie-stained SDS-PAGE is shown. The absorption ratio of 254/280 nm is shown next to the chromatogram. The molecular weight of the marker is given in kDa.

To investigate whether the presence of BacE in the void resulted from affinity to nucleic acids as DNA or RNA, the absorption ratio of 254/280 nm was calculated. However, a ratio of 1.54 showed that the samples only contained protein.

The bactofilin BacE from *B. subtilis* shows a similar behavior to bactofilins purified from *M. xanthus* or *C. crescentus* and seems to form larger assemblies [153]. To confirm if BacE also forms long polymers *in vitro*, samples need to be analyzed by negative-stain electron microscopy. However, this was not yet done within the scope of this work.

3.5.2 Purification of BacF reveals a nucleic-acid bound

Like BacE, the gene encoding BacF from *B. subtilis* was cloned to pET24d and expressed in *E. coli* BL21(DE3) as described in chapter 6.6.1. After cell disruption, the protein was enriched via Ni-NTA-chromatography (data not shown) and further purified by SEC using a HiLoad 16/600 Superdex 200 column.

Purification of BacF revealed the presence of large protein assemblies and/or aggregation on SEC. A large fraction of the protein eluted in the void fraction, however a second peak showed purer BacF, albeit at a lower concentration (**Figure 40**).

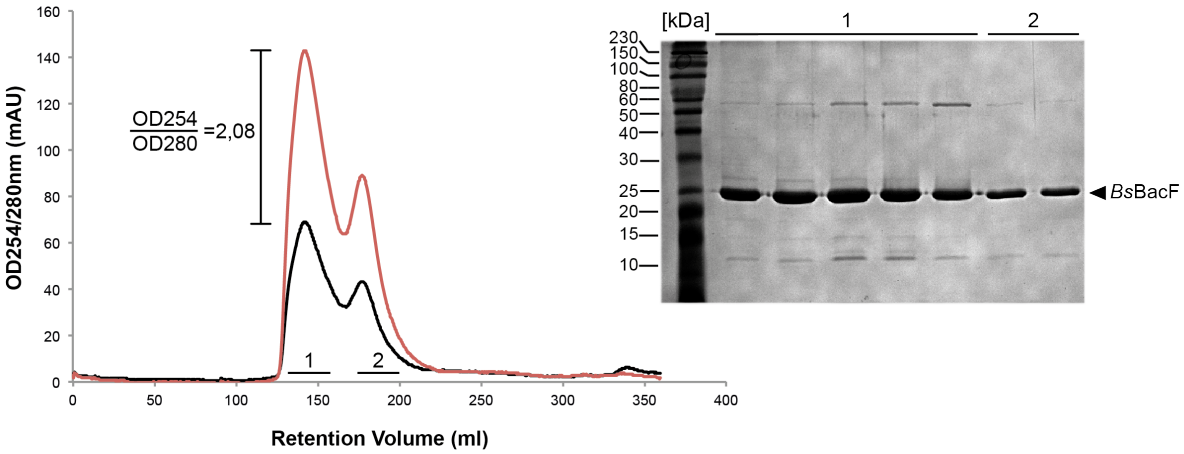

Figure 40: Purification of *B. subtilis* BacF. The chromatogram from size exclusion chromatography (SEC) and the respective coomassie-stained SDS-PAGE is shown. The a*Bs*orption ratio of 254/280 nm is shown next to the chromatogram. The molecular weight of the marker is given in kDa.

Interestingly, a closer look at the absorption ratio of 254/280 nm resulted in a value of 2.08. This might indicate RNA in the elution fractions, as the absorption ratio of pure RNA is 2.00. However, as contamination by nucleic acids during Ni-NTA-affinity chromatography could not be excluded, further verification of RNA present was required.

3.5.3 BacE and BacF form a complex *in vitro*

The two bactofilin proteins of *B. subtilis* are found in a transcriptional unit with *bacE* being the adjacent upstream gene. Purification of either of both proteins revealed that a large sub fraction multimerized and/or aggregated. SDS-PAGE of SEC fractions did not show a degradation of BacE and BacF, which could therefore be excluded as reason for the aggregation. Another reason could be the absence of an interaction partner yielding in the expose of charged or not-properly folded regions. To address whether both bactofilins might require their respective partner, the interaction was investigated by interactions assays.

Both proteins were co-expressed in *E. coli* BL21(DE3) and purified by Ni-NTA-affinity chromatography. Both proteins were fused to a hexahistidine tag and co-expressed with a respective untagged partner to exclude a steric hindrance.

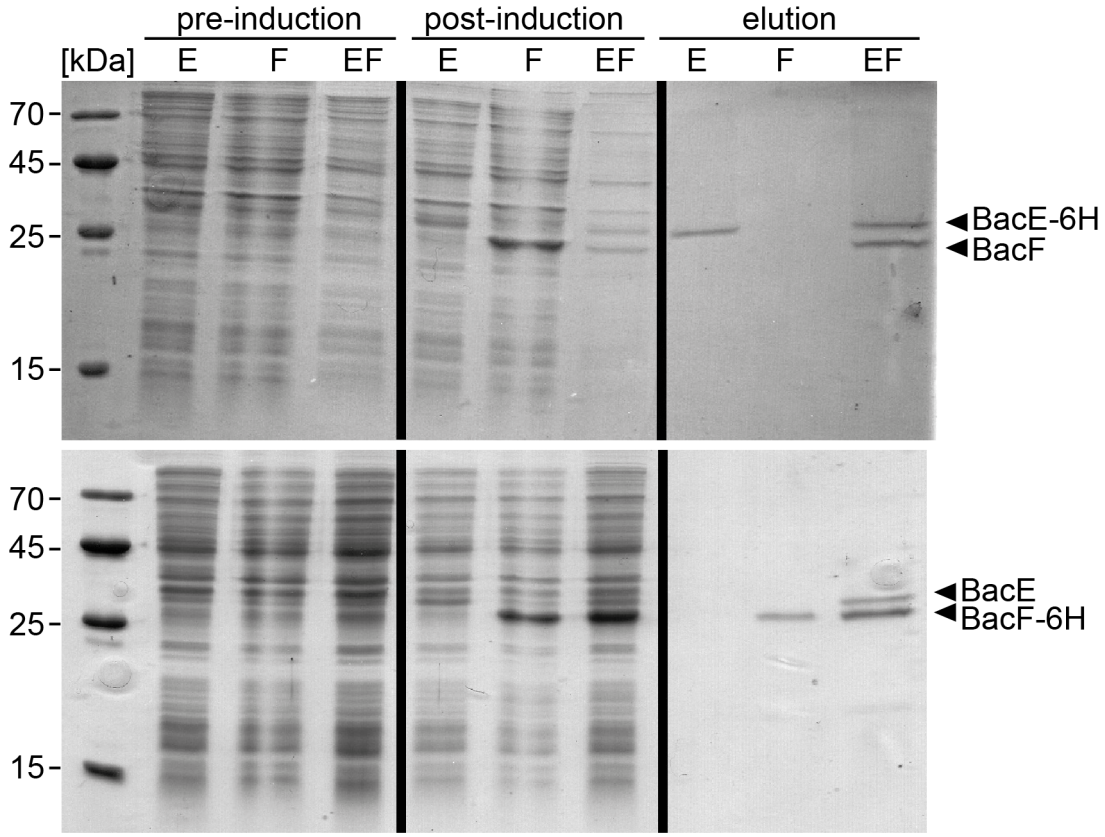

Figure 41: Ni-NTA-affinity purification of the BacE/BacF complex. Coomassie-stained SDS-PAGE of two different experimental set ups is shown. For further information see text. The figure originates from [151].

Interaction of BacE and BacF could be observed in both experiments (**Figure 41**). Conversely, the yield of BacE/BacF complex was even lower compared to purification of the single components.

3.5.4 FliW interacts with BacE and forms a heterotetrameric complex

Co-expression of BacE and BacF did not resolve the multimerization/aggregation problem and thus did not allow the setup of crystallization experiment for structure determination. Rajagopala and co-workers however, identified some other putative interaction partners of the bactofilins. To characterize the interaction of FliY or FliS with BacE and/or BacF, all proteins were co-expressed in *E. coli* BL21(DE3). As no interaction by Ni-NTA-affinity purification could be observed (data not shown), other flagellar components were investigated for interaction with either of the bactofilin proteins.

For BacE, I could identify the flagellar assembly factor FliW as putative interaction partner (**Figure 42A**). The BacE/FliW interaction could be biochemically verified because purified GST-FliW showed an interaction with purified BacE (**Figure 42A**, lane 1), but not with BacF

(**Figure 42A**, lane 2), in pull down assays. The BacE/BacF complex was also included in the interaction assay (**Figure 42A**, lane 3) but the faint signal on the coomassie-stained SDS-PAGE corresponding to BacE and BacF indicated only a residual interaction with GST-FliW.

As a next step, BacE and FliW were co-expressed in *E. coli* BL21(DE3) and enriched by Ni-NTA-chromatography and SEC using a HiLoad 16/600 Superdex 200 column. Both proteins formed a stable complex in SEC but two distinct complex species could be identified. A stoichiometric complex was visible in the fractions eluting at 175 ml (**Figure 42B**, 2) and some BacE/FliW complex again eluted in the column void.

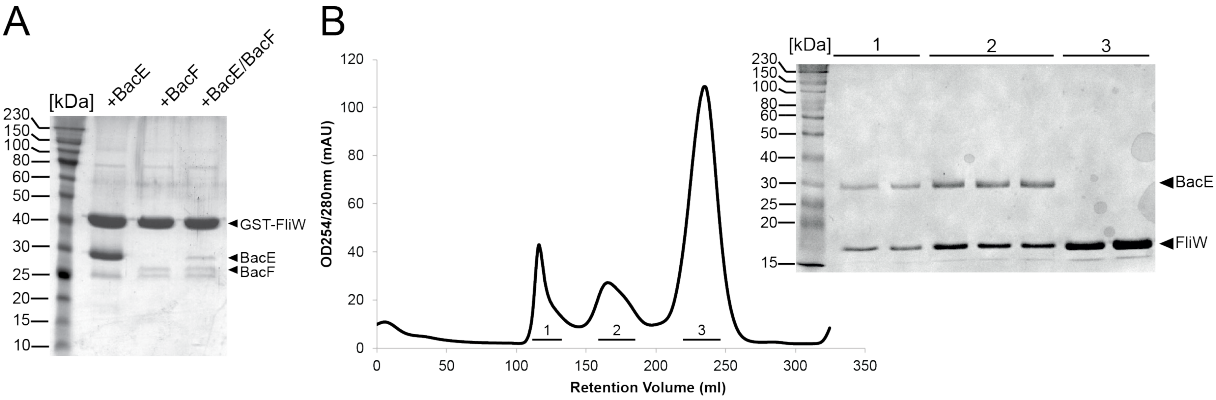

Figure 42: Interaction assay of BacE and FliW and purification of the BacE/FliW complex. A. SDS-PAGE of an interaction assay employing GST-tagged FliW, BacE and BacF. For further information see text. **B.** Purification of BacE/FliW. The SDS-PAGE and respective SEC chromatogram is shown. The molecular weight of the marker is given in kDa.

The BacE/FliW complex from fractions summarized in 2 was pooled and concentrated to a final concentration of 30 mg/ml. Prior to crystallization, the integrity and mono-dispersity of the sample was analysed by Static and Dynamic-light scattering (SLS/DLS). In addition to information about the sample quality, this technique allows to determine the molecular weight and size of the particles analysed [154].

The samples of BacE/FliW analyzed, proved to be homogenous by DLS and had an apparent molecular weight of 78 kDa (**Figure 43**). This is very close to a 2:2 stoichiometry, which would reflect a heterotetramer of BacE(2)/FliW(2). Calculated molecular weight of the complex is 84 kDa (25 kDa x2 + 17 kDa x2). These data show that BacE and FliW form a heterotetramer, and identify the first interaction partner of a bactofilin from *B. subtilis*.

A

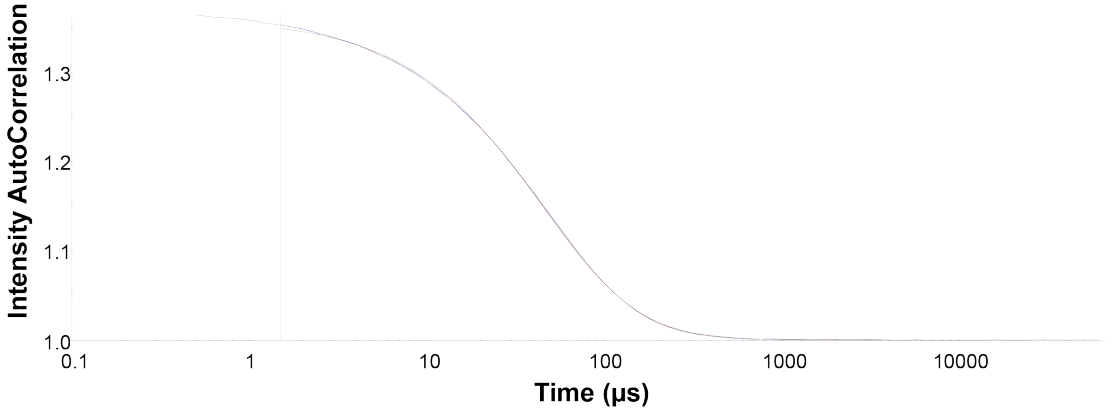

B

Item	Diameter (nm)	Intensity (Cnt/s)	DLS Temp (°C)	Baseline	Mw-S (kDA)	PD Index
BacE/FliW	14.4	534658	25.0	1000	78.22	0.237

	Item	Diameter (nm)	Intensity (Cnt/s)	DLS Temp (C)	Baseline	Mw-S (kDa)	Static Scattering Detector (V)	PD Index
1	Acq 1	14.4	534658	25.0	1.000	78.22	0.33	0.237
2	Acq 2	14.3	564547	25.0	1.000	80.08	0.35	0.241
3	Acq 3	14.2	553370	25.0	1.000	78.80	0.34	0.244
Mean		14.3	550858	25.0	1.000	97.83	0.41	0.241
S		0.1	15102	0.0	0.000	33.47	0.14	0.003
%S		1.0	3	0.0	0.020	34.21	32.71	1.357
S^2		0.0	228055554	0.0	0.000	1120.10	0.02	0.000
Min		14.2	534658	25.0	1.000	78.22	0.33	0.237
Max		14.4	564547	25.0	1.000	80.08	0.35	0.244

Figure 43: DLS/SLS measurement of BacE/FliW. A. Correlation curve of the BacE/FliW DLS-measurement. Shown is a comparison of the intensity of a signal at a time point compared to the intensity after a short delay. Depending on the particle size, the correlation of the signal takes a longer time to decay. A stable correlation curve indicates homogenous particles. **B.** Table of BacE/FliW SLS-measurements. Three acquisitions have been taken over a time period of 30 seconds each. Two measurements indicate a molecular weight of approximately 78 kDa,

Several crystallization attempts were conducted, which did not result in the observation of crystals. Again, homologues of *G. thermodenitrificans* BacE and FliW were employed but again without success.

3.5.5 Both CsrA and flagellin/FliS displace BacE from FliW

FliW has been identified as interaction partner of BacE from *B. subtilis in vitro*. SEC revealed that only a sub-fraction of BacE/FliW complex eluted within one peak, while a considerable amount of both proteins already eluted within the void fraction of the column (compare **Figure 42**). This might indicate that another component (e.g nucleic acid or protein) is necessary to stabilize the BacE/FliW complex.

The interaction of several binding partners with FliW has been biochemically characterized during this work (compare 3.1.7 and 3.3.2). To integrate BacE into the FliW-CsrA-flagellin network, an interaction assay employing GST-FliW as prey protein was performed. BacE, flagellin/FliS and CsrA interacted in a stoichiometric manner with FliW, whereas no binding could be observed for BacF (**Figure 44**). In addition to that, both flagellin/FliS and CsrA could replace BacE from FliW. Only an under stoichiometric amount corresponding to BacE was visible on an coomassie-stained SDS PAGE, although all proteins were included in equimolar amounts (**Figure 44**).

To further characterize the binding of BacE/FliW in the context of flagellin/FliS, an interaction assay with increasing amounts of flagellin/FliS was performed.

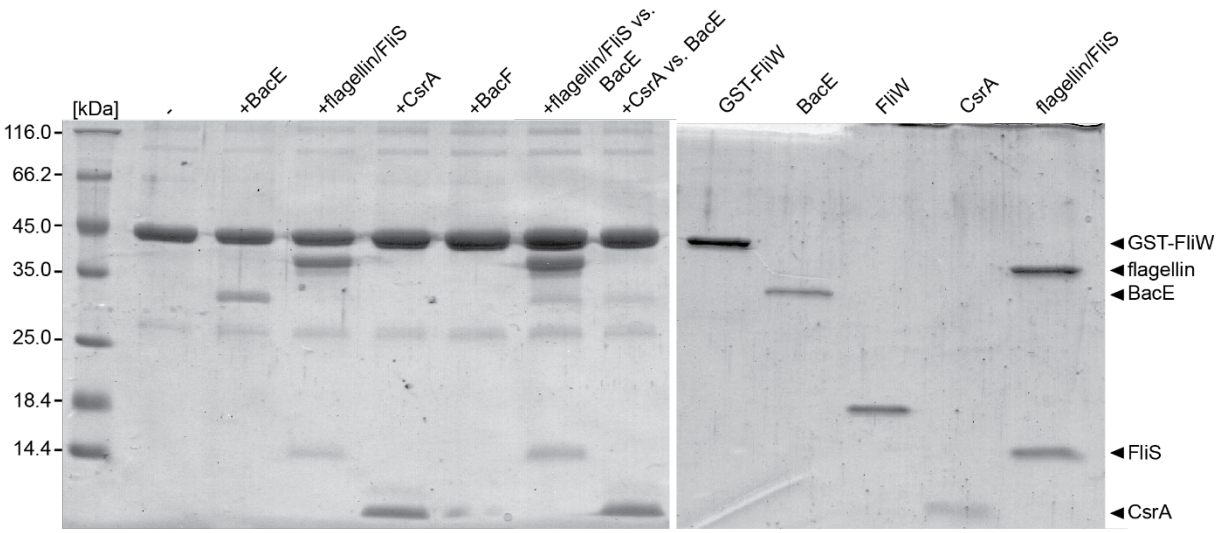

Figure 44: Interaction of FliW, CsrA, flagellin/FliS and BacE. (right) The coomassie-stained SDS PAGE of GST-interaction assays is shown. GST-FliW served as prey, whereas CsrA, flagellin/FliS and BacE were used as bait. (left) Input controls (10 µM) of all proteins used for the interaction assay. The molecular weight of the marker is given in kDa.

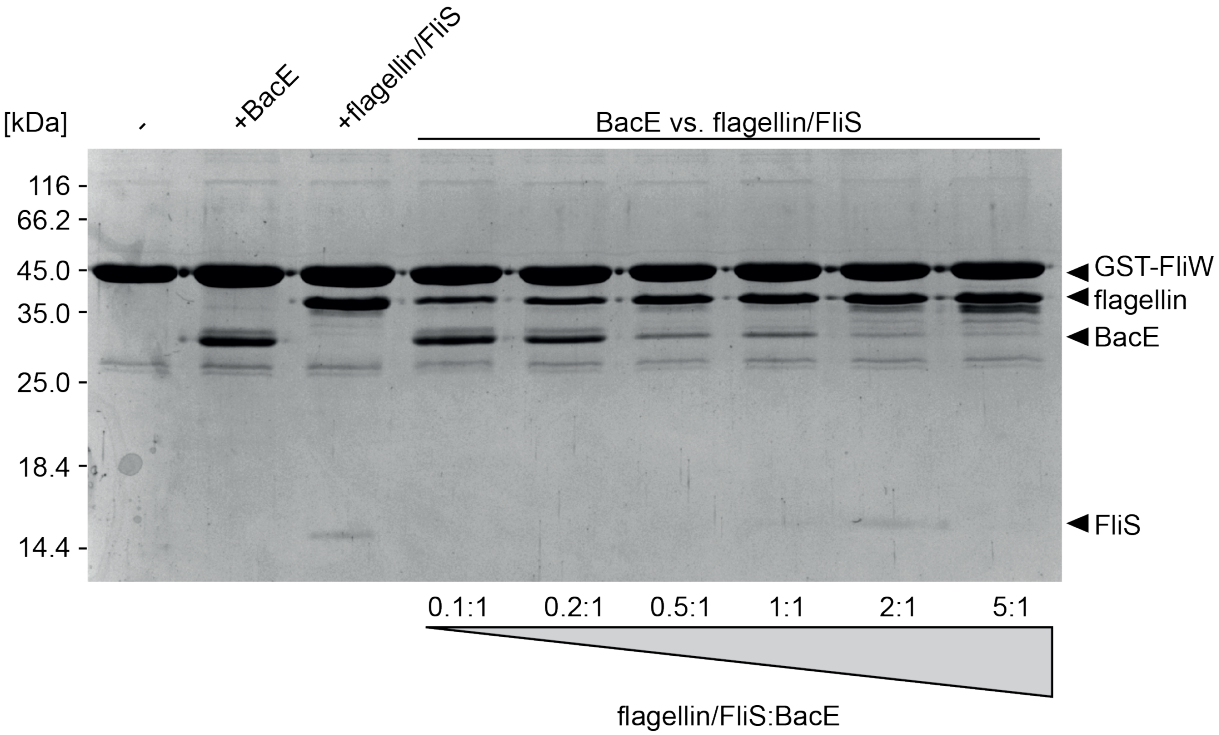

Figure 45: Interaction of BacE and FliW in the presence of flagellin/FliS. The coomassie-stained SDS-PAGE shows GST-FliW as prey and BacE and flagellin/FliS as bait proteins. The molecular weight of the marker is given in kDa.

GST-FliW was immobilized on glutathione-sepharose beads at a concentration of 2 µM and incubated with 20 µM of BacE and flagellin/FliS to confirm the interaction with FliW (**Figure 45**, lane 2 and 3). Next, BacE was incubated with GST-FliW in the presence of increasing amounts of flagellin/FliS. A ratio from flagellin/FliS:BacE of 0.5:1 was sufficient to displace the majority of BacE from FliW (**Figure 45**). An excess of flagellin/FliS even led to a complete displacement of BacE from FliW indicating that FliW prefers flagellin over BacE.

3.5.6 Construct optimization for BacE crystallization

All attempts to crystallize BacE alone or in complex with interaction partners (e.g. FliW and BacF) were unsuccessful. Employing the homologue of *G. thermodenitrificans* did also not result in crystallization as successfully applied in the case of CsrA/FliW. Therefore, different approaches to increase both, solubility and generate crystal-packing forces, were tested.

The second protein structure ever determined was the one of chicken egg lysozyme [155], which also proved to be excellently suited for crystallography earlier [156]. Nowadays, it is still commonly used to demonstrate the process of crystallization to students during their studies and to facilitate crystallization of other proteins.

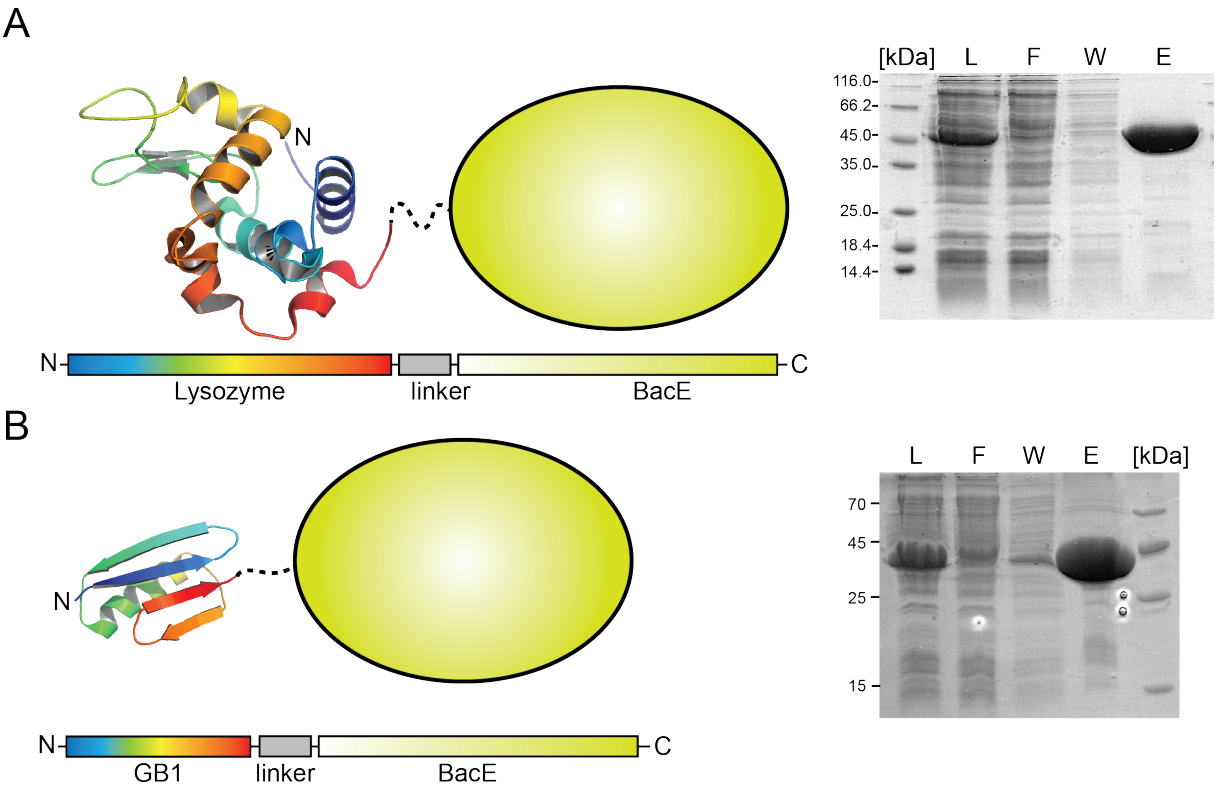

Figure 46: Construct design of T4L-*Gt*BacE and GB1-*Gt*BacE. A. Lysozyme and GB1 are colored in rainbow colors from N- to C-terminus and display in cartoon representation. The coomassie-stained SDS-PAGEs show fractions collected from a Ni-NTA-purification. (L) column load, (F) column flow through, (W) column wash, (E) column elution. The molecular weight of the marker is given in kDa.

Another protein domain that has proven to increase the solubility of target proteins and is usually used in nuclear magnetic resonance (NMR) experiments, is the immunoglobulin beta 1 binding domain of protein G (GB1). Although it has not been reported to facilitate crystallization, it could be used to increase the yield of BacE after purification and possibly change the migration behavior on SEC.

Therefore, lysozyme from T4 phage and GB1 were N-terminally fused to BacE from *G. thermodenitrificans* and expressed in *E. coli* BL21(DE3). To allow certain flexibility, a short GS-linker was included in both constructs (**Figure 46**). Both proteins could be expressed in large amounts and showed no degradation or insolubilities. Interestingly, precipitation of both fusion constructs could be observed at 4 °C but not at room temperature.

After enrichment by Ni-NTA-chromatography the proteins were further purified by SEC using a HiLoad 16/600 Superdex 200 column (**Figure 47**). Interestingly, both fusion proteins migrated as a stable fraction on SEC, indicating that the N-terminal fusion either interfered with intramolecular contacts disrupting a larger assembly of BacE or facilitated a proper folding (**Figure 47**).

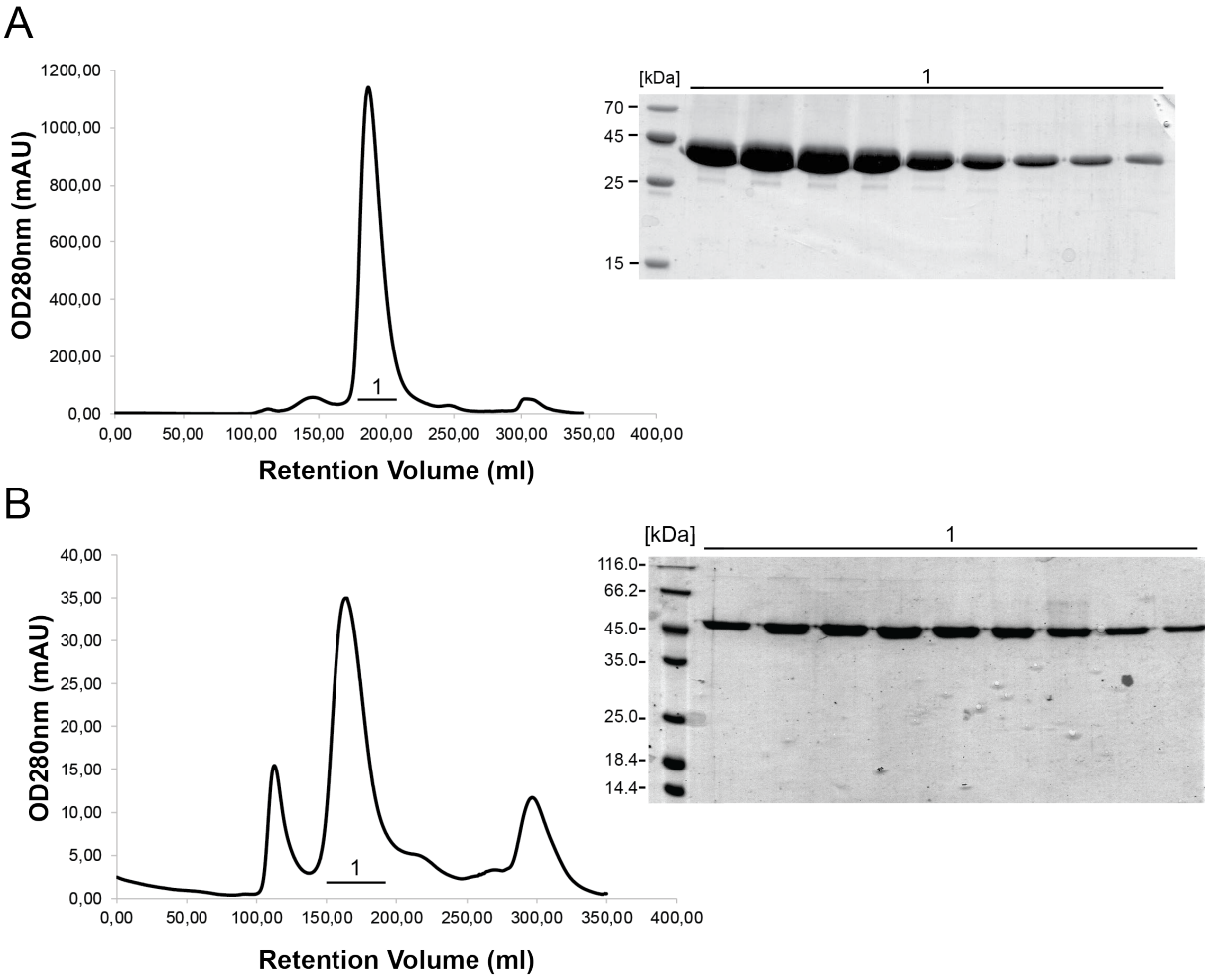

Figure 47: Purification of GB1-*Gt*BacE and T4L-*Gt*BacE. The chromatograms from size exclusion chromatography (SEC) and the respective coomassie-stained SDS-PAGEs are shown. The molecular weight of the marker is given in kDa.

In addition to that, purification of both proteins yielded amounts sufficient for crystallography (GB1-*Gt*BacE: 33 mg/ml, T4L-*Gt*BacE: 15 mg/ml).

3.5.7 Crystallization of GB1-BacE from *G. thermodenitrificans*

To crystallize GB1-*Gt*BacE, a crystallization experiment was set up with 33 mg/ml and 16.5 mg/ml of protein in a sitting-drop experiment. 500 nl of protein was mixed with the same amount of mother liquor. GB1-*Gt*BacE crystallized in several conditions within two weeks of incubation at room temperature (**Figure 48A-D**). Prior data collection, crystals were flash-frozen in liquid nitrogen employing a cryo-solution that consisted of crystallization buffer supplemented with 10 % (v/v) 2-Methyl-2,4-pentanediol (MPD).

Most of the crystals diffracted only to 8-10 Å resolution and therefore had to be improved. However, crystals obtained in 0.1 M Ammonium acetate, 0.1 M citrate pH 5.6, 30 % MPD diffracted to ~4 Å, which was close to a resolution promising for structure solution (**Figure 48C**).

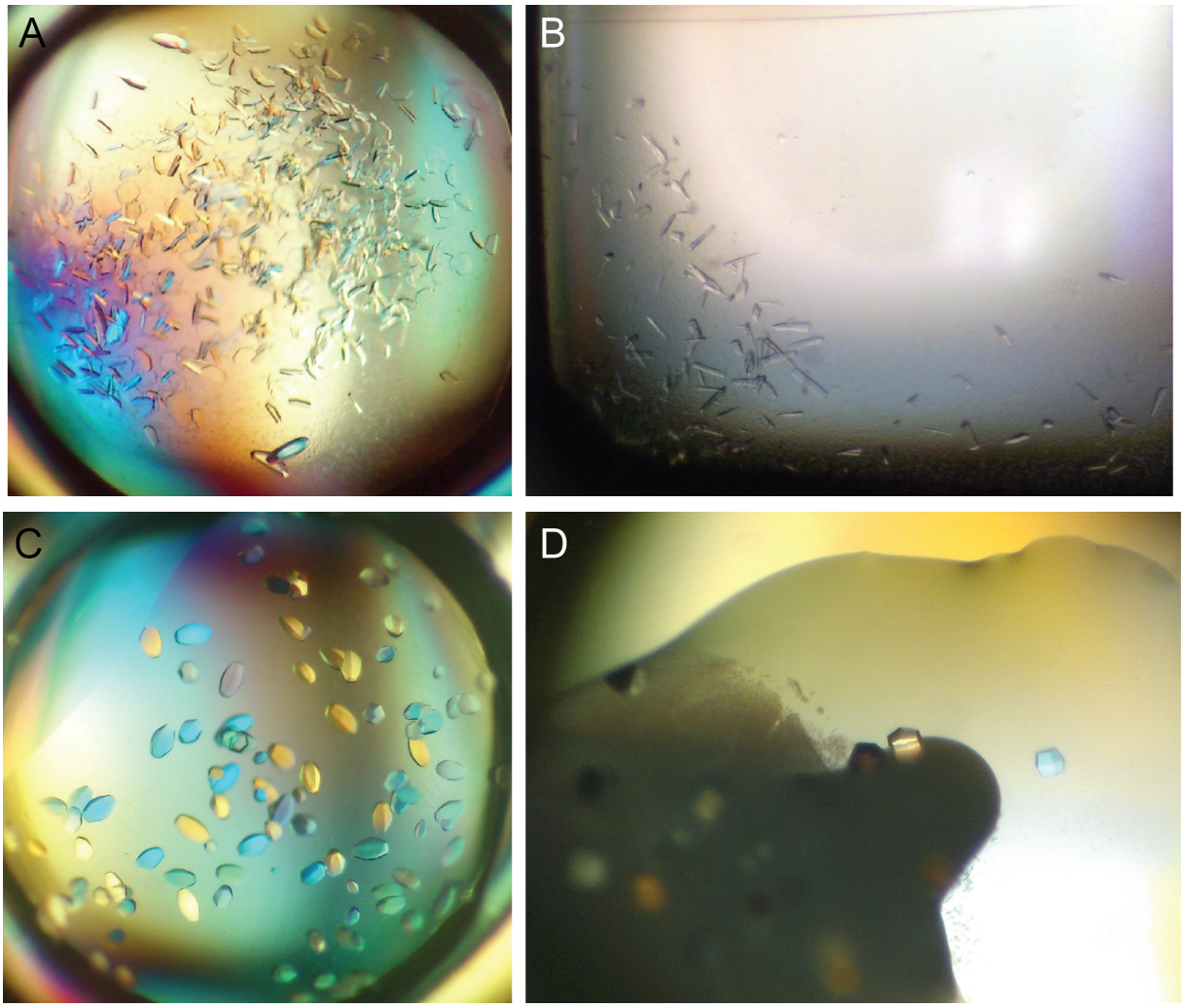

Figure 48: Crystallization of GB1-*Gt*BacE. A 0.1 M Tris pH 7.0, 0.2 M Ammonium sulphate, 40 % MPD **B.** 0.1 M Citrate pH 5.5, 30 % 1,2-propanediol, 20 % MPD **C.** 0.1 M Ammonium acetate, 0.1 M citrate pH 5.6, 30 % MPD **D.** 0.2 M CaAc, 0.1 M MES pH 6.0, 10% Isopropanol.

Fine screening of one condition improved crystal quality significantly (0.24 M Ammonium acetate, 0.1 M citrate pH 5.6, 30 % (v/v) MPD) but several attempts to increase the crystal quality by micro- or macro seeding were unsuccessful and therefore an additive screen was setup consisting of 24 unique conditions (**Table 4**). A 96-well plate was used for the additive screen, allowing adding the solutions to four different conditions (24x4). 27 µl of crystallization cocktail was layered in the reservoir of the crystallization plate, 3 µl of additive

solution added and mixed thoroughly. Again, 500 nl of protein was mixed with the same amount of precipitant solution (+additive).

GB-*Gt*BacE crystallized in various conditions and was subsequently analyzed by X-ray diffraction. Several additives could indeed increase the resolution of diffracting crystals up to 3.2 Å resolution (**Figure 49**, **Table 4**).

Table 4: Additive screen used for the crystallization of GB1-*Gt*BacE. Conditions are marked that increased the resolution substantially (XX) or moderately (X).

Well	Agent	Classification	Final conc	Crystallization hit
1	0.1 M Zinc Chloride	Multivalent	10 mM	
2	0.1 M Fe(III)Citrate	Multivalent	10 mM	
3	0.1 M I3C	Multivalent	10 mM	
4	1 M Glycin	Linker	100 mM	X
5	0.1 M Taurine	Linker	10 mM	
6	2 M Sodium Chloride	Salt	200 mM	XX
7	1 M Ammonium sulfate	Salt	100 mM	XX
8	1 M Sodium Citrate	Salt	100 mM	
9	0.1 M EDTA	Chelating Agent	10 mM	
10	1 M Guanidine HCl	Chaotrope	100 mM	
11	0.1 M Urea	Chaotrope	10 mM	
12	-	-	-	X
13	30 % w/v Sucrose	Carbohydrate	3 %	
14	30 % w/v Lactose	Carbohydrate	3 %	
15	30 % w/v Glucose	Carbohydrate	3 %	
16	30 % w/v Fructose	Carbohydrate	3 %	
17	30 % PEG 400	Polyol	3 %	
18	30 % PEG 3350	Polyol	3 %	
19	30 % PEG 6000	Polyol	3 %	
20	30 % PEG 8000	Polyol	3 %	XX
21	30 % v/v Glycerol	Polyol	3 %	
22	40 % v/v Acetone	Organic; Volatile	4 %	
23	30 % v/v Ethanol	Organic; Volatile	3 %	
24	30 % v/v Methanol	Organic; Volatile	3 %	

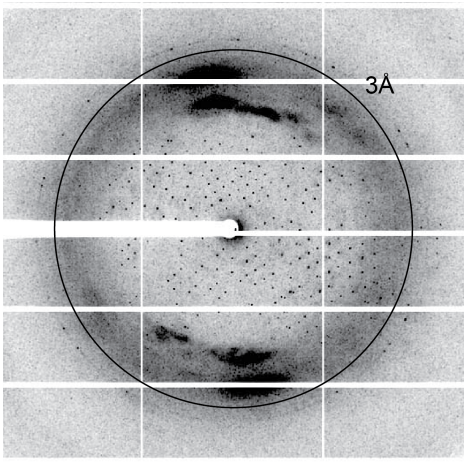

Figure 49: Diffraction image of a GB1-*Gt*BacE crystal. The crystal diffracts to ~3Å as depicted by the black circle but shows some anisotropy.

3.5.8 Structure solution of GB1*Gt*BacE

Improved crystals of GB1-*Gt*BacE were obtained that belonged to the hexagonal space group P622. Datasets were collected at the European Synchrotron Radiation Facility (ESRF, Grenoble), processed, integrated and scaled with XDS and merged with the program AIMLESS from the ccp4 suite (see section 6.8.). The unit cell had the parameters: a=83.73 Å, b=83.73 Å, c=179.28 Å; α= 90.0 ° β= 90.0 ° γ= 120.0 ° (**Table 5**). Calculation of the asymmetric unit (ASU) content by CCP4-integrated Matthews [157] predicted 330 amino acids residues with a solvent content of 50 %. This would refer to a monomer in the ASU.

A NCBI BLAST (http://blast.ncbi.nlm.nih.gov/Blast.cgi) search employing the PDB-blast algorithm did not result in homologous structures apart from the NMR structure of a bactofilin homologue from *Caulobacter vibroides* that became available during this study (PDB-identifier: 2N3D, [158]) and was therefore used as a search model for molecular replacement (MR). Despite several attempts of model truncation, including the use of MrBump, a program for automated structure solution [159], phase determination was not possible. A secondary structure prediction of BacE revealed the presence of only β-strands, which was reminiscent of 2N3D but obviously certain differences on tertiary structure level prevented molecular replacement. The use of several GB1 structures for MR was also unsuccessful, possibly due to the small size of GB1 (7 kDa) being insufficient for structure solution.

To overcome the difficulties of MR, experimental phasing by using selenomethionine (SeMet) labelled GB1-*Gt*BacE was employed.

Table 5: Data collection statistics of GB1-*Gt*BacE. Values in parenthesis refer to the highest resolution shell.

		GB1-*Gt*BacE (SeMet)	GB1-*Gt*BacE (native)
Data collection	Space group	P622	P622
	Cell dimensions		
	a, *b*, *c* (Å)	83.729	82.18
		83.729	82.18
		179.281	179.35
	α, β, γ (°)	90.00	90.00
		90.00	90.00
		120.00	120.00
	Energy (keV)	12.656	13.52
	Resolution (Å)	46.12 - 3.00	45.78 – 2.99
		(3.19 - 3.00)	(3.18 -2.99)
	R_{merge}	0.054 (0.844)	0.047 (0.575)
	$I / \sigma I$	16.9 (1.9)	10.8 (1.6)
	Completeness (%)	99.7 (99.0)	98.5 (98.8)
	Redundancy	10.3 (10.2)	4.2 (4.3)
	Anomalous completeness (%)	99.5 (97.9)	-
	Anomalous redundancy (%)	5.5 (5.4)	-

An overnight culture of *E. coli* BL21(DE3) in rich medium (LB) was used to inoculate minimal medium containing selen labelled methionine. The cultures were induced with 1 mM IPTG at OD_{600} of 0.5 and incubated at 37 °C overnight.

After Ni-NTA chromatography and SEC, the protein was concentrated to 33 mg/ml and used for crystallization experiments (data not shown). SeMet-GB1-*Gt*BacE crystallized in the same conditions as the native variant and additive screening further optimized crystals.

Prior data collection, crystals were flash-frozen in liquid nitrogen employing a cryo-solution that consisted of crystallization buffer supplemented with 20 % (v/v) MPD. The crystals diffracted to 3.4 Å and several datasets were collected at the absorption edge of selenium. An energy fluorescence scan revealed a strong signal and confirmed the incorporation of seleno-methionine in the protein and thus the crystals of GB1-*Gt*BacE.

The data were processed, integrated and scaled with XDS and merged with the program AIMLESS from the ccp4 suite (see chapter 6.8.). Crystals again belonged to the hexagonal space group P622 and could be integrated with the same unit cell parameters as native crystals. An anomalous signal was present to a resolution of 3.9 Å, indicating that experimental phasing could be successful.

Several programs were used for substructure determination, e.g. SHELXC/D/E combined with CCP4-integrated CRANK [160,161] and the PHENIX suite [162]. However, no substructure could be determined and phasing was not yet successful.

3.5.9 Purification, Crystallization and structure solution of GB1-BacE from *B. subtilis*

In a next step, the GB1 construct was used to improve the yield of BacE from *B. subtilis* and the fusion construct expressed in *E. coli* BL21(DE3) as described in 6.6.1. The protein was enriched by Ni-NTA chromatography and further purified by SEC using a HiLoad 16/600 Superdex 200 column (**Figure 50**). Contrary to the behavior of *Gt*BacE, the *B. subtilis* homologue retained its ability to multimerize or aggregate and eluted in the column void. The fractions were pooled, concentrated to 40 mg/ml and used for crystallization experiments.

GB1-*Bs*BacE crystallized after 3 weeks in 0.2 M Sodium thiocyanate, 20 % PEG 3350 and 0.2 M Sodium iodide, 20 % PEG 3350. Only small crystals could be detected, which did not re-appear upon fine screening of the conditions. Crystals were harvested in a cryo-solution containing the respective precipitant solution including 25 % glycerol and flash-frozen in liquid nitrogen.

Datasets were collected at the European Synchrotron Radiation Facility (ESRF, Grenoble), which belonged to the monoclinic space group $P2_1$. The unit cell had the dimensions: a= 42.64, b=78.13, c=48.41; α=90.00, β=99.33, γ=90.00. Calculation of the Matthews coefficient indicated that one monomer of 33 kDa would fit in the asymmetric unit assuming a solvent content of 49 %.

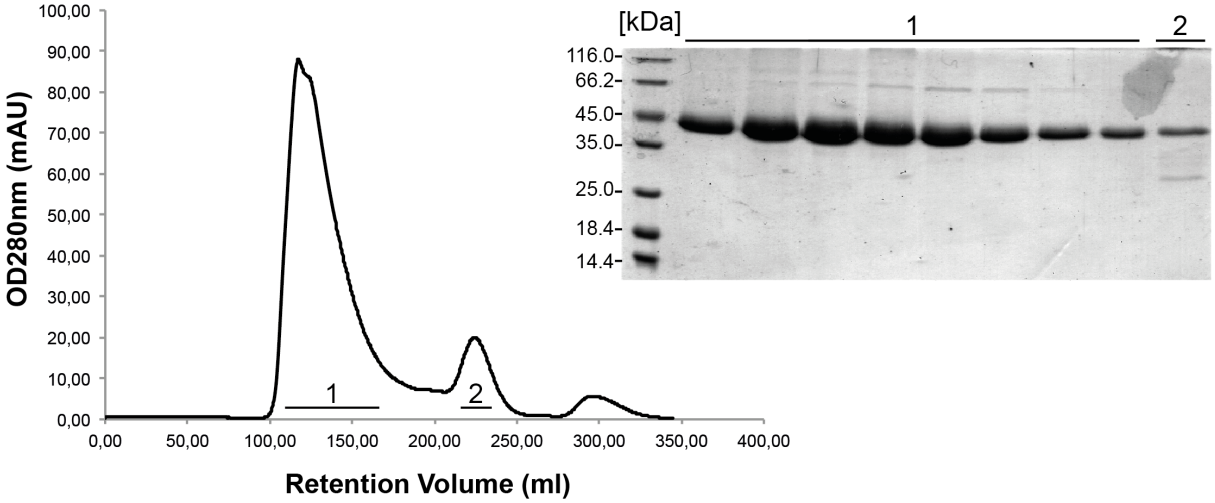

Figure 50: Purification of GB1-*Bs*BacE. The chromatogram from size exclusion chromatography (SEC) and the respective coomassie-stained SDS-PAGE is shown. The molecular weight of the marker is given in kDa.

The data were processed, integrated and scaled with XDS and merged with the program AIMLESS from the ccp4 suite (**Table 6**, see chapter 6.8). Several attempts for molecular replacement were unsuccessful (compare 3.5.8) but experimental phasing was not yet conducted and could therefore not be included in this work.

Table 6: Data collection statistics of GB1-*Bs*BacE. Values in parenthesis refer to the highest resolution shell.

		GB1-*Bs*BacE
Data collection	Space group	$P2_1$
	Cell dimensions	
	a, *b*, *c* (Å)	42.65
		78.13
		48.41
	α, β, γ (°)	90.00
		99.33
		90.00
	Resolution (Å)	47.77 – 2.10
		(2.16 -2.10)
	R_{merge}	0.28 (0.90)
	$I / \sigma I$	7.6 (4.0)
	Completeness (%)	99.8 (99.7)
	Redundancy	6.2 (6.0)
	Anomalous completeness (%)	-
	Anomalous redundancy (%)	-

3.5.10 Expression and purification of a bactofilin homologue from *H. pylori* and flagellar associated proteins from *S. putrefaciens* and *T. maritima*

So far, all attempts to solve the crystal structure of bactofilins from *B. subtilis* and the closely related *G. thermodenitrificans* were unsuccessful. The use of solubility/crystallization tags facilitated the crystallization process and increased the yield of purified protein but did not result in resolving the crystal structure.

A different approach however, was the search for bactofilin homologues in other organisms for crystallization experiments. The NCBI BLAST algorithm was used to find genes encoding bactofilin homologues in *H. pylori*, *S. putrefaciens* and *T. maritima*. Interestingly, another domain of unknown function (DUF) besides the bactofilin domain was predicted for the *B. subtilis* homologs BacE and BacF. The DUF342 seems to describe a different class of proteins of much larger size, which might share certain homologies to the bactofilin proteins (**Figure 51**).

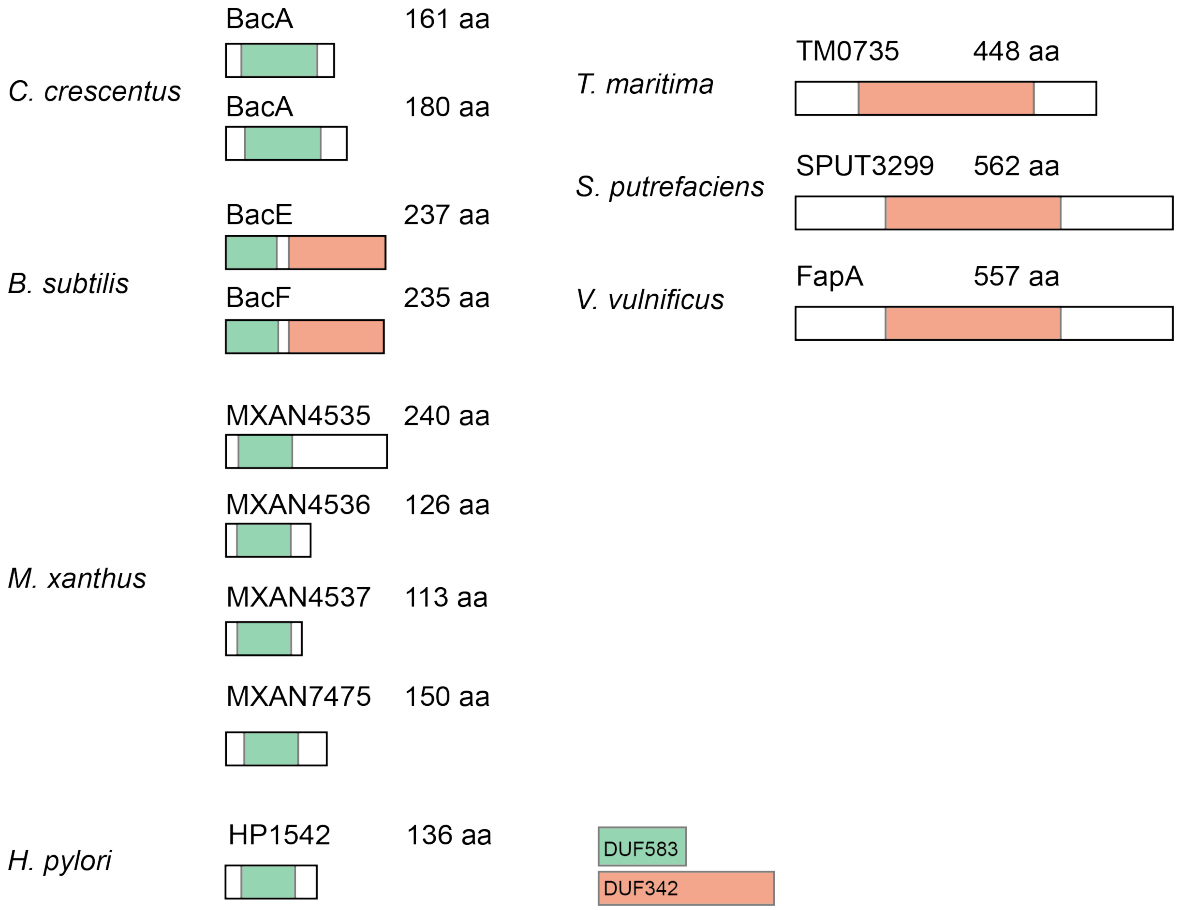

Figure 51: Architecture of bactofilin proteins and flagellar-associated proteins. Bactofilin homologues that have been described are listed on the left side including the bactofilin (DUF583) domain (green box). The DUF342-containing proteins are indicated with a red box.

The genes were cloned to pET24d, expressed and purified by Ni-NTA chromatography (**Figure 52**). The gene encoding SPUT3299 from *S. putrefaciens* did not express well by induction with 1 mM IPTG and was therefore omitted for further optimization in the future (only a faint signal in the coomassie-stained SDS PAGE at 62 kDa, **Figure 52**).

The Hp1542 homologue of *H. pylori* encodes a rather small bactofilin of 15 kDa, which resembles the size of bactofilins found and described in *M. xanthus* and *Camplyobacter* species (**Figure 52**). In addition to that, research in *Treponema pallidum* and *H. pylori* indicated a different connection of the bactofilins to the flagellar assembly apparatus via FliS [152]. The low yield obtained from purification of HP1542 required further improvements and interaction assays with flagellar components could not be included in this work.

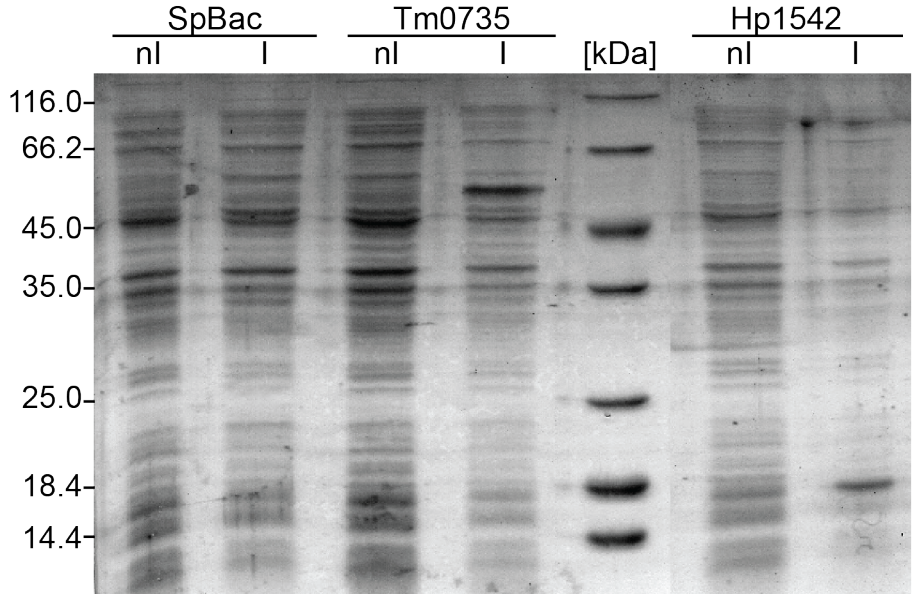

Figure 52: Expression of different bactofilin homologues in *Helicobacter pylori* and flagellar associated proteins in *Shewanella putrefaciens*, *Thermotoga maritima.* A coomassie-stained SDS-PAGE of samples containing whole cell lysate is shown prior and 3 hours after induction with 1 mM IPTG. The molecular weight of the marker is given in kDa.

Tm0735, which encodes the large (49 kDa) homologue of *T. maritima* expressed well and was therefore expressed in *E. coli* BL21(DE3). After cell disruption, the protein was enriched by Ni-NTA chromatography and SEC using a HiLoad 16/600 Superdex 200 column. The protein eluted at 200 ml in a stable fraction and could be concentrated to 80 mg/ml (**Figure 53**).

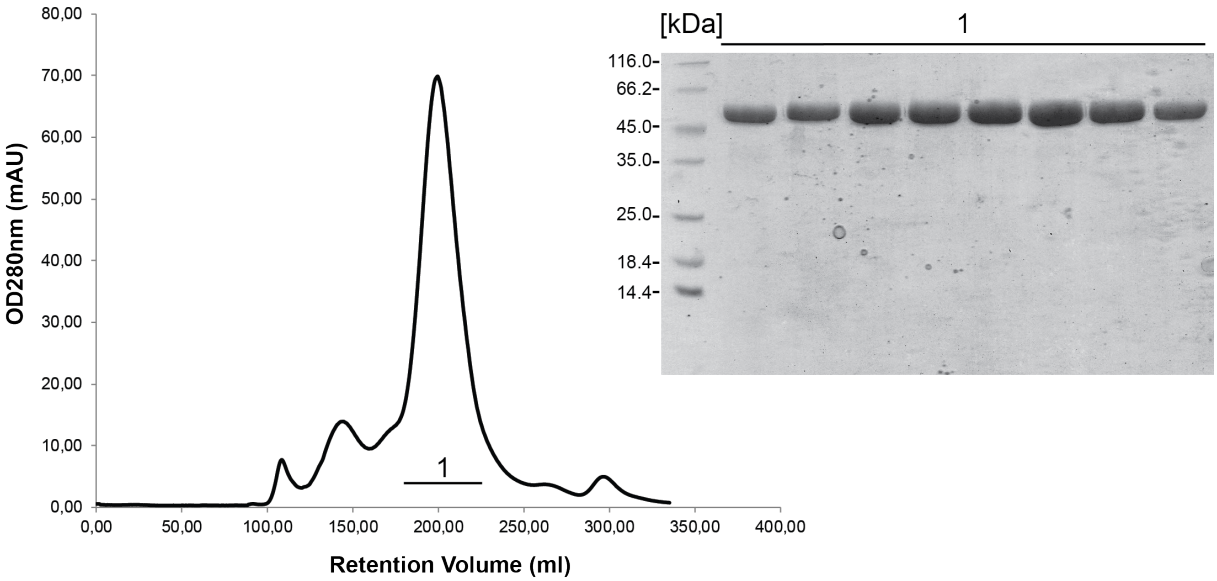

Figure 53: Purification of Tm0735. The chromatogram from size exclusion chromatography (SEC) and the respective coomassie-stained SDS-PAGE is shown. The molecular weight of the marker is given in kDa.

3.5.11 Crystallization of the putative bactofilin Tm0735 from *T. maritima*

Crystals of Tm0735 appeared over night at a concentration of 40 mg/ml in a condition containing 0.2 M Magnesium chloride, 0.1 M Tris pH 7.0, 2.5 M Sodium chloride. Crystals were optimized by macro-seeding (**Figure 54**). This technique requires the presence of initial crystals that are transferred with a nylon loop or whisker into a new well containing fresh protein and precipitant solution. The availability of a nucleation starting point often facilitates the growth of larger crystals and might improve the quality of crystals. However, in this case crystals grew much larger (up to 300 µm) but the resolution did not improve accordingly. Crystals tested at the ESRF only diffracted up to 5-6 Å and therefore need to be improved in the future to allow structure solution.

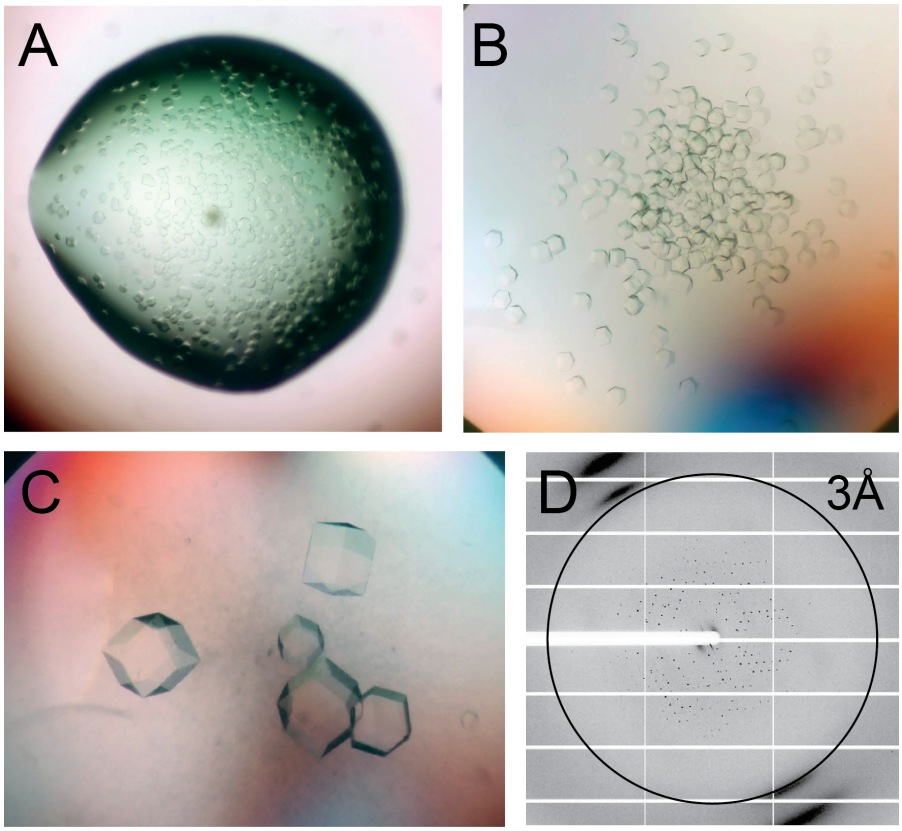

Figure 54: Crystallization of Tm0735. A. Crystals observed in 0.2 M Magnesium chloride, 0.1 M Tris pH 7.0, 2.5 M Sodium chloride were improved by macro-seeding (**B, C**) and diffracted to 5-6 Å. **D.** Diffraction pattern (numbered circle indicates the resolution).

4 DISCUSSION

4.1 FliW is a small regulatory protein with a novel fold

The gene encoding the FliW protein can be found in a variety of flagellated bacterial species and is often located within a transcriptional unit with *csrA* being the adjacent downstream gene [133]. The *fliW* gene was first discovered in *T. pallidum* and shown to be also present in *B. subtilis* and *C. jejuni* [145]. Initial results obtained in the study named above showed a drastic decrease in motility in a *fliW* deletion strain and suggested FliW to be a flagellar assembly factor like FliS. Titz and coworkers could also demonstrate that FliW binds to a region close to the C-terminus of flagellin thereby having a stabilizing effect [145]. The interaction of flagellin and FliW was further analyzed in *B. subtilis* and the role of CsrA integrated into the model of flagellin homeostasis [133].

To gain a deeper insight into the role of FliW in *B. subtilis*, its atomic structure was determined by X-ray crystallography (compare 3.1.5). The structure of FliW was analyzed and resembled a novel fold reminiscent of a very compact β-barrel (**Figure 9**). This β-barrel like architecture has first been described for a class of very diverse oligonucleotide/oligosaccharide binding proteins (OB)[163]. Although FliW shares no sequence homology to any of the classical OB-fold proteins and can barely be superposed to these proteins (r.m.s.d. values range from 5 to 9, data not shown), the overall structure shows some clear similarities. The β-barrel core is composed of five β-strands and a capping α-helix is located between β3 and β4, which is partially resembled by FliW (**Figure 55**, black arrow).

OB-fold members have been grouped into 27 functional families with activities ranging from molybdate-binding proteins to RNA chaperones [164,165]. It is hypothesized that these proteins derived from a common evolutionary ancestor but evidence is lacking. In addition to that, it can be difficult to distinguish between convergent and divergent evolution, especially when the protein functions show a high degree of diversity [166]. During this study, no direct interaction of FliW with oligonucleotides could be observed and the fold-differences render it therefore unlikely that FliW might be related to OB-fold proteins.

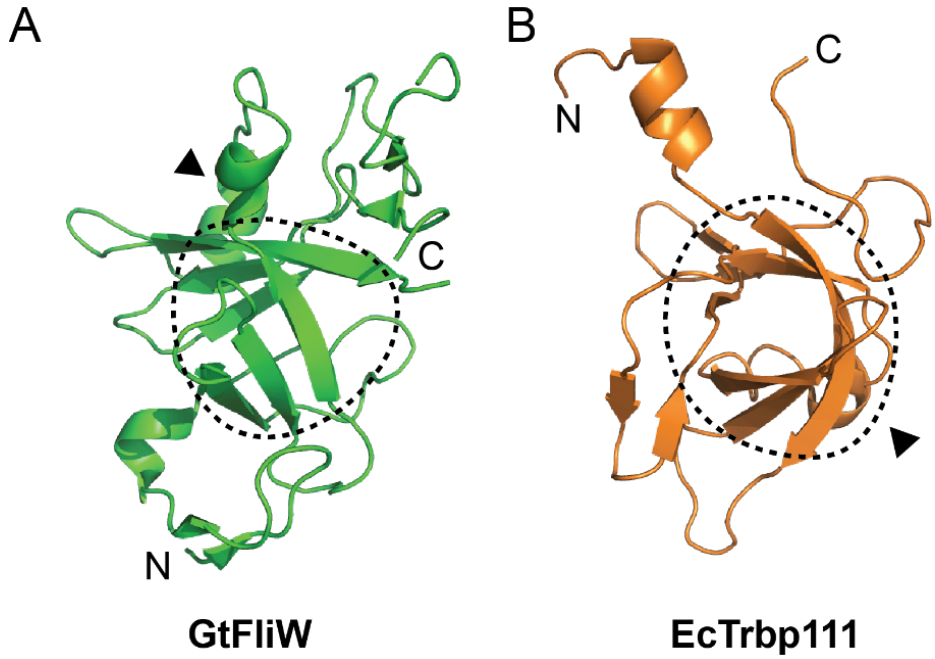

Figure 55: Superposition of *Gt*FliW and a tRNA-binding protein of *E. coli*. A. Crystal structure of *Gt*FliW in cartoon representation. The dotted line represents the β-barrel. **B.** Crystal structure of EcTrbp111 in cartoon representation. The dotted line represents the β-barrel. "N" and "C" represent N- and C-termini, respectively. Black arrows indicate the "capping" α-helix.

Nonetheless, the presence of a small β-barrel represents a very stable fold, as the barrel core is tightly kept together by strong hydrophobic interactions. Several surface cavities that originate from the large surface area of the compact core domain, allow contacts with several binding partners due to the possibility of different charge distributions on the surface (compare **Figure 9**). During this study, interactions of FliW with flagellin, CsrA and BacE have been confirmed. These findings show that the fold of FliW represents an elegant way to couple several properties necessary for a small, regulatory protein.

4.2 CsrA and FliW represent an ancient regulatory module

Although initial results on the phylogenetic conservation of FliW and CsrA were present within the study by Mukherjee and coworkers, an in-depths analysis including representative species of most eubacterial phyla was lacking [133].

The crystal structure of CsrA/FliW determined in this study (compare 3.1.10) clearly shows that FliW binds to a C-terminal extension at CsrA, hence referred to as CsrA-C. The presence of a C-terminal extension in all CsrA homologues was observed in all species harboring a copy of *fliW* within their genome (**Figure 6**). A closer look at the amino acid sequence of CsrA proteins revealed that enterobacterial homologues always had a length of 60-66 amino

acid residues. In contrast to that, the presence of CsrA-C resulted in a size of 74 to 81 amino acid residues. *Vice versa*, CsrA proteins from flagellated species missing FliW also lack the C-terminal elongation, while the RNA-binding domain is highly conserved (**Figure 5**).

The phylogenetic analysis confirmed that the majority of flagellated eubacterial species possess both proteins, CsrA and FliW as suggested previously [133,138,167]. Furthermore, presence of FliW also requires the presence of CsrA-C, which renders it likely that both are subject to co-evolution. This is further supported by the fact that the phylogenetic data show a low number of secondary losses of CsrA and FliW in the investigated species [90]. A secondary loss scenario would also explain the large differences between CsrA regulation in enterobacteria compared to other species [133]. If these bacterial species lost both CsrA and FliW during the course of evolution and regained CsrA alone, regulatory targets might have also changed.

Another interesting observation is the presence of the sRNAs termed "sponge" RNAs (CsrB/C and RsmX/Y/Z) only in γ-proteobacteria species serving as antagonists for CsrA activity [114,130,168]. In contrast to FliW, these antagonizing sRNAs provide multiple CsrA binding sites and prevent CsrA-binding to their mRNA target sites in a competitive manner. Physiologically, sRNAs are related to a plethora of antagonizing effects associated with motility, metabolism and biofilm formation (reviewed in: [110,111,131,169]). In *E. coli* and *Yersinia pseudotuberculosis*, CsrA has been shown to interact directly with the 5'-UTR of the *flhDC* mRNA and to stabilize the transcript [170–172]. FlhDC represent the master regulatory proteins of flagella biosynthesis in these organisms. In *Salmonella typhimurium*, deletion of the CsrA interacting sRNAs CsrB/C show increased transcription of the mRNA encoding the major flagellin protein FliA [173]. This contrasts with *B. subtilis* and *C. jejuni*, where the deletion of FliW decreases the production of flagellin [132,133].

A complete phylogenetic distribution of these sRNAs is nonetheless difficult to obtain since they are poorly conserved and already show large variations between closely related species [131]. To bypass the problem of a low sequence conservation of sponge RNAs such as CsrB/C, a recent study investigated the presence of a major signal transduction pathway controlling a variety of processes via CsrB/C [127]. The two-component system BarA/UvrY is a key regulatory unit that controls the transcription of CsrB and CsrC among other pathways [174,175]. BarA is a membrane-bound hybrid sensor kinase that trans-phosphorylates its cognate response regulator UvrY upon sensing of several stimuli (e.g. formate and acetate) [176]. The presence of BarA/UvrY strongly anticorrelated with the

presence of FliW and only six species out of 346 were identified that harboured both BarA and FliW [127].

The data obtained in the study by Zere and co-workers further show that BarA/UvrY is almost exclusively present in γ-proteobacteria and thereby confirm the phylogenetic inference conducted in this study [127]. Taken together, FliW seems to be the ancestral antagonist of CsrA activity in most bacterial species.

4.3 CsrA and FliW regulate flagellin homeostasis by an allosteric mechanism

The evolutionary conservation of CsrA/FliW could be confirmed during the course of this study. However, a closer inspection of the binding modes of FliW and sRNAs should reveal the substantial differences by which CsrA is regulated.

In *B. subtilis*, CsrA inhibits translation of flagellin by binding to two adjacent sites present within the 5'-UTR of *hag* [139]. Interaction of FliW binding with CsrA enables translation of flagellin, which itself can also sequester FliW [91,133]. This pattern of interactions permits FliW to antagonize initiation of flagellin translation (via CsrA) in a flagellin-dependent manner.

Here I have investigated the structural basis for how FliW antagonizes CsrA enabling ribosomes to access the SD present within the 5'-UTR of the *hag* mRNA. As mentioned earlier, the crystal structure of the CsrA/FliW complex reveals that FliW binds to CsrA primarily through its C-terminal extension (CsrA-C) but also through contacts with the CsrA RNA-binding domain. FliW shares overlapping interfaces with the SD at CsrA, which makes the simultaneous binding of FliW and SD extremely unlikely (**Figure 18B**). Moreover, FliW exhibits a prominent negative charge on one half of the molecule. This side of the protein localizes in close proximity to where the RNA is found in SD/CsrA structures. The strong electrostatic repulsions generated by this negative charge inhibit RNA binding.

Therefore, FliW allosterically antagonizes CsrA in a non-competitive manner by excluding the 5'-UTR from CsrA [177] (**Figure 56A**). The mechanism is in strong contrast to that of sRNAs also regulating CsrA. Recent structural analysis has elegantly demonstrated that the sRNA RsmZ sequesters CsrA by offering multiple CsrA binding sites that are similar to SD sequences [122,125] (**Figure 5**). As such, sRNAs regulate CsrA by acting as competitive inhibitors of the original SD sequences (**Figure 56B**). The analysis performed in this study

shows that FliW acts - in contrast to sRNAs – by a non-competitive mechanism through a highly specific binding site offered by CsrA-C (**Figure 56A**).

Therefore, FliW is highly specific to CsrA, but also to the process of flagellar assembly via its interaction with flagellin. FliW therefore links the presence of mature, cytoplasmic flagellin molecules with the production of new flagellin via CsrA. This mechanism is extremely important in the light that flagellin is one of the most abundant proteins in flagellated bacteria (one flagellar filament consists of over 20.000 flagellin copies), and therefore, should be homeostatically controlled. Why the γ-proteobacteria use sRNAs instead of FliW in regulating CsrA is unclear, but might be related to the adaptation of virulence mechanisms [111].

Taken together, I have shown that FliW and sRNAs control the activity of CsrA *via* two fundamentally different mechanisms. While FliW regulates CsrA activity by an allosteric mechanism and seems to be related to motility, sRNAs act as competitive inhibitors of CsrA on a global cellular scale.

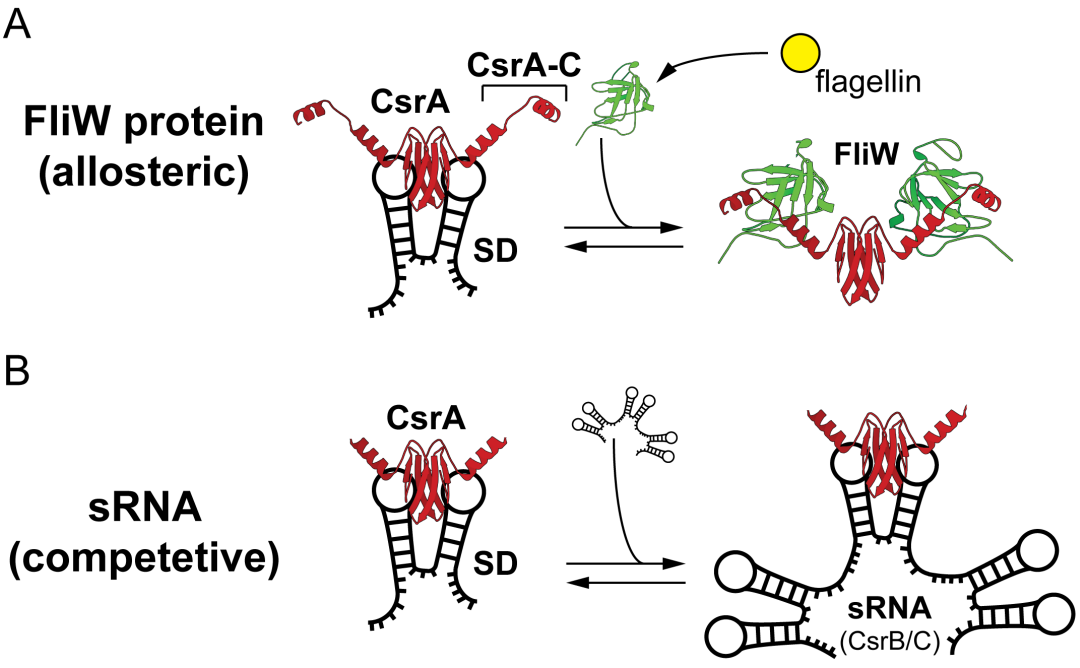

Figure 56: Model of CsrA regulation by FliW and sRNA. A. The different modes of CsrA (red) regulation by FliW (green, right side) and **B.** sRNA (black, right side) are depicted. Both, FliW and sRNA, antagonize the CsrA-dependent repression of translation initiation (left side). The figure originates from [90].

4.4 Bactofilins: a class of diverse scaffold proteins?

Bactofilins are involved in motility of different bacterial species

Another class of proteins that has been shown to be involved in the regulation of bacterial motility, are the bactofilins [152]. These ubiquitous proteins have been identified in *C. crescentus* and shown to be conserved in all bacterial phyla for which genome information is available [153]. In *C. crescentus* two bactofilin homologs (BacA and BacB) can be found in the genome that are constantly present throughout the cell cycle and involved in the transition from mobile to sessile life style [153]. Heterologous overproduction and purification of both proteins revealed long, filamentous structures when analyzed by electron microscopy [153]. The results indicated that bactofilin scaffolds serve as polar localization factors that recruit the peptidoglycan synthase PbpC to the stalked pole.

In *M. xanthus* four different bactofilin homologs are encoded in the genome, with three being part of one operon (*bacNOP* and *bacM*) [153]. Overproduction of all homologs again revealed the presence of long filaments, which seemed to be an intrinsic property of bactofilin proteins. Implications on T4P-mediated motility could be demonstrated in the absence of *bacP* [153,178]. These results indicate that, despite the huge differences between T4P-movement of *M. xanthus* and flagellar movement, bactofilins seem to play a role in both types of motility.

In *B. subtilis*, the genes encoding the bactofilins BacE and BacF have shown to be related to flagellar movement as their deletion led to reduced motility [152]. This phenotype was further investigated and both bactofilins were shown to localize in assemblies of 70 nm beneath the cytoplasmic membrane. Conversely, the localization pattern resembled that of flagellar basal bodies and not the cell division site as in *C. jejuni* and *M. xanthus* [151]. The observations from *B. subtilis* furthermore showed that BacE formed fewer subcellular assemblies than BacF and also rested only a few milliseconds compared to the static assemblies of BacF. These findings indicate different roles of the two homologs but further investigation of the differences by e.g. generation of deletion strains of either of the two genes was not possible. A closer look at the deletion strain of both bactofilins revealed that flagellar biogenesis was halted at the stage of hook assembly [151].

A connection of the bactofilins with hook assembly, represents an interesting observation, which might be related to a post-transcriptional regulation of the hook protein FlgE. First evidence for a post-transcriptional regulation of FlgE was found in *S. typhimurium* [179]. Although the amount of *flgE* transcript was not reduced in strains lacking several rod proteins, FlgE levels were drastically decreased [179]. A later study could show that in the absence of

rod proteins, FlgE was secreted into the periplasm and subsequently degraded [180]. To this effect, the bactofilins might be involved in either the regulation of FlgE or the rod proteins, which has not been studied yet. In addition to that, the rod composition of *B. subtilis* is different than in *S. typhimurium* which makes it difficult to directly compare the rod/hook assembly in both organisms [181]. Whether productive rod assembly takes place in an *yhbE*/*yhbF* double deletion strain needs to be analyzed in the future.

Furthermore, the bactofilins were suspected to interact with the flagellin chaperone FliS and the C-ring component FliY, which could not be confirmed in this study [152]. However, presence of a BacE/FliW complex in *B. subtilis* revealed an interesting connection of bactofilins with the process of filament assembly. This could be a first indication of a more intricate interconnection of hook and filament assembly than anticipated so far. Of note, a failure to build a hook structure also prevents the establishment of a filament [76,181]. Therefore, bactofilins could exert their effect on filament construction indirectly, via their function in hook assembly, but the findings on their stoichiometric interaction with flagellin chaperones *in vitro* and *in vivo* provide compelling evidence for a further level of regulation of filament assembly.

The observation that bactofilins form assemblies of 70 nm size and show a mobile localization pattern [151], especially in case of BacE, suggest that in addition to an assumed scaffolding function observed for other bacteria [153,178,182], bactofilins can drive reactions and/or assemblies in a highly dynamic manner, possibly in many other bacterial species.

The diversity of DUF583 proteins

To gain a deeper structural understanding of bactofilin proteins, a systematic search for bactofilin homologs was performed using the NCBI BLAST tool. Interestingly, apart from the bactofilin domain another domain family was proposed to be present in BacE and BacF from *B. subtilis*. The DUF342 describes a domain family of unknown function according to the CDD/SPARCLE algorithm used by the NCBI tool [183]. Proteins with this domain prediction were found in *S. putrefaciens* and *T. maritima* and already described in *Vibrio vulnificus* [184] (**Figure 51**).

The FapA termed DUF342 protein in *V. vulnificus* was discovered when monitoring the effect of glucose on flagellar motility. Deletion of the gene encoding FapA entirely abolished flagellar motility and complementation *in trans* could not restore flagellar biogenesis [184]. The *fapA* gene is encoded in the downstream region of a chemotaxis operon in *V. vulnificus* and transcription seems to be tightly controlled. Obviously, exceeding a certain threshold (*in*

trans expression was approximately nine-fold higher than wildtype) disturbed the fine-tuning of the hierarchical process of flagellar assembly [184]. The results obtained further indicated a connection of FapA to the sugar phosphotransferase system (PTS) via one domain of the phosphorylated form of the glucose-specific enzyme 2 (EIIA).

Whether the flagellar assembly factor described in *V. vulnificus* and other homologs described by DUF342 are indeed related to bactofilins remains to be shown. However, the bactofilin fold displaying a β-helical architecture might serve as a structural basis for diverse features [158,185,186]. Despite the vague structural similarities, both bactofilin and DUF342-possessing proteins seem to be involved in the flagellar assembly process. Further structural and biochemical information has to be obtained to confirm a relationship between these proteins.

4.5 Homeostasis and secretion of flagellin is regulated by a sophisticated mechanism

Based on the results obtained in this study and supported by the literature available, a working model for the coupling of homeostasis and secretion of flagellin was developed (**Figure 57**).

(I) Co-translational recognition of flagellin nascent chains

The production of flagellin is initiated after secretion of the anti-σ-factor FlgM, which enables the σD dependent transcription of the *hag* gene [106]. Another prerequisite for filament assembly is the completion of the hook-basal body complex as shown earlier [82,181]. Two scenarios describe how flagellin production is enabled: In the case of high amounts of free FliW, CsrA is sequestered and translation of flagellin enabled. On the other hand, untimely production of flagellin (e.g. prior to hook completion) would sequester FliW molecules to prevent a cytoplasmic aggregation of flagellin, thereby freeing CsrA [91] (**Figure 57I**). The biochemical data obtained in this study show that the N-terminal 70 residues of flagellin are sufficient for FliW binding (**Figure 29**), although these findings are in contrast to earlier observations [145]. Recognition of the N-terminus of flagellin by FliW render a scenario possible, in which FliW captures flagellin co-translationally. However, a binding of FliW to ribosomes translating flagellin could not be demonstrated reliably (**Figure 38**). Translation might simply be too rapid to provide evidence for FliW binding. Further experiments are necessary employing a stalled version of flagellin that stays associated with the ribosome.

(II) FliS guides flagellin to the export gate FlhA-C

Once flagellin has fully emerged from the ribosome exposing the C-terminal domain, it is recognized by its cognate chaperone FliS (**Figure 57II**). FliS wraps around the D0-C domain and interacts with flagellin via a complex network also employing part of the D1-C domain (**Figure 21 and figure 22**). Research in *B. subtilis* and *A. aeolicus* demonstrated that the presence of FliS is essential for flagellin secretion [55,91], albeit research in *S. typhimurium* showed a secretion of several FliC variants even in the absence of FliS [187].

Interestingly, these findings indicate a substantial difference between the enterobacteria and *B. subtilis* in terms of FliS function. In *B. subtilis*, deletion of FliS led to a 10-fold reduction of intracellular flagellin levels [133]. In contrast to that, flagellin levels are elevated by 6-fold in *Yersinia tuberculosis* when FliS is depleted [188]. Furthermore, FliS and FliA (σD) compete for FlgM binding and FliS inhibits the secretion of FlgM [188,189]. The interaction of FlgM and FliS was also confirmed in *S. typhimurium* and might therefore be another unique feature of enterobacteria [190]. Moreover, the lack of a CsrA/FliW complex possibly necessitated a differential regulation of flagellin production.

Taken together, FliS is essential to guide flagellin to FlhA-C. Although enterobacteria have developed a different mechanism of flagellin regulation by employing FliS as negative regulator of FlgM, the general mechanism of flagellin guidance to the fT3SS by FliS seems to be conserved.

(III) Flagellin is secreted via the fT3SS

Flagellin is recognized by the fT3SS only when in complex with its chaperone FliS (**Figure 30, Figure 57III**). In spite of the observation that fT3S seems to be "leaky" and flagellin secretion might occur spontaneously in the absence of its chaperone [187], assembly of an intact and fully functional filament can only take place when FliS is present [29].

FlhA provides a general sorting platform to all proteins that are secreted via the fT3SS [25,27,29,87]. Recent studies could also show how the process of fT3S is energized: The secretion process relies on the proton motive force (PMF) as well as the sodium motive force (SMF) [191,192]. Furthermore, the studies show that certain residues within FlhA are essential for proton-shuttling and induce a conformational change within the cytoplasmic domain of FlhA [192].

The process of fT3S is furthermore assisted by the soluble ATPase complex that consists of the proteins FliI, FliH and FliJ [41]. The role of this complex, has however not been clarified entirely. Flagellar assembly can proceed in strains lacking the ATPase complex, albeit not as

efficiently as in wild type strains [193]. In the iT3SS, the ATPase complex was shown to be involved in chaperone release and unfolding of the substrates prior to export [194]. Despite the similarities of fT3SS and iT3SS, an unfolding step for substrates has never been shown for flagellar related export. Conversely, a model predicting the export of flagellin subunits at a constant rate, assumes a partial, α-helical fold of flagellin monomers during their export, which would resemble the conformation observed in crystal structures [195]. As the variable domain of several species also comprises a very flexible fold, it might well be that flagellin travels in a completely folded state through the growing tunnel [142,144](compare **Figure 23**). Cryo-electron microscopy studies estimated the inner diameter of the tunnel to be approximately 2 nm, which would allow the passage of a folded flagellin molecule [137].
This idea is further supported by the results obtained in this study. Why would a cell invest in a sophisticated quality control mechanism resulting in a properly folded flagellin molecule, if it is again unfolded prior to secretion?

(IV) Recycling of FliW and FliS and further regulation

The recycling step of flagellar chaperones represents one of the most enigmatic steps during fT3S (**Figure 57IV**). One component of the ATPase complex, FliJ, is involved in binding empty chaperones after the cognate substrate has been released [196]. FliJ is also connected to FlhA-C but whether this interaction facilitates the release or recycling of chaperones has not been demonstrated yet [197,198].
If "unloaded" chaperones are not immediately redirected to their next cargo, they might also represent ideal targets for further regulatory steps. The bactofilin BacE interacts with FliW in *B. subtilis* (compare **figure 42**). Whether this interaction directly affects the process of flagellin production and homeostasis or involves regulatory steps at an earlier stage of flagellar assembly, is currently unclear. Notably, FliS is also subject to further regulation in enterobacteria [188,190]. A deeper understanding of how chaperones are released at the export gate and subsequently guided to their next target, might also reveal integration of regulatory elements at this step.

(V) CsrA blocks translation by binding to the SD sequence of the *hag* mRNA

Another round of flagellin translation is repressed by free CsrA that binds to the SD sequence of the flagellin mRNA (**Figure 56V**). This process has been comprehensively discussed in chapter 4.2 and 4.3 and will not be further discussed in this paragraph.

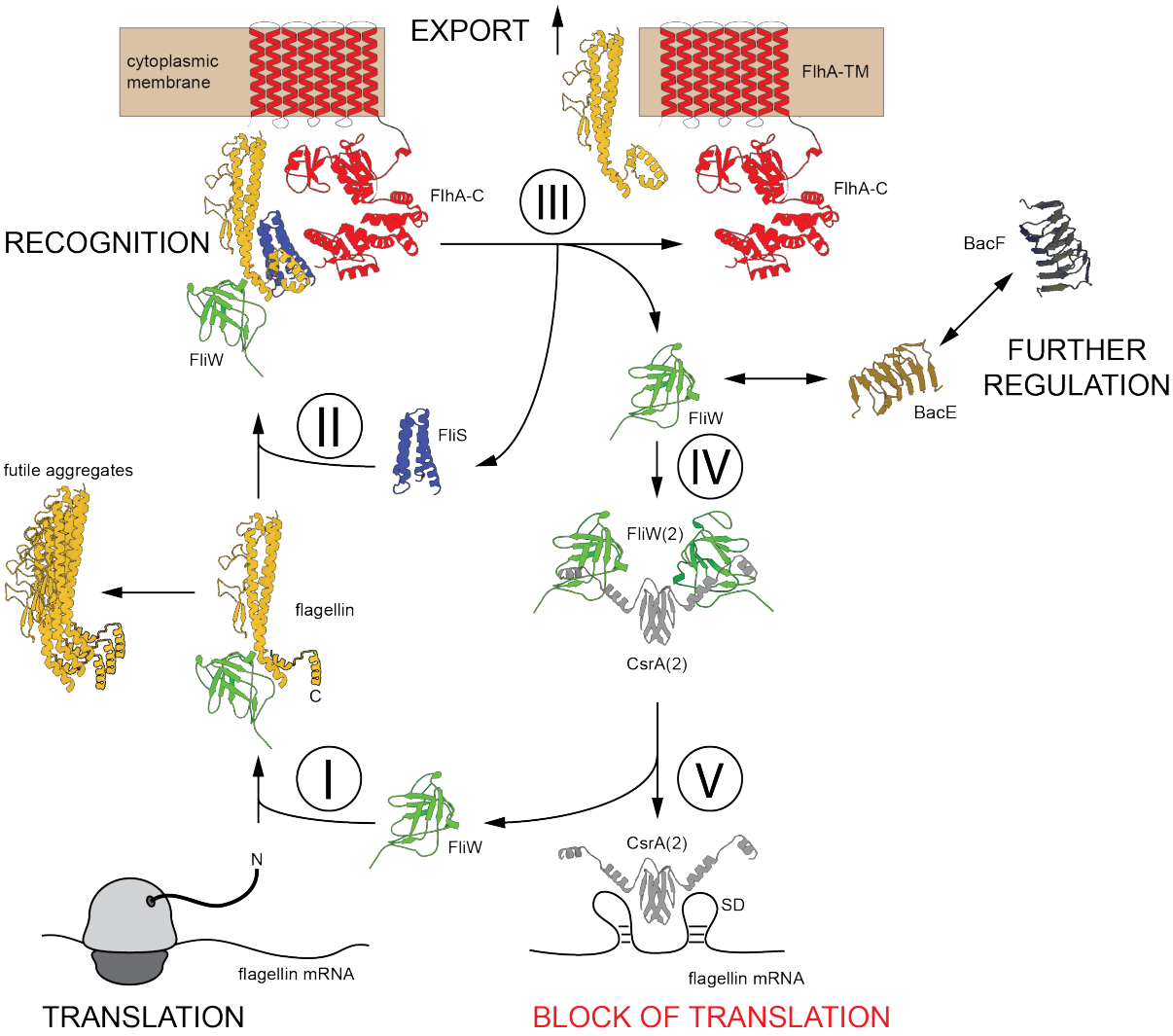

Figure 57: Coupling of flagellin homeostasis and secretion. The scheme illustrates how FliS, FliW and CsrA regulate the production and secretion of flagellin. I. The flagellin nascent chain emerges from the ribosome and FliW binds to its N-terminus. II. The cognate chaperone FliS binds to the C-terminus of flagellin and the heterotrimeric complex is recognized by FlhA-C. III. Flagellin is secreted from the export gate and assembles into the growing filament. Both, FliS and FliW are released and are available for another cycle of flagellin delivery. IV. FliW sequesters CsrA from the SD sequence and allows another round of flagellin translation. In addition to that, the bactofilin BacE can bind to FliW, albeit this regulatory step is not fully explained by the present data. BacF, however, can interact with BacE. V. Another flagellin molecule is produced by the ribosome and sequesters FliW from CsrA. This enables occlusion of the SD sequence until free FliW can bind to CsrA to allow another round of translation. Crystal structures used to generate this figure have been either solved in this study (flagellin/FliS, FliW and CsrA/FliW) or fetched from the PDB (FlhA-C: PDB-identifier 3MIX [27]; BacA: PDB-identifier 2N3D [158]). "N" and "C" represent N- and C-termini, respectively.

Finally, the results obtained in this study allowed the proposition of a model for regulation of flagellin homeostasis and secretion in the Gram-positive bacterium *B. subtilis* (**Figure 56**). Obtaining structural information on the CsrA/FliW and flagellin/FliS complex filled several gaps that could not be resolved earlier. Still, many pieces are missing, especially concerning the process of fT3S. Current models of late stage assembly should be extended to include another level of regulation by e.g. bactofilins in *B. subtilis*.

5 CONCLUSION

The findings presented within this study show that the proteins CsrA, FliW and FliS are part of a sophisticated machinery coupling the production of an abundant protein with its export. Moreover, a phylogenetic analysis confirmed that this type of flagellin regulation represents the ancestral state in eubacteria but somehow got lost during the evolution of enterobacteria, which use sRNA instead of FliW to regulate CsrA activity. Employing two chaperones (or one chaperone and one assembly factor) to prevent premature polymerization and efficient guidance to the T3SS is also a common phenomenon during injectisome assembly. The needle protein YscF is protected by the two proteins YscG and YscE [199]. Despite its structural divergence, the needle of an injectisome is reminiscent of a flagellar filament and both are formed by polymerization of a single protein. Admittedly, flagellum and injectisome are evolutionary related and one might therefore assume similarities on the structural and regulatory level.

However, the concept of co-translational capturing and specialized chaperones can also be applied on distinct processes, even in eukaryotes. One example is the biogenesis of ribosomes requiring a plethora of assembly factors that have to deliver ribosomal proteins from the cytoplasm to the nucleus and prevent premature aggregation [147,200]. Proteins that are incorporated into pre-ribosomal particles often interact extensively with ribosomal RNAs (rRNAs) and therefore exhibit patches of charged amino acid residues. Without an effective tethering of these regions by cognate chaperone proteins, translation of these proteins would be followed by aggregation and degradation, respectively. Furthermore, an efficient targeting to the prospective incorporation site is essential.

Taken together, employing dedicated chaperones for capturing and targeting of abundant and insoluble or aggregation-prone proteins represents a common scheme in nature. It is conserved from prokaryotes to eukaryotes and used in different cellular processes ranging from type-III-secretion to ribosomal biogenesis. However, because a co-translational event is extremely rapid, future research requires a careful spatiotemporal resolution to investigate these processes.

6 MATERIALS AND METHODS

6.1 Bacterial strains

The *E. coli* strains DH5α (Thermo Scientific) and *E. coli* XL1blue (Agilent Technologies) were used for propagation of entry and expression vectors. *E. coli* BL21(DE3) strains were used for heterologous expression of proteins (Invitrogen) (**Table 7**).

Table 7: Strains used in this work.

	Strain	Genotype	Reference
B. subtilis	NCIB 3610	wild type	
	NCIB 3610	*comI*Q12L	[201]
	NCIB 3610 DS1677	*Δhag*	[202]
	NCIB 3610 DS6188	*ΔcsrA*	[133]
	NCIB 3610 DS6189	*ΔfliWcsrA*	
	NCIB 3610 DS6245	*ΔfliW*	
E. coli	BL21 (DE3)	F- *ompT hsdS*$_B$ (r_B-m_B-) *gal dcm* (DE3)	Invitrogen
	BL21 (DE3) pLysS	F- *ompT hsdS*$_B$ (r_B-m_B-) *gal dcm* (DE3) pLysS (Cam^R)	Invitrogen
	Dh5α	F^- Φ80*lac*ZΔM15 Δ(*lac*ZYA-*arg*F) U169 *rec*A1 *end*A1 *hsd*R17(r_k^-, m_k^+) *pho*A *sup*E44 *thi*-1 *gyr*A96 *rel*A1 λ	Invitrogen
	XL1blue	*recA1 endA1 gyrA96 thi-1 hsdR17 supE44 relA1 lac*[F′ *proABlacI*^{q}*ZΔM15* Tn*10* (Tet_r)]	Stratagene

6.2 Bacterial growth conditions

Solid and liquid LB media was obtained from Roth and prepared according to the instructions of the manufacturer and sterilized by autoclavation at 121 °C for 20 minutes. *E. coli* strains were grown at 30 °C to 37 °C for cloning and plasmid propagation. For selective growth, antibiotics were added to the media in the following final concentrations: 100 µg/ml Ampicillin, 50 µg/ml Kanamycin. *B. subtilis* strains were grown in the presence of 5 µg/ml Chloramphenicol, or 100 µg/ml spectinomycin. All antibiotic stock solutions were sterile filtrated with a filter of 0.2 µm pore size (Sigma-Aldrich).

6.3 Chemicals and consumables

All chemicals were purchased from Sigma Aldrich (Germany), Roth (Germany), AppliChem (Germany) and VWR (Germay). Consumable plastic ware (reaction tubes, falcon tubes, pipette tips, syringes) was obtained from Sarstedt and Braun.

6.4 Oligonucleotides and Plasmids

Oligonucleotides were purchased from MWG Eurofins or Sigma-Aldrich and diluted with deionized water to a final concentration of 10 mM (Suppl. Table 1). All plasmids generated in this study are listed in supplemental table 2.

6.5 Molecular biology

6.5.1 Enzymes and molecular cloning equipment

All restriction enzymes and supplemental reagents (e.g. dNTPs, reaction buffers, BSA) for molecular biology techniques were supplied by New England Biolabs (NEB) and Fermentas. Quick-Load® Purple 2-Log DNA Ladder (0.1 - 10.0 kb, NEB) and GeneRuler 1 kb DNA Ladder (Thermo Scientific) was used as size standard for agarose gels. gBlocks® Gene Fragments used in this study were generated by Integrated DNA Technologies (IDT). Sequencing of plasmids generated in this work or amplified DNA was done by Eurofins Genomics.

6.5.2 Polymerase chain reaction (PCR)

PCR amplification of each gene was performed using Q5® and Phusion® High-Fidelity DNA Polymerase (NEB) according to the manufacturer's protocol. 100 µM dNTP's (NEB), 200 µM of each Oligonucleotide and 0.01 U/µl polymerase was used to set up a PCR reaction. An estimation of the optimal annealing temperature for each oligonucleotide was calculated by the webpage OligoCalc (http://biotools.nubic.northwestern.edu/OligoCalc.html). Two types of thermocyclers were used in this study: T100™ Thermal Cycler (BioRad) and ³Prime

Thermal Cycler (Techne). The program used was personally adjusted for each reaction according to the oligonucleotides and templates used and the manufacturers manual.

6.5.3 Transformation and isolation of plasmid DNA

Transformation of chemically competent *E. coli* strains was performed with 50 – 200 ng of plasmid and 100 µl of cells. The cells were incubated with plasmid DNA for 10 minutes on ice and then transferred to a neoBlock 1 (Neolab) for 45 seconds of incubation at 42 °C. Afterwards, 300 µl of SOC media was added, the cells transferred to 37 °C and incubated for one hour at 200 rpm. The whole aliquot was transferred to selective media and incubated at 37 °C overnight.

To extract plasmid DNA, 5 ml cultures of *E. coli* were inoculated from one colony and incubated overnight at 37 °C and 200 rpm. The cells were harvested by centrifugation at 4000 rpm for 5 minutes in a Heraeus Meagfuge 40R (Thermo Scientific) and further processed according to the manufacturers manual supplied with the GeneJET Plasmid Miniprep Kit (Thermo Scientific). The plasmid DNA was finally eluted in 50 µl deionized water.

6.5.4 Agarose gel electrophoresis

DNA restriction fragments and PCR amplified DNA were analyzed by agarose gel electrophoresis. Depending on the DNA fragment size, gels were prepared with an agarose concentration ranging from 0.8 % to 2 % (w/v). The agarose was dissolved in running buffer (90 mM Tris, 30 mM Taurine, 0.5 mM EDTA) by microwave heating and poured into gel casts. 5 µl of a 0.025 % ethidium bromide solution (Roth) was added to 100 ml of gel solution. Gel Loading Dye, Purple (6X, NEB) was added in appropriate amounts to the samples prior to loading. A voltage of 100 V was applied and DNA visualized with a Gel iX20 Imager (intas).

6.5.5 Restriction analysis and gel extraction

The insertion of a gene of interested into a plasmid backbone was verified by restriction analysis. The plasmid DNA was digested with respective restriction enzymes according to the manufacturer's instructions and the DNA sample analyzed by agarose gel electrophoresis.

If DNA fragments should be further used for molecular cloning, the DNA was extracted from agarose gels using a GeneJET Gel Extraction Kit (Thermo scientific) according to the manufacturers manual.

6.6 Protein biochemistry

6.6.1 Protein purification

For the heterologous expression of proteins, *E. coli* BL21(DE3) were grown in selective LB media according to 5. 2.. Protein overproduction was performed under auto-induction conditions by adding 1.75 % (w/v) D(+)-lactose-monohydrate to the media, followed by incubation at 30 °C for 16 hours and 180 rpm. If IPTG was used as inducer, cells were grown to an OD_{600} of 0.5-0.7, supplied with 1 mM IPTG and incubated at 37 °C for 3 hours and 180 rpm. Cells were harvested for 20 minutes at 4 °C and 3500 rpm and the pellet suspended in lysis buffer (20 mM HEPES-Na pH 8.0, 20 mM $MgCl_2$, 20 mM KCl, 250 mM NaCl, 40 mM Imidazole). Cell lysis was performed using a M-110L Microfluidizer® Materials Processor (Microfluidics) and the lysate clarified by centrifugation (20.000 rpm, 20 minutes, 4 °C).
The lysate was strictly kept on ice and applied onto a 1 or 5 ml HisTrap™ Fast Flow (GE Healthcare Life Sciences), depending on the culture size. HisTrap columns were equilibrated with 10 column volumes (CV) of lysis buffer prior loading of the lysate. The column was washed with 10 CV of lysis buffer and the protein eluted with elution buffer (lysis buffer + 460 mM Imidazole). Protein fractions were concentrated to a volume of 1-5 ml using Amicon Ultra-15 centrifugal filter units (Merck Millipore) with an appropriate molecular weight cut-off (MWCO) and applied to a SEC column (HiLoad 16/600 Superdex 200, HiLoad 16/600 Superdex 75; GE Healthcare Life Sciences). SEC was performed with a ÄKTApurifier 10 and a ÄKTAprime (both GE Healthcare) and the column equilibrated with 1 CV of SEC-buffer (20 mM HEPES-Na pH 7.5, 20 mM $MgCl_2$, 20 mM KCl, 200 mM NaCl). Protein containing elution fractions were pooled and concentrated to 200-1000 µl according to the experimental requirements. Protein concentration was estimated with a NanoDrop™ Lite spectrophotometer (Thermo Scientific).

6.6.2 SDS-PAGE

Sodium-dodecyl-sulfate polyacrylamide gel electrophoresis (SDS-PAGE) was performed to separate proteins according to their size. 15 % polyacrylamide gels were prepared using a Mini-PROTEAN 3 Multi-Casting Chamber (Biorad) and stored at 4 °C. A 5x loading buffer (100 mM Tris-HCl (pH 6.3), 10% (v/v) glycerol, 2 mg/ml SDS, 3% (v/v) β-mercaptoethanol, 1 mg/ml brom-phenol blue) was added to samples for SDS-PAGE analysis. Samples containing whole cell extracts or ribosomes were denatured prior to electrophoresis at 98 °C for 5 minutes. A voltage of 200 to 270 V was applied with a Mini Pro 300V Power Supply (neolab) in a Mini-PROTEAN® Tetra Cell (Biorad) for 35 to 55 minutes. SDS-PAGES were stained with Coomassie Brilliant Blue R-250. A solution containing 60 % (v/v) H_2O, 30 % (v/v) ethanol and 10 % (v/v) acetic acid served to destain the gels.

6.6.3 Western Blot and Immunodetection

Western Blot analysis was performed according to [203]. A Trans-Blot® SD Semi-Dry Transfer Cell (Biorad) was used to transfer proteins onto a nitrocellulose membrane (GE healthcare) and assembled according to the manufacturer's instructions.
After transfer, the membrane was incubated in blocking solution for either one hour or overnight (1x TBS buffer, 5 % (w/v) skimmed milk, 0.025 % (v/v) Nonidet® P40 (applichem)). Antibodies were generously received from Daniel Kearns, Indiana University, Bloomington (α-FliW) and Kürsad Turgay, Leibniz-University Hannover (α-flagellin). The antibodies were incubated in blocking buffer in the following dilution for 2 to 4 hours: α-flagellin: 1:40.000, α-FliW: 1:10.000. The membrane was washed with blocking buffer three times afterwards and incubate with a secondary antibody Goat Anti-Rabbit IgG H&L (HRP) (abcam) for 30 minutes according to the manufacturer's instructions. The membrane was again washed three times in blocking solution and once with 1x TBS, 0.025 % (v/v) Nonidet® P40 (applichem). The immunoblot was incubated in a luminol solution according to [204] and chemiluminescence detected with a ChemiDoc™ XRS+ System (Biorad).

6.6.4 Ribosome purification from *B. subtilis*

B. subtilis strains were inoculated from an overnight culture (1:100) in 500 ml LB medium and grown to an OD_{600} of 0.7. Chloramphenicol was added to a final concentration of 50

µg/ml and cells rapidly cooled down on ice. After cell harvest at 4°C for 20 min. at 4000 rpm, cells were re-suspended in ribosome buffer 1 (25 mM HEPES pH 7.5, 30 mM MgOAc, 150 mM KOAc, 10 % (w/v) Sucrose, 50 µg/ml Chloramphenicol, 0.025% (v/v) DDM) and lysed with a M-110L Microfluidizer® Materials Processor (Microfluidics). Cell debris was removed at 25.000g for 30 min and the supernatant load on a 17.5 % (w/v) sucrose cushion. Ribosomes were harvested by ultracentrifugation at 200.000 g for 2 h at 4 °C in an Optima™ XE ultracentrifuge (Beckman Coulter).
The ribosomal pellet was re-suspended in 200 µl ribosome buffer 1 and either used for interaction assays or gradient ultra-centrifugation.

6.6.5 Ribosome interaction assays

Approximately 0.5 mmol of ribosomes was incubated on ice with 5 mmol of purified FliW protein for 30 min. The reaction volume was afterwards increased to 2 ml by the addition of ribosome binding buffer 1, separated in two aliquots, loaded on either a high salt (700 mM KOAc) or low salt (100 mM KOAc) cushion and centrifuged for 2 h at 200.000 g and 4 °C in an Optima™ XE ultracentrifuge (Beckman Coulter). Ribosomal pellets were again resuspended in 100 µl ribosome buffer 1 and TCA precipitated. After precipitation, protein pellets were dissolved in 5x SDS loading buffer (see 5.4.2.) and 5 µl used for SDS-PAGE separation.

6.6.6 Gradient ultra-centrifugation

Sucrose gradients were prepared with ribosome buffer 1 (25 mM HEPES pH 7.5, 30 mM MgOAc, 150 mM KOAc, 50 µg/ml Chloramphenicol, 0.025% (v/v) DDM), supplemented with 10 % (w/v) and 60 % (w/v) sucrose. A Gradient Master™ (Biocomp) was employed to mix the two solutions according to the manufacturers manual. Purified ribosomes (see 5.6.4.) were loaded on top of the gradient and centrifugated for 2h at 200.000g and 4 °C. The gradient was afterwards separated with the Gradient Master™ and fractions collected and analyzed by using the fractionator and UV-cell of an ÄKTAprime (GE Healthcare). Fractions were precipitated with TCA and analyzed by coomassie-stained SDS PAGE and Western blot.

6.6.7 Ni-NTA affinity binding assays

For in vitro pull down assays, all proteins were produced as explained in 6.6.1. The bait protein contained a hexa-histidine tag at its N-terminus, while the prey protein did not. Cells were re-suspended in a lysis buffer containing 20 mM HEPES-Na pH 8.0, 250 mM NaCl, 20 mM MgCl2, 20 mM KCl and 40 mM imidazole. After cell lysis and removal of cell debris by centrifugation (4 °C, 20.000 g, 20 minutes), the lysate was incubated with Ni-NTA-agarose beads (Qiagen) for 5 minutes on ice. After three washing steps with lysis buffer, bound protein was eluted in a buffer containing 20 mM HEPES-Na pH 8.0, 250 mM NaCl, 20 mM MgCl2, 20 mM KCl and 500 mM imidazole. Elutes were analyzed by coomassie-stained SDS-PAGE.

6.6.8 Glutathione-S-transferase (GST) binding assays

GST interaction assays were performed with 1x PBS buffer (137 mM NaCl, 2.7 mM KCl, 10 mM Na_2HPO_4, 1.8 mM KH_2PO_4) at 4 °C by the use of spin columns Mobicol "classic" (MoBiTec). A total amount of 1 nmol of SEC-purified GST-tagged protein was immobilized on 15 µl Glutathione Sepharose 4B (GE Healthcare) and incubated on a turning wheel for 10 minutes. 5 equivalents of putative interaction partner proteins were added to the beads and incubated for 20 minutes on a turning wheel. After removal of residual protein by centrifugation (4 °C, 4000 rpm, 1 minute), the column was washed three times with PBS buffer. Proteins were eluted with 80 µl of GSH elution buffer (50 mM Tris pH. 7.9, 20 mM glutathione) and analysed by coomassie stained SDS-PAGE.

6.7 Protein crystallization

Crystallization experiments were performed at room temperature using the JCSG Core Suites I – IV (qiagen). Proteins were crystallized by the sitting-drop method using SWISSCI MRC 2 Well and 3 Well (Jena Bioscience) crystallization plates. 300 – 500 nl of protein solution were mixed with mother liquor in a 1:1 or 1:2 ratio and a reservoir volume of 50 (2 well) or 30 µl (3 well) was used. The experiments were set up with a Crystal Gryphon (Art Robbins) according to the manufacturers manual.

6.8 Data collection and structure determination

Prior data collection, crystals were flash-frozen in liquid nitrogen after incubation in a cryo-protecting solution containing either 20 % (v/v) glycerol or MPD. Crystals were harvested with Adjustable Mounted CryoLoops™ (Hampton Research) of different diameters and data collected at the European Synchrotron Radiation Facility (ESRF, Grenoble).
The data were processed, integrated and scaled with XDS [205]and merged with the program AIMLESS from the CCP4 suite [206,207]. The resolution cutoff was determined with the program AIMLESS and according to several values from the CORRECT-file obtained by the XDS-program. Cross validation of refinement was performed with 5 % of the total reflections (R_{free}).
The merged-MTZ file was either used for molecular replacement (MR) using the CCP4-implemented PhaserMR or experimental phasing as described in the respective result chapter.
Refinement was performed with PHENIX.refine [208]and models manually built and corrected with COOT [209]. The final models were uploaded to the protein data bank (PDB) with respective identifiers stated in the result chapter.

6.9 Small-angle X-ray scattering (SAXS)

Samples for small-angle X-ray scattering were prepared according to section 6.6.1. Prior to storage in liquid nitrogen, aliquots with 100 µl of protein and/or complexes in a concentration series from 1 mg/ml to 20 mg/ml were prepared and used for SAXS analysis. The data were collected at the European Synchrotron Radiation Facility (ESRF) at beamline BM29. Data collection for each protein was started and ended with a measurement of the buffer used during purification of the protein. Data processing was performed with the ATSAS package [210].

6.10 Electron microscopy

Electron microscopy was performed in close collaboration with Dr. Thomas Heimerl from the Philipps-University Marburg. Samples were diluted to a concentration of 5 – 10 µM and 5 µl spotted on a on formvar coated copper-grids, stabilized with evaporated carbon film and negatively stained by applying 5 µl of a 2 % (w/v) uranyl acetate solution. The grids were dried and analyzed with a 200 kV Transmission Electron Microscope JEM-2100 (JEOL).

6.11 Hydrogen/deuterium-exchange mass-spectrometry

6.11.1 Data acquisition

For HDX analysis of flagellin/FliS, FliW and FlhA-C, 200 pmol (4 µl of 50 µM solution) of protein were incubated without or in the presence of binding partners for 5 min at 37 °C prior to H/D exchange. Binding partners were added to the respective protein in equimolar concentrations. The mixtures were diluted 10-fold in D_2O-containing SEC buffer to start the H/D exchange and incubated at 37 °C. The reactions were stopped after different incubation times (i.e. 30, 120, 600 sec) through addition of an equal volume of ice-cold quench buffer and directly injected into an ACQUITY UPLC M-class system with HDX technology (Waters). Preparation of samples during HDX analysis of flagellin/FliS, FliW and FlhA was aided by a two-arm robotic autosampler (LEAP Technologies).

All proteins were digested online using an Enzymate BEH Pepsin column 2.1 x 30 mm (Waters) at a flow rate of 100 µl/min ddH_2O + 0.1 % (v/v) formic acid at 11 °C and the resulting peptic peptides trapped for 3 min using an AQUITY UPLC BEH C18 1.7 µm 2.1 x 5 mm VanGuard Pre-column (Waters) kept at 0.5 °C (209). Thereafter, the trap column was placed in line with an ACQUITY UPLC BEH C18 1.7 µm 1.0 x 100 mm column (Waters) and the peptides eluted at 0.5 °C using a gradient of water + 0.1 % formic acid (Hdx buffer A) and acetonitrile + 0.1 % formic acid (HDX buffer B) at 40 µl/min flow rate: 5% B (0 min), 5-35% B (0-7 min), 35-85% B (7-8 min), 85% B (8-10 min), 85-95% B (10-10.1 min), 95% B (10.1-11 min), 95-5% B (11-11.1 min), 5% B (11.1-16 min). Mass spectra were acquired in positive ion mode using a SYNAPT G2-Si mass spectrometer equipped with an electrospray ionization source (Waters). Deuterated peptides were detected in High Definition MS (HDMS, [211]) mode including ion mobility separation (IMS). Lock mass spectra were obtained every 30-45 s using [Glu1]-Fibrinopeptide B standard (Waters). Undeuterated peptides of all proteins were obtained similar as described above by 10-fold dilution in H_2O-containing SEC buffer and detected in Enhanced High Definition MS ($HDMS^E$) mode including IMS of precursor ions within the gas phase and alternating high and low energies applied to the transfer cell (Waters). All measurements were performed in triplicates. Blank runs were performed between each sample to avoid peptide carry-over.

6.11.2 Data analysis

Analysis of HDX data was aided by the softwares Protein LynX Global Server (PLGS) and DynamX 3.0 (both Waters). Identification of undeuterated peptides was performed using PLGS with custom-created databases and the setting ‘no enzyme’. Only peptides identified in at least two replicates of each nucleotide-bound state were used for assignment of deuterium incorporation in DynamX 3.0. Thresholds of 0.5 min and 25 ppm for retention time and *m/z* values, respectively, were applied for assignment of the deuterated peptides to their undeuterated counterparts. Deuterium incorporation into each peptide was calculated by subtracting the centroid of the isotope distribution of the undeuterated from the deuterated peptides. Relative deuteration was calculated as the quotient between absolute deuteration and the number of backbone amide hydrogens of the peptide [211].

7 REFERENCES

1. Jarrell KF, McBride MJ: **The surprisingly diverse ways that prokaryotes move** . *Nat. Rev. Microbiol.* 2008, **6**:466–476.
2. Berg HC, Anderson RA: **Bacteria swim by rotating their flagellar filaments.** . *Nature* 1973, **245**:380–2.
3. Kearns DB: **A field guide to bacterial swarming motility.** . *Nat. Rev. Microbiol.* 2010, **8**:634–44.
4. Macnab RM: **How bacteria assemble flagella.** . *Annu. Rev. Microbiol.* 2003, **57**:77–100.
5. Wall D, Kaiser D: **Type IV pili and cell motility.** . *Mol. Microbiol.* 1999, **32**:1–10.
6. Skerker JM, Berg HC: **Direct observation of extension and retraction of type IV pili.** . *Proc. Natl. Acad. Sci. U. S. A.* 2001, **98**:6901–4.
7. Giltner CL, Nguyen Y, Burrows LL: **Type IV Pilin Proteins: Versatile Molecular Modules** . *Microbiol. Mol. Biol. Rev.* 2012, **76**:740–772.
8. Pelicic V: **Type IV pili: e pluribus unum?** . *Mol. Microbiol.* 2008, **68**:827–837.
9. Kearns DB: **MICROBIOLOGY: Bright Insight into Bacterial Gliding** . *Science (80-.).* 2007, **315**:773–774.
10. Mignot T: **The elusive engine in Myxococcus xanthus gliding motility** . *Cell. Mol. Life Sci.* 2007, **64**:2733–2745.
11. Miyata M, Hamaguchi T: **Prospects for the gliding mechanism of Mycoplasma mobile** . *Curr. Opin. Microbiol.* 2016, **29**:15–21.
12. LEIFSON E: **Staining, shape and arrangement of bacterial flagella.** . *J. Bacteriol.* 1951, **62**:377–89.
13. Stallmeyer MJ, Aizawa S, Macnab RM, DeRosier DJ: **Image reconstruction of the flagellar basal body of Salmonella typhimurium.** . *J. Mol. Biol.* 1989, **205**:519–28.
14. Sosinsky GE, Francis NR, DeRosier DJ, Wall JS, Simon MN, Hainfeld J: **Mass determination and estimation of subunit stoichiometry of the bacterial hook-basal body flagellar complex of Salmonella typhimurium by scanning transmission electron microscopy.** . *Proc. Natl. Acad. Sci. U. S. A.* 1992, **89**:4801–5.
15. Liu J, Howell JK, Bradley SD, Zheng Y, Zhou ZH, Norris SJ: **Cellular Architecture of Treponema pallidum: Novel Flagellum, Periplasmic Cone, and Cell Envelope as Revealed by Cryo Electron Tomography** . *J. Mol. Biol.* 2010, **403**:546–561.
16. Qin Z, Lin W, Zhu S, Franco AT, Liu J: **Imaging the Motility and Chemotaxis Machineries in Helicobacter pylori by Cryo-Electron Tomography** . *J. Bacteriol.* 2017, **199**:e00695-16.
17. DeRosier D: **Bacterial Flagellum: Visualizing the Complete Machine In Situ** . *Curr. Biol.* 2006, **16**:R928–R930.
18. Altegoer F, Bange G: **Undiscovered regions on the molecular landscape of flagellar assembly** . *Curr. Opin. Microbiol.* 2015, **28**:98–105.
19. Chevance FF V, Hughes KT: **Coordinating assembly of a bacterial macromolecular machine.** . *Nat. Rev. Microbiol.* 2008, **6**:455–65.
20. Larsen SH, Adler J, Gargus JJ, Hogg RW: **Chemomechanical coupling without ATP: the source of energy for motility and chemotaxis in bacteria.** . *Proc. Natl. Acad. Sci. U. S. A.* 1974, **71**:1239–43.
21. Kojima S: **Dynamism and regulation of the stator, the energy conversion complex of the bacterial flagellar motor** . *Curr. Opin. Microbiol.* 2015, **28**:66–71.
22. Brown DA, Berg HC: **Temporal stimulation of chemotaxis in Escherichia coli.** .

Proc. Natl. Acad. Sci. U. S. A. 1974, **71**:1388–92.
23. Berg HC, Brown DA: **Chemotaxis in Escherichia coli analysed by three-dimensional tracking.** . *Nature* 1972, **239**:500–4.
24. Blocker A, Komoriya K, Aizawa S-I: **Type III secretion systems and bacterial flagella: insights into their function from structural similarities.** . *Proc. Natl. Acad. Sci. U. S. A.* 2003, **100**:3027–30.
25. Minamino T: **Protein export through the bacterial flagellar type III export pathway.** . *Biochim. Biophys. Acta* 2014, **1843**:1642–8.
26. Saijo-Hamano Y, Imada K, Minamino T, Kihara M, Shimada M, Kitao A, Namba K: **Structure of the cytoplasmic domain of FlhA and implication for flagellar type III protein export.** . *Mol. Microbiol.* 2010, **76**:260–8.
27. Bange G, Kümmerer N, Engel C, Bozkurt G, Wild K, Sinning I: **FlhA provides the adaptor for coordinated delivery of late flagella building blocks to the type III secretion system.** . *Proc. Natl. Acad. Sci. U. S. A.* 2010, **107**:11295–300.
28. Moore SA, Jia Y: **Structure of the cytoplasmic domain of the flagellar secretion apparatus component FlhA from Helicobacter pylori.** . *J. Biol. Chem.* 2010, **285**:21060–9.
29. Kinoshita M, Hara N, Imada K, Namba K, Minamino T: **Interactions of bacterial flagellar chaperone-substrate complexes with FlhA contribute to co-ordinating assembly of the flagellar filament.** . *Mol. Microbiol.* 2013, **90**:1249–61.
30. Morimoto Y V, Ito M, Hiraoka KD, Che Y-S, Bai F, Kami-Ike N, Namba K, Minamino T: **Assembly and stoichiometry of FliF and FlhA in Salmonella flagellar basal body.** . *Mol. Microbiol.* 2014, **91**:1214–26.
31. Li H, Sourjik V: **Assembly and stability of flagellar motor in Escherichia coli.** . *Mol. Microbiol.* 2011, **80**:886–99.
32. Abrusci P, Vergara-Irigaray M, Johnson S, Beeby MD, Hendrixson DR, Roversi P, Friede ME, Deane JE, Jensen GJ, Tang CM, et al.: **Architecture of the major component of the type III secretion system export apparatus.** . *Nat. Struct. Mol. Biol.* 2013, **20**:99–104.
33. Meshcheryakov VA, Kitao A, Matsunami H, Samatey FA: **Inhibition of a type III secretion system by the deletion of a short loop in one of its membrane proteins.** . *Acta Crystallogr. D. Biol. Crystallogr.* 2013, **69**:812–20.
34. Smith TG, Pereira L, Hoover TR: **Helicobacter pylori FlhB processing-deficient variants affect flagellar assembly but not flagellar gene expression.** . *Microbiology* 2009, **155**:1170–80.
35. Zarivach R, Deng W, Vuckovic M, Felise HB, Nguyen H V, Miller SI, Finlay BB, Strynadka NCJ: **Structural analysis of the essential self-cleaving type III secretion proteins EscU and SpaS.** . *Nature* 2008, **453**:124–7.
36. Ferris HU, Furukawa Y, Minamino T, Kroetz MB, Kihara M, Namba K, Macnab RM: **FlhB regulates ordered export of flagellar components via autocleavage mechanism.** . *J. Biol. Chem.* 2005, **280**:41236–42.
37. Hirano T, Yamaguchi S, Oosawa K, Aizawa S: **Roles of FliK and FlhB in determination of flagellar hook length in Salmonella typhimurium.** . *J. Bacteriol.* 1994, **176**:5439–49.
38. Ohnishi K, Fan F, Schoenhals GJ, Kihara M, Macnab RM: **The FliO, FliP, FliQ, and FliR proteins of Salmonella typhimurium: putative components for flagellar assembly.** . *J. Bacteriol.* 1997, **179**:6092–9.
39. Barker CS, Meshcheryakova I V., Kostyukova AS, Samatey FA: **FliO Regulation of FliP in the Formation of the Salmonella enterica Flagellum** . *PLoS Genet.* 2010, **6**:e1001143.
40. Barker CS, Meshcheryakova I V., Inoue T, Samatey FA: **Assembling Flagella in**

Salmonella Mutant Strains Producing a Type III Export Apparatus without FliO . *J. Bacteriol.* 2014, **196**:4001–4011.

41. Imada K, Minamino T, Uchida Y, Kinoshita M, Namba K: **Insight into the flagella type III export revealed by the complex structure of the type III ATPase and its regulator.** . *Proc. Natl. Acad. Sci. U. S. A.* 2016, **113**:3633–8.
42. Paul K, Erhardt M, Hirano T, Blair DF, Hughes KT: **Energy source of flagellar type III secretion.** . *Nature* 2008, **451**:489–92.
43. Ueno T, Oosawa K, Aizawa S: **M ring, S ring and proximal rod of the flagellar basal body of Salmonella typhimurium are composed of subunits of a single protein, FliF.** . *J. Mol. Biol.* 1992, **227**:672–7.
44. Jones CJ, Macnab RM, Okino H, Aizawa S: **Stoichiometric analysis of the flagellar hook-(basal-body) complex of Salmonella typhimurium.** . *J. Mol. Biol.* 1990, **212**:377–87.
45. Kojima S, Shinohara A, Terashima H, Yakushi T, Sakuma M, Homma M, Namba K, Imada K: **Insights into the stator assembly of the Vibrio flagellar motor from the crystal structure of MotY.** . *Proc. Natl. Acad. Sci. U. S. A.* 2008, **105**:7696–701.
46. Morimoto Y V, Nakamura S, Hiraoka KD, Namba K, Minamino T: **Distinct roles of highly conserved charged residues at the MotA-FliG interface in bacterial flagellar motor rotation.** . *J. Bacteriol.* 2013, **195**:474–81.
47. Morimoto Y V, Minamino T: **Structure and function of the bi-directional bacterial flagellar motor.** . *Biomolecules* 2014, **4**:217–34.
48. Beeby M, Ribardo DA, Brennan CA, Ruby EG, Jensen GJ, Hendrixson DR: **Diverse high-torque bacterial flagellar motors assemble wider stator rings using a conserved protein scaffold.** . *Proc. Natl. Acad. Sci. U. S. A.* 2016, **113**:E1917-26.
49. Yuan J, Branch RW, Hosu BG, Berg HC: **Adaptation at the output of the chemotaxis signalling pathway** . *Nature* 2012, **484**:233–236.
50. Minamino T, Imada K: **The bacterial flagellar motor and its structural diversity.** . *Trends Microbiol.* 2015, **23**:267–274.
51. Zhao X, Zhang K, Boquoi T, Hu B, Motaleb MA, Miller KA, James ME, Charon NW, Manson MD, Norris SJ, et al.: **Cryoelectron tomography reveals the sequential assembly of bacterial flagella in Borrelia burgdorferi.** . *Proc. Natl. Acad. Sci. U. S. A.* 2013, **110**:14390–5.
52. Cohen EJ, Hughes KT: **Rod-to-hook transition for extracellular flagellum assembly is catalyzed by the L-ring-dependent rod scaffold removal.** . *J. Bacteriol.* 2014, **196**:2387–95.
53. Matsunami H, Barker CS, Yoon Y-H, Wolf M, Samatey FA: **Complete structure of the bacterial flagellar hook reveals extensive set of stabilizing interactions** . *Nat. Commun.* 2016, **7**:13425.
54. Yoon Y-H, Barker CS, Bulieris P V, Matsunami H, Samatey FA: **Structural insights into bacterial flagellar hooks similarities and specificities.** . *Sci. Rep.* 2016, **6**:35552.
55. Evdokimov AG, Phan J, Tropea JE, Routzahn KM, Peters HK, Pokross M, Waugh DS: **Similar modes of polypeptide recognition by export chaperones in flagellar biosynthesis and type III secretion.** . *Nat. Struct. Biol.* 2003, **10**:789–93.
56. Fraser GM, Bennett JCQ, Hughes C: **Substrate-specific binding of hook-associated proteins by FlgN and FliT, putative chaperones for flagellum assembly** . *Mol. Microbiol.* 1999, **32**:569–580.
57. Muskotál A, Király R, Sebestyén A, Gugolya Z, Végh BM, Vonderviszt F: **Interaction of FliS flagellar chaperone with flagellin.** . *FEBS Lett.* 2006, **580**:3916–20.
58. Shibata S, Alam M, Aizawa S-I: **Flagellar Filaments of the Deep-sea Bacteria Idiomarina loihiensis Belong to a Family Different from those of Salmonella typhimurium**. *J. Mol. Biol.* 2005, **352**:510–516.

59. Galkin VE, Yu X, Bielnicki J, Heuser J, Ewing CP, Guerry P, Egelman EH: **Divergence of Quaternary Structures Among Bacterial Flagellar Filaments** . *Science (80-.).* 2008, **320**:382–385.
60. Faulds-Pain A, Birchall C, Aldridge C, Smith WD, Grimaldi G, Nakamura S, Miyata T, Gray J, Li G, Tang JX, et al.: **Flagellin Redundancy in Caulobacter crescentus and Its Implications for Flagellar Filament Assembly** . *J. Bacteriol.* 2011, **193**:2695–2707.
61. Bubendorfer S, Ishihara M, Dohlich K, Heiss C, Vogel J, Sastre F, Panico M, Hitchen P, Dell A, Azadi P, et al.: **Analyzing the Modification of the Shewanella oneidensis MR-1 Flagellar Filament** . *PLoS One* 2013, **8**:e73444.
62. Schuhmacher JS, Thormann KM, Bange G: **How bacteria maintain location and number of flagella?** . *FEMS Microbiol. Rev.* 2015, doi:10.1093/femsre/fuv034.
63. Boll JM, Hendrixson DR: **A regulatory checkpoint during flagellar biogenesis in campylobacter jejuni initiates signal transduction to activate transcription of flagellar genes**. *MBio* 2013, **4**:1–10.
64. Cross BCS, Sinning I, Luirink J, High S: **Delivering proteins for export from the cytosol.** . *Nat. Rev. Mol. Cell Biol.* 2009, **10**:255–64.
65. Grudnik P, Bange G, Sinning I: **Protein targeting by the signal recognition particle.** . *Biol. Chem.* 2009, **390**:775–82.
66. Wang P, Kuhn A, Dalbey RE: **Global change of gene expression and cell physiology in YidC-depleted Escherichia coli.** . *J. Bacteriol.* 2010, **192**:2193–209.
67. Lynch MJ, Levenson R, Kim EA, Sircar R, Blair DF, Dahlquist FW, Crane BR: **Co-Folding of a FliF-FliG Split Domain Forms the Basis of the MS:C Ring Interface within the Bacterial Flagellar Motor** . *Structure* 2017, doi:10.1016/j.str.2016.12.006.
68. Sircar R, Borbat PP, Lynch MJ, Bhatnagar J, Beyersdorf MS, Halkides CJ, Freed JH, Crane BR: **Assembly States of FliM and FliG within the Flagellar Switch Complex** . *J. Mol. Biol.* 2015, **427**:867–886.
69. Schuhmacher JS, Rossmann F, Dempwolff F, Knauer C, Altegoer F, Steinchen W, Dörrich AK, Klingl A, Stephan M, Linne U, et al.: **MinD-like ATPase FlhG effects location and number of bacterial flagella during C-ring assembly** . *Proc. Natl. Acad. Sci.* 2015, **112**:201419388.
70. Sourjik V, Armitage JP: **Spatial organization in bacterial chemotaxis.** . *EMBO J.* 2010, **29**:2724–33.
71. McMurry JL, Murphy JW, González-Pedrajo B: **The FliN-FliH interaction mediates localization of flagellar export ATPase FliI to the C ring complex.** . *Biochemistry* 2006, **45**:11790–8.
72. Notti RQ, Bhattacharya S, Lilic M, Stebbins CE: **A common assembly module in injectisome and flagellar type III secretion sorting platforms.** . *Nat. Commun.* 2015, **6**:7125.
73. Lin T, Gao L, Zhao X, Liu J, Norris SJ, Division C: **Mutations in the Borrelia burgdorferi Flagellar Type III Secretion System Genes fliH and fliI Profoundly Affect Spirochete Flagellar** . *MBio* 2015, **6**:1–13.
74. Erhardt M, Mertens ME, Fabiani FD, Hughes KT: **ATPase-independent type-III protein secretion in Salmonella enterica.** . *PLoS Genet.* 2014, **10**:e1004800.
75. Bai F, Morimoto Y V, Yoshimura SDJ, Hara N, Kami-Ike N, Namba K, Minamino T: **Assembly dynamics and the roles of FliI ATPase of the bacterial flagellar export apparatus.** . *Sci. Rep.* 2014, **4**:6528.
76. Erhardt M, Namba K, Hughes KT: **Bacterial nanomachines: the flagellum and type III injectisome.** . *Cold Spring Harb. Perspect. Biol.* 2010, **2**:a000299.
77. Diepold A, Armitage JP: **Type III secretion systems: the bacterial flagellum and the injectisome.** . *Philos. Trans. R. Soc. Lond. B. Biol. Sci.* 2015, **370**.

78. Cherradi Y, Schiavolin L, Moussa S, Meghraoui A, Meksem A, Biskri L, Azarkan M, Allaoui A, Botteaux A: **Interplay between predicted inner-rod and gatekeeper in controlling substrate specificity of the type III secretion system** . *Mol. Microbiol.* 2013, **87**:1183–1199.
79. Burkinshaw BJ, Deng W, Lameignère E, Wasney GA, Zhu H, Worrall LJ, Finlay BB, Strynadka NCJ: **Structural analysis of a specialized type III secretion system peptidoglycan-cleaving enzyme.** . *J. Biol. Chem.* 2015, **290**:10406–17.
80. Monjarás Feria J, García-Gómez E, Espinosa N, Minamino T, Namba K, González-Pedrajo B: **Role of EscP (Orf16) in injectisome biogenesis and regulation of type III protein secretion in enteropathogenic Escherichia coli.** . *J. Bacteriol.* 2012, **194**:6029–45.
81. Ince D, Sutterwala FS, Yahr TL: **Secretion of Flagellar Proteins by the Pseudomonas aeruginosa Type III Secretion-Injectisome System** . *J. Bacteriol.* 2015, **197**:2003–2011.
82. Erhardt M, Singer HM, Wee DH, Keener JP, Hughes KT: **An infrequent molecular ruler controls flagellar hook length in Salmonella enterica.** . *EMBO J.* 2011, **30**:2948–61.
83. Hughes KT: **Flagellar hook length is controlled by a secreted molecular ruler.** . *J. Bacteriol.* 2012, **194**:4793–6.
84. Erhardt M, Hirano T, Su Y, Paul K, Wee DH, Mizuno S, Aizawa S, Hughes KT: **The role of the FliK molecular ruler in hook-length control in Salmonella enterica.** . *Mol. Microbiol.* 2010, **75**:1272–84.
85. Morris DP, Roush ED, Thompson JW, Moseley MA, Murphy JW, McMurry JL: **Kinetic characterization of Salmonella FliK-FlhB interactions demonstrates complexity of the Type III secretion substrate-specificity switch.** . *Biochemistry* 2010, **49**:6386–93.
86. Mizuno S, Amida H, Kobayashi N, Aizawa S-I, Tate S-I: **The NMR structure of FliK, the trigger for the switch of substrate specificity in the flagellar type III secretion apparatus.** . *J. Mol. Biol.* 2011, **409**:558–73.
87. Minamino T, Kinoshita M, Hara N, Takeuchi S, Hida A, Koya S, Glenwright H, Imada K, Aldridge PD, Namba K: **Interaction of a bacterial flagellar chaperone FlgN with FlhA is required for efficient export of its cognate substrates.** . *Mol. Microbiol.* 2012, **83**:775–88.
88. Imada K, Vonderviszt F, Furukawa Y, Oosawa K, Namba K: **Assembly characteristics of flagellar cap protein HAP2 of Salmonella: decamer and pentamer in the pH-sensitive equilibrium.** . *J. Mol. Biol.* 1998, **277**:883–91.
89. Shimizu R, Taguchi F, Marutani M, Mukaihara T, Inagaki Y, Toyoda K, Shiraishi T, Ichinose Y: **The DeltafliD mutant of Pseudomonas syringae pv. tabaci, which secretes flagellin monomers, induces a strong hypersensitive reaction (HR) in non-host tomato cells.** . *Mol. Genet. Genomics* 2003, **269**:21–30.
90. Altegoer F, Rensing SA, Bange G: **Structural basis for the CsrA-dependent modulation of translation initiation by an ancient regulatory protein.** . *Proc. Natl. Acad. Sci. U. S. A.* 2016, **113**:10168–73.
91. Mukherjee S, Babitzke P, Kearns DB: **FliW and FliS function independently to control cytoplasmic flagellin levels in Bacillus subtilis.** . *J. Bacteriol.* 2013, **195**:297–306.
92. Aldridge P, Hughes KT: **Regulation of flagellar assembly.** . *Curr. Opin. Microbiol.* 2002, **5**:160–5.
93. Mukherjee S, Kearns DB: **The structure and regulation of flagella in Bacillus subtilis.** . *Annu. Rev. Genet.* 2014, **48**:319–40.
94. Cozy LM, Kearns DB: **Gene position in a long operon governs motility**

development in *Bacillus subtilis* . *Mol. Microbiol.* 2010, **76**:273–285.
95. Kearns DB, Losick R: **Cell population heterogeneity during growth of Bacillus subtilis.** . *Genes Dev.* 2005, **19**:3083–94.
96. Márquez LM, Helmann JD, Ferrari E, Parker HM, Ordal GW, Chamberlin MJ: **Studies of sigma D-dependent functions in Bacillus subtilis.** . *J. Bacteriol.* 1990, **172**:3435–43.
97. Helmann JD, Márquez LM, Chamberlin MJ: **Cloning, sequencing, and disruption of the Bacillus subtilis sigma 28 gene.** . *J. Bacteriol.* 1988, **170**:1568–74.
98. Senesi S, Ghelardi E, Celandroni F, Salvetti S, Parisio E, Galizzi A: **Surface-associated flagellum formation and swarming differentiation in Bacillus subtilis are controlled by the ifm locus.** . *J. Bacteriol.* 2004, **186**:1158–64.
99. Calvio C, Celandroni F, Ghelardi E, Amati G, Salvetti S, Ceciliani F, Galizzi A, Senesi S: **Swarming Differentiation and Swimming Motility in Bacillus subtilis Are Controlled by swrA, a Newly Identified Dicistronic Operon** . *J. Bacteriol.* 2005, **187**:5356–5366.
100. Veening J-W, Kuipers OP: **Gene position within a long transcript as a determinant for stochastic switching in bacteria** . *Mol. Microbiol.* 2010, **76**:269–272.
101. Cozy LM, Phillips AM, Calvo RA, Bate AR, Hsueh Y-H, Bonneau R, Eichenberger P, Kearns DB: **SlrA/SinR/SlrR inhibits motility gene expression upstream of a hypersensitive and hysteretic switch at the level of σ(D) in Bacillus subtilis.** . *Mol. Microbiol.* 2012, **83**:1210–28.
102. Chai Y, Norman T, Kolter R, Losick R: **An epigenetic switch governing daughter cell separation in Bacillus subtilis.** . *Genes Dev.* 2010, **24**:754–65.
103. Sorenson MK, Ray SS, Darst SA: **Crystal structure of the flagellar sigma/anti-sigma complex sigma(28)/FlgM reveals an intact sigma factor in an inactive conformation.** . *Mol. Cell* 2004, **14**:127–38.
104. Khanra N, Rossi P, Economou A, Kalodimos CG: **Recognition and targeting mechanisms by chaperones in flagellum assembly and operation.** . *Proc. Natl. Acad. Sci. U. S. A.* 2016, **113**:9798–803.
105. Hsueh Y-H, Cozy LM, Sham L-T, Calvo RA, Gutu AD, Winkler ME, Kearns DB: **DegU-phosphate activates expression of the anti-sigma factor FlgM in Bacillus subtilis.** . *Mol. Microbiol.* 2011, **81**:1092–108.
106. Calvo RA, Kearns DB: **FlgM is secreted by the flagellar export apparatus in Bacillus subtilis.** . *J. Bacteriol.* 2015, **197**:81–91.
107. Karlinsey JE, Tanaka S, Bettenworth V, Yamaguchi S, Boos W, Aizawa SI, Hughes KT: **Completion of the hook-basal body complex of the Salmonella typhimurium flagellum is coupled to FlgM secretion and fliC transcription.** . *Mol. Microbiol.* 2000, **37**:1220–31.
108. Steitz JA, Jakes K: **How ribosomes select initiator regions in mRNA: base pair formation between the 3' terminus of 16S rRNA and the mRNA during initiation of protein synthesis in Escherichia coli.** . *Proc. Natl. Acad. Sci. U. S. A.* 1975, **72**:4734–8.
109. Shine J, Dalgarno L: **Determinant of cistron specificity in bacterial ribosomes.** . *Nature* 1975, **254**:34–8.
110. Romeo T, Vakulskas CA, Babitzke P: **Post-transcriptional regulation on a global scale: form and function of Csr/Rsm systems.** . *Environ. Microbiol.* 2013, **15**:313–24.
111. Vakulskas CA, Potts AH, Babitzke P, Ahmer BMM, Romeo T: **Regulation of Bacterial Virulence by Csr (Rsm) Systems** . *Microbiol. Mol. Biol. Rev.* 2015, **79**:193–224.
112. Romeo T, Gong M, Liu MY, Brun-Zinkernagel AM: **Identification and molecular**

characterization of csrA, a pleiotropic gene from Escherichia coli that affects glycogen biosynthesis, gluconeogenesis, cell size, and surface properties. . *J. Bacteriol.* 1993, **175**:4744–55.

113. Sabnis NA, Yang H, Romeo T: **Pleiotropic regulation of central carbohydrate metabolism in Escherichia coli via the gene csrA.** . *J. Biol. Chem.* 1995, **270**:29096–104.
114. Liu Y, Cui Y, Mukherjee A, Chatterjee AK: **Characterization of a novel RNA regulator of Erwinia carotovora ssp. carotovora that controls production of extracellular enzymes and secondary metabolites.** . *Mol. Microbiol.* 1998, **29**:219–34.
115. Gutiérrez P, Li Y, Osborne MJ, Pomerantseva E, Liu Q, Gehring K: **Solution structure of the carbon storage regulator protein CsrA from Escherichia coli.** . *J. Bacteriol.* 2005, **187**:3496–501.
116. Heeb S, Kuehne SA, Bycroft M, Crivii S, Allen MD, Haas D, Cámara M, Williams P: **Functional analysis of the post-transcriptional regulator RsmA reveals a novel RNA-binding site.** . *J. Mol. Biol.* 2006, **355**:1026–36.
117. Schubert M, Lapouge K, Duss O, Oberstrass FC, Jelesarov I, Haas D, Allain FH-T: **Molecular basis of messenger RNA recognition by the specific bacterial repressing clamp RsmA/CsrA.** . *Nat. Struct. Mol. Biol.* 2007, **14**:807–13.
118. Rife C, Schwarzenbacher R, McMullan D, Abdubek P, Ambing E, Axelrod H, Biorac T, Canaves JM, Chiu H-J, Deacon AM, et al.: **Crystal structure of the global regulatory protein CsrA from Pseudomonas putida at 2.05 A resolution reveals a new fold.** . *Proteins* 2005, **61**:449–53.
119. Mercante J, Suzuki K, Cheng X, Babitzke P, Romeo T: **Comprehensive alanine-scanning mutagenesis of Escherichia coli CsrA defines two subdomains of critical functional importance.** . *J. Biol. Chem.* 2006, **281**:31832–42.
120. Dubey AK, Baker CS, Romeo T, Babitzke P: **RNA sequence and secondary structure participate in high-affinity CsrA-RNA interaction.** . *RNA* 2005, **11**:1579–87.
121. Mercante J, Edwards AN, Dubey AK, Babitzke P, Romeo T: **Molecular geometry of CsrA (RsmA) binding to RNA and its implications for regulated expression.** . *J. Mol. Biol.* 2009, **392**:511–28.
122. Duss O, Michel E, Yulikov M, Schubert M, Jeschke G, Allain FH-T: **Structural basis of the non-coding RNA RsmZ acting as a protein sponge.** . *Nature* 2014, **509**:588–92.
123. Weilbacher T, Suzuki K, Dubey AK, Wang X, Gudapaty S, Morozov I, Baker CS, Georgellis D, Babitzke P, Romeo T: **A novel sRNA component of the carbon storage regulatory system of Escherichia coli.** . *Mol. Microbiol.* 2003, **48**:657–70.
124. Sonnleitner E, Haas D: **Small RNAs as regulators of primary and secondary metabolism in Pseudomonas species.** . *Appl. Microbiol. Biotechnol.* 2011, **91**:63–79.
125. Duss O, Michel E, Diarra dit Konté N, Schubert M, Allain FH-T: **Molecular basis for the wide range of affinity found in Csr/Rsm protein-RNA recognition.** . *Nucleic Acids Res.* 2014, **42**:5332–46.
126. Morris ER, Hall G, Li C, Heeb S, Kulkarni RV, Lovelock L, Silistre H, Messina M, Cámara M, Emsley J, et al.: **Structural Rearrangement in an RsmA/CsrA Ortholog of Pseudomonas aeruginosa Creates a Dimeric RNA-Binding Protein, RsmN** . *Structure* 2013, **21**:1659–1671.
127. Zere TR, Vakulskas CA, Leng Y, Pannuri A, Potts AH, Dias R, Tang D, Kolaczkowski B, Georgellis D, Ahmer BMM, et al.: **Genomic Targets and Features of BarA-UvrY (-SirA) Signal Transduction Systems** . *PLoS One* 2015, **10**:e0145035.
128. Edwards AN, Patterson-Fortin LM, Vakulskas CA, Mercante JW, Potrykus K, Vinella

D, Camacho MI, Fields JA, Thompson SA, Georgellis D, et al.: **Circuitry linking the Csr and stringent response global regulatory systems** . *Mol. Microbiol.* 2011, **80**:1561–1580.

129. Vakulskas CA, Pannuri A, Cortés-Selva D, Zere TR, Ahmer BM, Babitzke P, Romeo T: **Global effects of the DEAD-box RNA helicase DeaD (CsdA) on gene expression over a broad range of temperatures** . *Mol. Microbiol.* 2014, **92**:945–958.
130. Romeo T: **Global regulation by the small RNA-binding protein CsrA and the non-coding RNA molecule CsrB.** . *Mol. Microbiol.* 1998, **29**:1321–30.
131. Heroven AK, Böhme K, Dersch P: **The Csr/Rsm system of Yersinia and related pathogens: A post-transcriptional strategy for managing virulence** . *RNA Biol.* 2012, **9**:379–91.
132. Dugar G, Svensson SL, Bischler T, Wäldchen S, Reinhardt R, Sauer M, Sharma CM: **The CsrA-FliW network controls polar localization of the dual-function flagellin mRNA in Campylobacter jejuni.** . *Nat. Commun.* 2016, **7**:11667.
133. Mukherjee S, Yakhnin H, Kysela D, Sokoloski J, Babitzke P, Kearns DB: **CsrA-FliW interaction governs flagellin homeostasis and a checkpoint on flagellar morphogenesis in Bacillus subtilis.** . *Mol. Microbiol.* 2011, **82**:447–61.
134. Wilkinson DA, Chacko SJ, Vénien-Bryan C, Wadhams GH, Armitage JP: **Regulation of flagellum number by FliA and FlgM and role in biofilm formation by Rhodobacter sphaeroides.** . *J. Bacteriol.* 2011, **193**:4010–4.
135. Ding L, Wang Y, Hu Y, Atkinson S, Williams P, Chen S: **Functional characterization of FlgM in the regulation of flagellar synthesis and motility in Yersinia pseudotuberculosis.** . *Microbiology* 2009, **155**:1890–900.
136. Auvray F, Thomas J, Fraser GM, Hughes C: **Flagellin polymerisation control by a cytosolic export chaperone.** . *J. Mol. Biol.* 2001, **308**:221–9.
137. Yonekura K, Maki-Yonekura S, Namba K: **Complete atomic model of the bacterial flagellar filament by electron cryomicroscopy.** . *Nature* 2003, **424**:643–50.
138. Karna SLR, Prabhu RG, Lin Y-H, Miller CL, Seshu J: **Contributions of environmental signals and conserved residues to the functions of carbon storage regulator A of Borrelia burgdorferi.** . *Infect. Immun.* 2013, **81**:2972–85.
139. Yakhnin H, Pandit P, Petty TJ, Baker CS, Romeo T, Babitzke P: **CsrA of Bacillus subtilis regulates translation initiation of the gene encoding the flagellin protein (hag) by blocking ribosome binding.** . *Mol. Microbiol.* 2007, **64**:1605–20.
140. Rost B: **Twilight zone of protein sequence alignments.** . *Protein Eng.* 1999, **12**:85–94.
141. Holm L, Sander C: **Dali: a network tool for protein structure comparison.** . *Trends Biochem. Sci.* 1995, **20**:478–80.
142. Maruyama Y, Momma M, Mikami B, Hashimoto W, Murata K: **Crystal structure of a novel bacterial cell-surface flagellin binding to a polysaccharide.** . *Biochemistry* 2008, **47**:1393–402.
143. Samatey FA, Imada K, Nagashima S, Vonderviszt F, Kumasaka T, Yamamoto M, Namba K: **Structure of the bacterial flagellar protofilament and implications for a switch for supercoiling.** . *Nature* 2001, **410**:331–7.
144. Song WS, Yoon S: **Crystal structure of FliC flagellin from Pseudomonas aeruginosa and its implication in TLR5 binding and formation of the flagellar filament.** . *Biochem. Biophys. Res. Commun.* 2014, **444**:109–15.
145. Titz B, Rajagopala S V, Ester C, Häuser R, Uetz P: **Novel conserved assembly factor of the bacterial flagellum.** . *J. Bacteriol.* 2006, **188**:7700–6.
146. Konarev P V., Volkov V V., Sokolova A V., Koch MHJ, Svergun DI, IUCr, C. B, R. K, J. KMH, M. MS, et al.: ***PRIMUS*: a Windows PC-based system for small-angle scattering data analysis** . *J. Appl. Crystallogr.* 2003, **36**:1277–1282.

147. Pausch P, Singh U, Ahmed YL, Pillet B, Murat G, Altegoer F, Stier G, Thoms M, Hurt E, Sinning I, et al.: **Co-translational capturing of nascent ribosomal proteins by their dedicated chaperones.** . *Nat. Commun.* 2015, **6**:7494.
148. Guttenplan SB, Shaw S, Kearns DB: **The cell biology of peritrichous flagella in Bacillus subtilis.** . *Mol. Microbiol.* 2013, **87**:211–29.
149. Sohmen D, Chiba S, Shimokawa-Chiba N, Innis CA, Berninghausen O, Beckmann R, Ito K, Wilson DN: **Structure of the Bacillus subtilis 70S ribosome reveals the basis for species-specific stalling.** . *Nat. Commun.* 2015, **6**:6941.
150. Lin L, Thanbichler M: **Nucleotide-independent cytoskeletal scaffolds in bacteria.** . *Cytoskeleton (Hoboken).* 2013, **70**:409–23.
151. El Andari J, Altegoer F, Bange G, Graumann PL: **Bacillus subtilis Bactofilins Are Essential for Flagellar Hook- and Filament Assembly and Dynamically Localize into Structures of Less than 100 nm Diameter underneath the Cell Membrane.** . *PLoS One* 2015, **10**:e0141546.
152. Rajagopala S V, Titz B, Goll J, Parrish JR, Wohlbold K, McKevitt MT, Palzkill T, Mori H, Finley RL, Uetz P: **The protein network of bacterial motility.** . *Mol. Syst. Biol.* 2007, **3**:128.
153. Kühn J, Briegel A, Mörschel E, Kahnt J, Leser K, Wick S, Jensen GJ, Thanbichler M: **Bactofilins, a ubiquitous class of cytoskeletal proteins mediating polar localization of a cell wall synthase in Caulobacter crescentus.** . *EMBO J.* 2010, **29**:327–39.
154. Gast K, Fiedler C: **Dynamic and Static Light Scattering of Intrinsically Disordered Proteins** . In *Intrinsically Disordered Protein Analysis*. . Springer New York; 2012:137–161.
155. BLAKE CCF, KOENIG DF, MAIR GA, NORTH ACT, PHILLIPS DC, SARMA VR: **Structure of Hen Egg-White Lysozyme: A Three-dimensional Fourier Synthesis at 2 Å Resolution** . *Nature* 1965, **206**:757–761.
156. ALDERTON G, FEVOLD HL: **Direct crystallization of lysozyme from egg white and some crystalline salts of lysozyme.** . *J. Biol. Chem.* 1946, **164**:1–5.
157. Matthews BW: **Solvent content of protein crystals.** . *J. Mol. Biol.* 1968, **33**:491–7.
158. Shi C, Fricke P, Lin L, Chevelkov V, Wegstroth M, Giller K, Becker S, Thanbichler M, Lange A: **Atomic-resolution structure of cytoskeletal bactofilin by solid-state NMR.** . *Sci. Adv.* 2015, **1**:e1501087.
159. Keegan RM, Winn MD, IUCr, L. MT, A. SA, J. Z, Z. Z, W. M, J. LD, M. B, et al.: **Automated search-model discovery and preparation for structure solution by molecular replacement** . *Acta Crystallogr. Sect. D Biol. Crystallogr.* 2007, **63**:447–457.
160. Sheldrick GM: **Experimental phasing with *SHELXC* / *D* / *E*: combining chain tracing with density modification** . *Acta Crystallogr. Sect. D Biol. Crystallogr.* 2010, **66**:479–485.
161. Pannu NS, Waterreus WJ, Skubák P, Sikharulidze I, Abrahams JP, de Graaff RAG: **Recent advances in the CRANK software suite for experimental phasing.** . *Acta Crystallogr. D. Biol. Crystallogr.* 2011, **67**:331–7.
162. Zwart PH, Afonine P V., Grosse-Kunstleve RW, Hung L-W, Ioerger TR, McCoy AJ, McKee E, Moriarty NW, Read RJ, Sacchettini JC, et al.: **Automated Structure Solution with the PHENIX Suite** . In *Methods in molecular biology (Clifton, N.J.)*. . 2008:419–435.
163. Murzin AG: **OB(oligonucleotide/oligosaccharide binding)-fold: common structural and functional solution for non-homologous sequences.** . *EMBO J.* 1993, **12**:861–7.
164. Watson E, Matousek WM, Irimies EL, Alexandrescu AT: **Partially Folded States of Staphylococcal Nuclease Highlight the Conserved Structural Hierarchy of OB-Fold Proteins** † . *Biochemistry* 2007, **46**:9484–9494.

165. Murzin AG, Brenner SE, Hubbard T, Chothia C: **SCOP: a structural classification of proteins database for the investigation of sequences and structures.** . *J. Mol. Biol.* 1995, **247**:536–540.
166. Murzin AG: **How far divergent evolution goes in proteins.** . *Curr. Opin. Struct. Biol.* 1998, **8**:380–7.
167. Titz B, Rajagopala S V, Goll J, Häuser R, McKevitt MT, Palzkill T, Uetz P: **The binary protein interactome of Treponema pallidum--the syphilis spirochete.** . *PLoS One* 2008, **3**:e2292.
168. Valverde C, Heeb S, Keel C, Haas D: **RsmY, a small regulatory RNA, is required in concert with RsmZ for GacA-dependent expression of biocontrol traits in Pseudomonas fluorescens CHA0.** . *Mol. Microbiol.* 2003, **50**:1361–79.
169. Lucchetti-Miganeh C, Burrowes E, Baysse C, Ermel G: **The post-transcriptional regulator CsrA plays a central role in the adaptation of bacterial pathogens to different stages of infection in animal hosts**. *Microbiology* 2008, **154**:16–29.
170. Heroven AK, Böhme K, Rohde M, Dersch P: **A Csr-type regulatory system, including small non-coding RNAs, regulates the global virulence regulator RovA of Yersinia pseudotuberculosis through RovM.** . *Mol. Microbiol.* 2008, **68**:1179–95.
171. Wei BL, Brun-Zinkernagel AM, Simecka JW, Prüss BM, Babitzke P, Romeo T: **Positive regulation of motility and flhDC expression by the RNA-binding protein CsrA of Escherichia coli.** . *Mol. Microbiol.* 2001, **40**:245–56.
172. Yakhnin A V, Baker CS, Vakulskas CA, Yakhnin H, Berezin I, Romeo T, Babitzke P: **CsrA activates flhDC expression by protecting flhDC mRNA from RNase E-mediated cleavage.** . *Mol. Microbiol.* 2013, **87**:851–66.
173. Jonas K, Edwards AN, Ahmad I, Romeo T, Römling U, Melefors O: **Complex regulatory network encompassing the Csr, c-di-GMP and motility systems of Salmonella Typhimurium.** . *Environ. Microbiol.* 2010, **12**:524–40.
174. Suzuki K, Wang X, Weilbacher T, Pernestig A-K, Melefors O, Georgellis D, Babitzke P, Romeo T: **Regulatory circuitry of the CsrA/CsrB and BarA/UvrY systems of Escherichia coli.** . *J. Bacteriol.* 2002, **184**:5130–40.
175. Camacho MI, Alvarez AF, Gonzalez Chavez R, Romeo T, Merino E, Georgellis D: **Effects of the Global Regulator CsrA on the BarA/UvrY Two-Component Signaling System** . *J. Bacteriol.* 2015, **197**:983–991.
176. Pernestig A-K, Melefors O, Georgellis D: **Identification of UvrY as the Cognate Response Regulator for the BarA Sensor Kinase in Escherichia coli** . *J. Biol. Chem.* 2001, **276**:225–231.
177. Mukherjee S, Oshiro RT, Yakhnin H, Babitzke P, Kearns DB: **FliW antagonizes CsrA RNA binding by a noncompetitive allosteric mechanism** . *Proc. Natl. Acad. Sci.* 2016, **113**:9870–9875.
178. Bulyha I, Lindow S, Lin L, Bolte K, Wuichet K, Kahnt J, van der Does C, Thanbichler M, Søgaard-Andersen L: **Two Small GTPases Act in Concert with the Bactofilin Cytoskeleton to Regulate Dynamic Bacterial Cell Polarity** . *Dev. Cell* 2013, **25**:119–131.
179. Bonifield HR, Yamaguchi S, Hughes KT: **The flagellar hook protein, FlgE, of Salmonella enterica serovar typhimurium is posttranscriptionally regulated in response to the stage of flagellar assembly.** . *J. Bacteriol.* 2000, **182**:4044–50.
180. Lee HJ, Hughes KT: **Posttranscriptional control of the Salmonella enterica flagellar hook protein FlgE.** . *J. Bacteriol.* 2006, **188**:3308–16.
181. Courtney CR, Cozy LM, Kearns DB: **Molecular characterization of the flagellar hook in Bacillus subtilis.** . *J. Bacteriol.* 2012, **194**:4619–29.
182. Koch MK, McHugh CA, Hoiczyk E: **BacM, an N-terminally processed bactofilin of Myxococcus xanthus, is crucial for proper cell shape.** . *Mol. Microbiol.* 2011,

80:1031–51.

183. Marchler-Bauer A, Bo Y, Han L, He J, Lanczycki CJ, Lu S, Chitsaz F, Derbyshire MK, Geer RC, Gonzales NR, et al.: **CDD/SPARCLE: functional classification of proteins via subfamily domain architectures.** . *Nucleic Acids Res.* 2017, **45**:D200–D203.
184. Park S, Park Y-H, Lee C-R, Kim Y-R, Seok Y-J: **Glucose induces delocalization of a flagellar biosynthesis protein from the flagellated pole.** . *Mol. Microbiol.* 2016, doi:10.1111/mmi.13424.
185. Vasa S, Lin L, Shi C, Habenstein B, Riedel D, Kühn J, Thanbichler M, Lange A: **β-Helical architecture of cytoskeletal bactofilin filaments revealed by solid-state NMR** . *Proc. Natl. Acad. Sci.* 2015, **112**:E127–E136.
186. Kassem MM, Wang Y, Boomsma W, Lindorff-Larsen K: **Structure of the Bacterial Cytoskeleton Protein Bactofilin by NMR Chemical Shifts and Sequence Variation** . *Biophys. J.* 2016, **110**:2342–2348.
187. Furukawa Y, Inoue Y, Sakaguchi A, Mori Y, Fukumura T, Miyata T, Namba K, Minamino T: **Structural stability of flagellin subunit affects the rate of flagellin export in the absence of FliS chaperone.** . *Mol. Microbiol.* 2016, **102**:405–416.
188. Xu S, Peng Z, Cui B, Wang T, Song Y, Zhang L, Wei G, Wang Y, Shen X: **FliS modulates FlgM activity by acting as a non-canonical chaperone to control late flagellar gene expression, motility and biofilm formation in *Y ersinia pseudotuberculosis*** . *Environ. Microbiol.* 2014, **16**:1090–1104.
189. Yokoseki T, Iino T, Kutsukake K: **Negative regulation by fliD, fliS, and fliT of the export of the flagellum-specific anti-sigma factor, FlgM, in Salmonella typhimurium.** . *J. Bacteriol.* 1996, **178**:899–901.
190. Galeva A, Moroz N, Yoon Y-H, Hughes KT, Samatey FA, Kostyukova AS: **Bacterial Flagellin-Specific Chaperone FliS Interacts with Anti-Sigma Factor FlgM** . *J. Bacteriol.* 2014, **196**:1215–1221.
191. Minamino T, Morimoto Y V, Hara N, Aldridge PD, Namba K: **The Bacterial Flagellar Type III Export Gate Complex Is a Dual Fuel Engine That Can Use Both H+ and Na+ for Flagellar Protein Export.** . *PLoS Pathog.* 2016, **12**:e1005495.
192. Erhardt M, Wheatley P, Kim EA, Hirano T, Zhang Y, Sarkar MK, Hughes KT, Blair DF: **Mechanism of type-III protein secretion: Regulation of FlhA conformation by a functionally critical charged-residue cluster** . *Mol. Microbiol.* 2017, doi:10.1111/mmi.13623.
193. Minamino T, Namba K: **Distinct roles of the FliI ATPase and proton motive force in bacterial flagellar protein export.** . *Nature* 2008, **451**:485–8.
194. Akeda Y, Galán JE: **Chaperone release and unfolding of substrates in type III secretion** . *Nature* 2005, **437**:911–915.
195. Stern AS, Berg HC: **Single-File Diffusion of Flagellin in Flagellar Filaments** . *Biophys. J.* 2013, **105**:182–184.
196. Evans LDB, Stafford GP, Ahmed S, Fraser GM, Hughes C: **An escort mechanism for cycling of export chaperones during flagellum assembly** . *Proc. Natl. Acad. Sci.* 2006, **103**:17474–17479.
197. Fraser GM, González-Pedrajo B, Tame JRH, Macnab RM: **Interactions of FliJ with the Salmonella type III flagellar export apparatus.** . *J. Bacteriol.* 2003, **185**:5546–54.
198. Ibuki T, Uchida Y, Hironaka Y, Namba K, Imada K, Minamino T: **Interaction between FliJ and FlhA, components of the bacterial flagellar type III export apparatus.** . *J. Bacteriol.* 2013, **195**:466–73.
199. Sun P, Tropea JE, Austin BP, Cherry S, Waugh DS: **Structural Characterization of the Yersinia pestis Type III Secretion System Needle Protein YscF in Complex with Its Heterodimeric Chaperone YscE/YscG** . *J. Mol. Biol.* 2008, **377**:819–830.

200. Pillet B, García-Gómez JJ, Pausch P, Falquet L, Bange G, de la Cruz J, Kressler D: **The Dedicated Chaperone Acl4 Escorts Ribosomal Protein Rpl4 to Its Nuclear Pre-60S Assembly Site** . *PLOS Genet.* 2015, **11**:e1005565.
201. Konkol MA, Blair KM, Kearns DB: **Plasmid-Encoded ComI Inhibits Competence in the Ancestral 3610 Strain of Bacillus subtilis** . *J. Bacteriol.* 2013, **195**:4085–4093.
202. Blair KM, Turner L, Winkelman JT, Berg HC, Kearns DB: **A molecular clutch disables flagella in the Bacillus subtilis biofilm.** . *Science* 2008, **320**:1636–8.
203. Garić D, Humbert L, Fils-Aimé N, Korah J, Zarfabian Y, Lebrun J-J, Ali S: **Development of buffers for fast semidry transfer of proteins.** . *Anal. Biochem.* 2013, **441**:182–4.
204. Mruk DD, Cheng CY: **Enhanced chemiluminescence (ECL) for routine immunoblotting: An inexpensive alternative to commercially available kits.** . *Spermatogenesis* 2011, **1**:121–122.
205. Kabsch W: **XDS.** . *Acta Crystallogr. D. Biol. Crystallogr.* 2010, **66**:125–32.
206. Evans PR, Murshudov GN: **How good are my data and what is the resolution?** . *Acta Crystallogr. D. Biol. Crystallogr.* 2013, **69**:1204–14.
207. Winn MD, Ballard CC, Cowtan KD, Dodson EJ, Emsley P, Evans PR, Keegan RM, Krissinel EB, Leslie AGW, McCoy A, et al.: **Overview of the CCP4 suite and current developments.** . *Acta Crystallogr. D. Biol. Crystallogr.* 2011, **67**:235–42.
208. Adams PD, Afonine P V, Bunkóczi G, Chen VB, Davis IW, Echols N, Headd JJ, Hung L-W, Kapral GJ, Grosse-Kunstleve RW, et al.: **PHENIX: a comprehensive Python-based system for macromolecular structure solution.** . *Acta Crystallogr. D. Biol. Crystallogr.* 2010, **66**:213–21.
209. Emsley P, Cowtan K: **Coot: model-building tools for molecular graphics.** . *Acta Crystallogr. D. Biol. Crystallogr.* 2004, **60**:2126–32.
210. Petoukhov M V., Franke D, Shkumatov A V., Tria G, Kikhney AG, Gajda M, Gorba C, Mertens HDT, Konarev P V., Svergun DI: **New developments in the *ATSAS* program package for small-angle scattering data analysis** . *J. Appl. Crystallogr.* 2012, **45**:342–350.
211. Li G-Z, Vissers JPC, Silva JC, Golick D, Gorenstein M V., Geromanos SJ: **Database searching and accounting of multiplexed precursor and product ion spectra from the data independent analysis of simple and complex peptide mixtures** . *Proteomics* 2009, **9**:1696–1719.

8 APPENDIX

8.1 Oligonucleotides

Supplement table 1: Oligonucleotides used in this study.

Org	Oligonucleotide	Sequence (5'-3')
Bs	BacE_Bam_rv	aattggatccttacaactttgtgga
Bs	BacE_Nco_fw	ttaaccatggggcaccatcaccatcaccatatggatgtagtggaa
Bs	BacE_NcoI_nohis	ttaaccatggggatggatgtagtggaa
Bs	BacF_Nco_fw	ttaaccatggggcaccatcaccatcaccatatggagacaacaaaa
Bs	BacF_NcoI_nohis	ttaaccatggggatggagacaacaaaa
Bs	BacF_Bam_rv	aattggatccttacagttttgtttt
Bs	FliW_PciI_fw	ttaaacatgtcaatgatcattcatacg
Bs	FliW_XhoI_6H_rv	aattctcgagctaatggtgatggtgatggtggcatgattctcc
Bs	FliW_BamHI_rv	aattggatccctagcatgattctcc
Bs	FliW_XhoI_rv	aattctcgagctagcatgattctcc
Bs	Bs_FliS_fw	ttaaccatggggcaccatcaccatcaccatatggcgatccaaaat
Bs	Bs_FliS_rv	aattctcgagtcaatggtgatggtgatggtgtgcgatcccgcc
Bs	BsHag_F	ttaaccatgggcagaattaaccaca
Bs	BsHagN50_6H_R	aattggatccttagtgatggtgatggtgatgttcagagatcgcaag
Bs	BsHagN60_6H_R	aattggatccttagtgatggtgatggtgatgttcaagacctctgat
Bs	BsHagdN72_6H_R	aattggatccttagtgatggtgatggtgatg
Bs	BsHagdN20_F	ttaa ccatgg gcagtgcgagccaaaag
Bs	BsHagdN40_F	ttaa ccatgg gcgcgggagatgacgca
Bs	BsCsrAN55D_F	tcaggaagaagaaaaccgtgctgcagcg
Bs	BsCsrAN55D_R	cgctgcagcacggttttcttcttcctga
Bs	BsCsrAR44A_F	tgatatccacgcaaaagaaattt
Bs	BsCsrAR44A_R	Aaatttcttttgcgtggatatca
Bs	BsCsrAK31E_F	Ggatcaagtggaacttggaattg
Bs	BsCsrAK31E_R	caattccaagttccacttgatcc
Gt	GtBacE_fw	ttaaccatgggggaacgtcgtgatttg
Gt	GtBacE_rv	aattggatcctcacccttttctctac
Gt	GtBacE_6H_fw	ttaaccatggggcaccatcaccatcaccatgaacgtcgtgatttg
Gt	GtBacF_fw	ttaaccatgggggcagcaagaaactta
Gt	GtBacF_rv	aattggatccctatctttgtctttt
Gt	GtBacF_6H_fw	ttaaccatggggcaccatcaccatcaccatgcagcaagaaactta
Gt	GtFliW_fw	ttaaccatggggaaaatcgcgacaaa
Gt	GtFliW_rv	aattggatccttatttcgccacttt
Gt	GtFliW_6H_rv	aattggatccttaatggtgatggtgatggtgtttcgccacttttt
Gt	GtCsrA_fw	ttaaccatggggcttgtactaacgcgc
Gt	GtCsrA_rv	aattggatcctcatgcttgtttccc
Gt	GtCF_F	ttaacaactcgctgcgcatcgacattgtcacgta
Gt	GtCF_R	aattggaagaaagtcggccgcctttcttcgctat
Gt	GtCsrA_fw	ttaaccatggggcttgtactaacgcgcaaattg

Gt	GtCsrA_rv	aattggatcctcatgcttgtttccccccttt
Gt	GtCsrA_6H_fw	ttaaccatggggcaccatcaccatcaccatcttgtactaacgcgc
Gt	GtCsrA_6H_rv	aattggatcctcaatggtgatggtgatggtgtgcttgtttcccccc
Gt	GtFliWI25D_R	cttgggaagcaagttgatttaacaaacacgaac
Gt	GtFliWI25D_F	gttcgtgtttgttaaatcaacttgcttcccaag
Gt	GtFliWQ123D_R	aagcgacttgggaaggatgttattttaacaaac
Gt	GtFliWQ123D_F	gtttgttaaaataacatccttcccaagtcgctt
Gt	GtFliWF44D_R	ctcgaagacacaccggatatcattttacaatcg
Gt	GtFliWF44D_F	cgattgtaaaatgatatccggtgtgtcttcgag
Hp	Hp1542_F	aatt ccatgg gc gcaatctttgataac
Hp	Hp1542_R	aattggatccttaatggtgatggtgatggtg tttattttcaatttt
Tm	Tm0735_F	ttaa ccatgg gc aaggtagagatcaca
Tm	Tm0735_R	ttaa ctcgag tta atggtgatggtgatggtg cgctgaataccctcc
Tm	Tm0735_dN25_NcoI_F	ttaa ccatgg gc cttacaaaggaagagctttt
Sp	SpBac_F	ttaa ccatgg gc ttgccacctgaactt
Sp	SpBac_R	ttaa ggatcc tta atggtgatggtgatggtg gcttggtgtgggagt

8.2 Plasmids

Supplement table 2: List of plasmids generated in this study.

Org	**Vector**	**Insert**	**Tag**
Bs	pET16b	*csrA*	-
Bs	pET16b	$csrA_{\Delta C30}$	-
Bs	pET16b	$csrA_{\Delta C17}$	-
Bs	pET24b	*fliW*	-
Bs	pGAT3	*fliW*	C6H
Bs	pET16b	*bacF*	N6H
Bs	pET24d	$flhA_{\Delta N301}$	N6H
Bs	pET16b	hag_{N40}	-
Bs	pET16b	hag_{N72}	-
Bs	pET16b	*hag*	-
Bs	pET16b	hag_{N50}	C6H
Bs	pET16b	hag_{N60}	C6H
Bs	pET16b	hag_{N72}	C6H
Bs	pET16b	*bacE*	6H
Gt	pEMGB1	*bacF*	N6H
Gt	pEMGB1	*bacE*	N6H
Bs	pGAT3	*bacF*	6H
Gt	pET24d	*bacF*	N6H
Bs	pET24d	*hag*	6H
Gt	pET24d	*fliW*	C6H
Gt	pET24d	*fliW*	-
Gt	pET16b	*csrA*	C6H
Gt	pET16b	*csrA*	-

Gt	pET16b	*csrA*	N6H
Gt	pET16b	*bacE*	-
Gt	pET24d	*bacE*	6H
Gt	pET16b	*bacF*	-
Bs	pET16b	*hag*	-
Gt	pET24d	$fliW_{N125D}$	6H
Gt	pET24d	$fliW_{N123D}$	6H
Gt	pET24d	$fliW_{F44D}$	6H
Bs	pET24d	*T4L-bacE*	6H
Hp	pET24d	*Hp1542*	6H
Sp	pET24d	*bac*	6H
Tm	pET24d	*Tm0735*	6H
Bs	pET24d	hag_{N40-72}	C6H
Bs	pET24d	hag_{N20-72}	C6H
Bs	pET16b	hag_{N40-72}	C6H
Bs	pEMGB1	*bacE*	6H

Erklärung der selbstständigen Erarbeitung der Dissertation

Hiermit erkläre ich, dass ich die vorliegende Dissertation:

„Structural and functional studies on the homeostasis and type-III-secretion of flagellin“

selbstständig und ohne unerlaubte Hilfsmittel angefertigt habe. Es wurden keine anderen, als der von mir ausdrücklich angegebenen Hilfsmittel verwendet. Die Dissertation wurde in der jetzigen oder in einer ähnlichen Form noch bei keiner anderen Hochschule eingereicht.

Es handelt sich bei den heute von mir eingereichten Exemplaren um in Wort und Bild völlig übereinstimmende Exemplare.

Des Weiteren erkläre ich, dass die digitalen Abbildungen ausschließlich originale Daten enthalten und in keinem Fall inhaltsverändernde Bildbearbeitung vorgenommen wurde.

Marburg, den 13.02.2017

_____

Florian Altegoer